

DEVELOPMENT OF PIEZOELECTRIC CERAMICS
FOR ULTRASONIC MOTOR APPLICATIONS

A THESIS SUBMITTED TO
THE GRADUATE SCHOOL OF NATURAL AND APPLIED SCIENCES
OF
MIDDLE EAST TECHNICAL UNIVERSITY

BY

VOLKAN KALEM

IN PARTIAL FULFILLMENT OF THE REQUIREMENTS
FOR
THE DEGREE OF DOCTOR OF PHILOSOPHY
IN
METALLURGICAL AND MATERIALS ENGINEERING

JANUARY 2011

Approval of the thesis:

**DEVELOPMENT OF PIEZOELECTRIC CERAMICS FOR ULTRASONIC
MOTOR APPLICATIONS**

submitted by **VOLKAN KALEM** in partial fulfillment of the requirements for the degree of **Doctor of Philosophy in Metallurgical and Materials Engineering Department, Middle East Technical University** by,

Prof. Dr. Canan Özgen _____
Dean, Graduate School of **Natural and Applied Sciences**

Prof. Dr. Tayfur Öztürk _____
Head of Department, **Metallurgical and Materials Engineering**

Prof. Dr. Muharrem Timuçin _____
Supervisor, **Metallurgical and Materials Engineering Dept., METU**

Examining Committee Members:

Prof. Dr. Macit Özenbaş _____
Metallurgical and Materials Engineering Dept., METU

Prof. Dr. Muharrem Timuçin _____
Metallurgical and Materials Engineering Dept., METU

Prof. Dr. Abdullah Öztürk _____
Metallurgical and Materials Engineering Dept., METU

Assoc. Prof. Dr. Nuri Durlu _____
Mechanical Engineering Dept., TOBB ETU

Assoc. Prof. Dr. F. Arcan Dericioğlu _____
Metallurgical and Materials Engineering Dept., METU

Date: 12.01.2011

I hereby declare that all information in this document has been obtained and presented accordance with the academic rules and ethical conduct. I also declare that, as required by these rules and conduct, I have fully cited and referenced all material and results that are not original to this work.

Name, Last name : Volkan Kalem

Signature :

ABSTRACT

DEVELOPMENT OF PIEZOELECTRIC CERAMICS FOR ULTRASONIC MOTOR APPLICATIONS

Kalem, Volkan

Ph.D., Department of Metallurgical and Materials Engineering

Supervisor: Prof. Dr. Muharrem Timuçin

January 2011, 157 pages

This study has been carried out to develop and manufacture piezoelectric ceramic materials which are utilized for ultrasonic motor (USM) applications. For this purpose, the effect of compositional modifications on the dielectric and piezoelectric properties of lead zirconate titanate (PZT) based ceramics was investigated.

PZT based powders were produced using the mixed oxide method. The base composition was selected as $\text{Pb}(\text{Zr}_{0.54}\text{Ti}_{0.46})\text{O}_3$. The samples in the proximity of morphotropic phase boundary were doped with strontium, lanthanum, lead manganese niobate (PMnN) and lead manganese antimonate (PMS) in order to improve the structural characteristics and electromechanical properties which are very important for USM applications. The dielectric constant, planar coupling coefficient, mechanical quality factor, piezoelectric strain constant and tangent loss values were evaluated in accordance with standard IRE (Institute of Radio Engineers) test procedures.

The results on dielectric and piezoelectric properties showed that piezoelectric ceramics with high mechanical quality factor, high piezoelectric strain constant and low tangent loss could be produced by using the aforementioned dopants. As a result, a new piezoelectric ceramic named as 0.97[PSLZT]-0.024[PMnN]-0.006[PMS] was produced with $K^T= 1913$, $Q_m= 1240$, $d_{33}= 540$ pC/N, $\tan \delta= 0.89\%$, $k_p= 0.57$ and $T_c= 235$ °C. This composition is a good candidate for high power applications.

The ceramic samples with the developed compositions were used to produce an ultrasonic-wave type motor and the performance of the USM was evaluated in terms of speed, torque and efficiency.

Keywords: PZT, Dielectric, Piezoelectric, Ultrasonic Motor.

ÖZ

ULTRASONİK MOTOR UYGULAMALARI İÇİN PİEZOELEKTRİK SERAMİKLERİN GELİŞTİRİLMESİ

Kalem, Volkan

Doktora, Metalurji ve Malzeme Mühendisliği Bölümü

Tez Yöneticisi: Prof. Dr. Muharrem Timuçin

Ocak 2011, 157 sayfa

Bu çalışma, ultrasonik motor (USM) uygulamalarında kullanılan piezoelektrik seramik malzemelerin geliştirilmesi ve üretimi için yapılmıştır. Bu amaçla, kompozisyon değişimlerinin; kurşun zirkonat titanat (PZT) seramiklerinin dielektrik ve piezoelektrik özellikleri üzerindeki etkileri incelenmiştir.

PZT tozları, oksit karışım metodu ile üretilmiştir. Temel PZT kompozisyonu olarak $Pb(Zr_{0.54}Ti_{0.46})O_3$ bileşimi seçilmiştir. Morfotropik faz sınırları içinde kalan numuneler; USM uygulamaları için çok önemli olan yapısal ve elektromekanik özellikleri geliştirmek amacıyla stronsiyum, lantan, kurşun mangan niobit (PMnN) ve kurşun mangan antimonit (PMS) ile katkılandırılmıştır. Dielektrik sabiti, düzlemsel bağlaşım katsayısı, mekanik kalite faktörü, piezoelektrik gerinim sabiti ve kayıp tanjantı; standart IRE testlerine göre saptanmıştır.

Dielektrik ve piezoelektrik özelliklere ait sonuçlar; yukarıda bahsedilen katkıların kullanımı ile yüksek mekanik kalite faktörü, yüksek piezoelektrik gerinim sabiti ve düşük kayıp tanjantına sahip piezoelektrik seramiklerin üretilebildiğini göstermiştir. Sonuç olarak, $K^T= 1913$, $Q_m= 1240$, $d_{33}= 540$ pC/N, $\tan \delta= 0.89\%$,

$k_p = 0.57$ and $T_c = 235 \text{ }^\circ\text{C}$ özelliklerine sahip $0.97[\text{PSLZT}]-0.024[\text{PMnN}]-0.006[\text{PMS}]$ isimli yeni bir piezoelektrik seramik kompozisyonu üretilmiştir. Geliştirilen kompozisyonlarda üretilen seramik numuneler ultrasonik-dalga tipi motor üretmek için kullanılmış ve motorun performansı; hız, dönme momenti ve verimlilik cinsinden saptanmıştır.

Anahtar Kelimeler: PZT, Dielektrik, Piezoelektrik, Ultrasonik Motor.

To my parents,

ACKNOWLEDGEMENTS

I would like to take this opportunity to express my sincerest gratitude to my thesis advisor, Prof. Dr. Muharrem Timuçin, for his invaluable guidance, patience, and support during the course of this work.

Thanks are also extended to Prof. Dr. Macit Özenbaş and Assoc. Prof. Dr. Nuri Durlu for providing me many valuable suggestions and helpful discussions on this work and serving on the thesis committee. I also appreciate the help and time spent by the other committee members: Prof. Dr. Abdullah Öztürk and Assoc. Prof. Dr. Arcan Dericioğlu. Sincere thanks to Dr. İbrahim Çam for his valuable criticisms and help during experimental work on both the ultrasonic motor and the piezoelectric characterization.

I would like to thank to Cengiz Tan and Necmi Avcı for their helps in SEM and XRD studies. I wish to give a special thank to Yankı Uzunçakmak for her helpful discussion and support, and for all the fun times throughout the graduate school. I would also like to thank to all of the office- and room-mates that I have had the pleasure of knowing over the last six years. I would like to express my sincere thanks to Derya Kapusuz and Filiz Arıkanlı for always being supportive in my life.

And last but absolutely not least, I thank Mom and Dad, Züleyha and Özer Kalem and my family for their understanding and encouragement during my graduate education.

This work has been financially supported by the State Planning Organization (DPT) of Turkey through Faculty Development Program (ÖYP) Project No: 2002K120510.

TABLE OF CONTENTS

ABSTRACT	iv
ÖZ	vi
ACKNOWLEDGEMENTS	ix
TABLE OF CONTENTS	x
LIST OF TABLES	xiii
LIST OF FIGURES	xvi
CHAPTERS	
1. INTRODUCTION	1
2. THEORETICAL BACKGROUND	6
2.1 Piezoelectricity	6
2.2 The Dielectric and Piezoelectric Parameters of Importance	13
2.2.1 Dielectric Constant, K	13
2.2.2 Loss Tangent, $\tan \delta$	14
2.2.3 Piezoelectric Strain Coefficient, d	15
2.2.4 Electromechanical Coupling Factor, k	15
2.2.5 Mechanical Quality Factor, Q_m	16
2.3 Materials	16
3. GENERAL EXPERIMENTAL PROCEDURE	19
3.1 Method.....	19
3.2 Preparation of Ceramic Powders.....	19
3.3 Sintering of Ceramic Samples.....	20
3.4 Ceramic Characterization	22
3.4.1 Phase Analysis and Microstructure	22
3.4.2 Sintered Density	24
3.4.3 Measurement of Dielectric and Piezoelectric Parameters	24

3.5 Particle Size.....	27
3.6 Stoichiometry	28
3.7 Curie Temperature (T_c).....	29
3.8 Hysteresis Loops	30
4. PSZT-PSLZT CERAMICS	34
4.1 Introduction.....	34
4.2 Compositions Studied.....	36
4.3 Results and Discussion	37
4.3.1 PSZT Ceramics.....	37
4.3.2 PSLZT Ceramics	44
4.4 Conclusions of the PSZT – PSLZT Ceramics	65
5. PSLZT CERAMICS MODIFIED BY Mn, Nb AND Sb	67
5.1 Introduction.....	67
5.1.1 Manganese	71
5.1.2 Antimony	73
5.1.3 Niobates and Antimonates	74
5.2 Compositions Studied.....	80
5.3 Results and Discussion	84
5.3.1 PMnN Addition	84
5.3.2 Zr/Ti Ratio.....	94
5.3.3 PMS Addition.....	100
5.4 Conclusions of the PSLZT Ceramics Modified by Mn, Nb and Sb.....	110
6. ULTRASONIC MOTOR (USM) APPLICATION	111
6.1 Hard-Drive Applications and Requirements.....	111
6.2 Ultrasonic Motors.....	112
6.3 Operating Principle and Features	113
6.4 Experimental Procedure.....	116
6.5 Results and Discussion	121
6.6 Conclusions of the Ultrasonic Motor Application	127
7. SUMMARY AND CONCLUSIONS	131

REFERENCES	136
APPENDICES	
A. PIEZOELECTRIC CHARACTERIZATION DATA OF PZT CERAMICS...	
.....	150
B. X-RAY AND DENSITY DATA OF PZT CERAMICS.....	153
CURRICULUM VITAE	157

LIST OF TABLES

TABLES

Table 3.1 ICP-OES analysis of modified PZT samples sintered at 1240 °C for 2h.	29
Table 4.1 Physical and electrical properties of $\text{Pb}_{0.95}\text{Sr}_{0.05}(\text{Zr}_z\text{Ti}_{1-z})\text{O}_3$ ceramics. ...	38
Table 4.2 Physical and electrical properties of $\text{Pb}_{0.95-y}\text{Sr}_{0.05}\text{La}_y(\text{Zr}_{0.54}\text{Ti}_{0.46})\text{O}_3$ ceramics.....	44
Table 4.3 Physical and electrical properties of $\text{Pb}_{0.94}\text{Sr}_{0.05}\text{La}_{0.01}(\text{Zr}_z\text{Ti}_{1-z})\text{O}_3$ ceramics.....	51
Table 4.4 Physical and electrical properties of $\text{Pb}_{0.99-x}\text{Sr}_x\text{La}_{0.01}(\text{Zr}_{0.54}\text{Ti}_{0.46})\text{O}_3$ ceramics.....	58
Table 5.1 PZT-based ceramic compositions developed for high power applications.	69
Table 5.2 Chemical formulations of PZT samples.....	82
Table 5.3 Physical and electrical properties of $(1-x)[\text{PSLZT}]-x[\text{PMnN}]$ ceramics.	84
Table 5.4 Physical and electrical properties of $0.97[\text{PSLZT}]-0.03[\text{PMnN}]$ ceramics with different Zr/Ti ratio.	95
Table 5.5 Physical and electrical properties of $0.97[\text{PSLZT}]-0.03-y[\text{PMnN}]-$ $(y)[\text{PMS}]$ ceramics with different Zr/Ti ratio.	101
Table 6.1 Compositions of the ceramics investigated for ultrasonic motor study.	124

Table 7.1 The ceramics, with optimum dielectric and piezoelectric properties, developed in this study.....	134
Table A.1 Sample diameter (\varnothing), resonance frequency (f_r), antiresonance frequency (f_a), impedance at resonance ($ Z_m $), and capacitance at 1 kHz (C) values for PSZT ceramics measured in HP 4194A Impedance/Gain-Phase Analyzer.	150
Table A.2 Sample diameter (\varnothing), resonance frequency (f_r), antiresonance frequency (f_a), impedance at resonance ($ Z_m $), and capacitance at 1 kHz (C) values for PSLZT ceramics measured in HP 4194A Impedance/Gain-Phase Analyzer.	151
Table A.3 Sample diameter (\varnothing), resonance frequency (f_r), antiresonance frequency (f_a), impedance at resonance ($ Z_m $), and capacitance at 1 kHz (C) values for (1-x-y)[PSLZT]-(x)[PMnN]-(y)[PMS] ceramics measured in HP 4194A Impedance/Gain-Phase Analyzer.	152
Table B.1 Lattice parameters, tetragonality, theoretical and experimental density values of $\text{Pb}_{0.95}\text{Sr}_{0.05}(\text{Zr}_z\text{Ti}_{1-z})\text{O}_3$ ceramics.....	153
Table B.2 Lattice parameters, tetragonality, theoretical and experimental density values of $\text{Pb}_{0.95-y}\text{Sr}_{0.05}\text{La}_y(\text{Zr}_{0.54}\text{Ti}_{0.46})\text{O}_3$ ceramics.....	154
Table B.3 Lattice parameters, tetragonality, theoretical and experimental density values of $\text{Pb}_{0.94}\text{Sr}_{0.05}\text{La}_{0.01}(\text{Zr}_z\text{Ti}_{1-z})\text{O}_3$ ceramics.	154
Table B.4 Lattice parameters, tetragonality, theoretical and experimental density values of $\text{Pb}_{0.99-x}\text{Sr}_x\text{La}_{0.01}(\text{Zr}_{0.54}\text{Ti}_{0.46})\text{O}_3$ ceramics.	155
Table B.5 Lattice parameters, tetragonality, theoretical and experimental density values of (1-x)[PSLZT]-(x)[PMnN] ceramics.....	155
Table B.6 Lattice parameters, tetragonality, theoretical and experimental density values of 0.97[PSLZT] – 0.03[PMnN] ceramics with different Zr/Ti ratio.	156

Table B.7 Lattice parameters, tetragonality, theoretical and experimental density values of $0.97[\text{PSLZT}] - (0.03-y)[\text{PMnN}] - (y)[\text{PMS}]$ ceramics.156

LIST OF FIGURES

FIGURES

Figure 1.1 Temperature rise in a vibrating piezoelectric body [4].	3
Figure 2.1 Relationship of piezoelectrics and subdivisions with symmetry groups (Reproduced from [8]).	8
Figure 2.2 Schematic of a two dimensional unit cell showing the directional dependency of piezoelectricity (Reproduced from [10]).	9
Figure 2.3 Crystal structure of a traditional piezoelectric ceramic [16].	11
Figure 2.4 Poling of a piezoelectric ceramic.	12
Figure 2.5 Direct and inverse behaviors of a piezoelectric element [16].	13
Figure 2.6 Designations of directions.	14
Figure 3.1 Production of PZT-based powder by the mixed oxide route.	21
Figure 3.2 PZT-based ceramics prepared for measurements.	22
Figure 3.3 Phase diagram of PbZrO_3 - PbTiO_3 system [20].	23
Figure 3.4 Fractional particle size distribution of ball-milled modified PZT powder.	27
Figure 3.5 Hysteresis loop for a ferroelectric crystal.	31
Figure 3.6 Modified Sawyer-Tower circuit.	33
Figure 4.1 SEM micrographs of $\text{Pb}_{0.95}\text{Sr}_{0.05}(\text{Zr}_z\text{Ti}_{1-z})\text{O}_3$ ceramics having variable Zr/Ti ratio: (a) PZT without Sr, (b) $z=0.52$, (c), $z=0.56$, and (d) $z=0.60$.	39
Figure 4.2 The XRD patterns of the $\text{Pb}_{0.95}\text{Sr}_{0.05}(\text{Zr}_z\text{Ti}_{1-z})\text{O}_3$ ceramics. The values of z in the figure indicate the Zr content in the PSZT.	40

Figure 4.3 Relative proportions of tetragonal and rhombohedral modifications in the $\text{Pb}_{0.95}\text{Sr}_{0.05}(\text{Zr}_z\text{Ti}_{1-z})\text{O}_3$ ceramics.....	41
Figure 4.4 Variations in the dielectric and piezoelectric properties of $\text{Pb}_{0.95}\text{Sr}_{0.05}(\text{Zr}_z\text{Ti}_{1-z})\text{O}_3$ ceramics.	42
Figure 4.5 Variations in Q_m and $\tan \delta$ with Zr/Ti ratio in $\text{Pb}_{0.95}\text{Sr}_{0.05}(\text{Zr}_z\text{Ti}_{1-z})\text{O}_3$ ceramics.....	43
Figure 4.6 SEM micrographs of $\text{Pb}_{0.95-y}\text{Sr}_{0.05}\text{La}_y(\text{Zr}_{0.54}\text{Ti}_{0.46})\text{O}_3$ ceramics with increasing La content: (a) $y=0.01$, (b) $y=0.03$, (c) $y=0.04$, and (d) $y=0.05$	46
Figure 4.7 The XRD patterns of the $\text{Pb}_{0.95-y}\text{Sr}_{0.05}\text{La}_y(\text{Zr}_{0.54}\text{Ti}_{0.46})\text{O}_3$ ceramics. The values of y in the figure indicate the La content in the PSLZT.	47
Figure 4.8 Relative proportions of tetragonal and rhombohedral modifications in the $\text{Pb}_{0.95-y}\text{Sr}_{0.05}\text{La}_y(\text{Zr}_{0.54}\text{Ti}_{0.46})\text{O}_3$ ceramics as a function of La doping.	48
Figure 4.9 Variations in the dielectric and piezoelectric properties of $\text{Pb}_{0.95-y}\text{Sr}_{0.05}\text{La}_y(\text{Zr}_{0.54}\text{Ti}_{0.46})\text{O}_3$ ceramics with increasing La substitution.	49
Figure 4.10 Variations in Q_m and $\tan \delta$ with La content in $\text{Pb}_{0.95-y}\text{Sr}_{0.05}\text{La}_y(\text{Zr}_{0.54}\text{Ti}_{0.46})\text{O}_3$ ceramics.....	50
Figure 4.11 SEM micrographs of $\text{Pb}_{0.94}\text{Sr}_{0.05}\text{La}_{0.01}(\text{Zr}_z\text{Ti}_{1-z})\text{O}_3$ ceramics with Zr content of (a) $z=0.52$, (b) $z=0.54$, (c) $z=0.58$, (d) $z=0.60$	52
Figure 4.12 The XRD patterns of the $\text{Pb}_{0.94}\text{Sr}_{0.05}\text{La}_{0.01}(\text{Zr}_z\text{Ti}_{1-z})\text{O}_3$ ceramics. The values of z in the figure indicate the Zr content in the PSLZT.	53
Figure 4.13 Relative proportions of tetragonal and rhombohedral modifications in the $\text{Pb}_{0.94}\text{Sr}_{0.05}\text{La}_{0.01}(\text{Zr}_z\text{Ti}_{1-z})\text{O}_3$ ceramics.	54
Figure 4.14 Variations in the dielectric and piezoelectric properties of $\text{Pb}_{0.94}\text{Sr}_{0.05}\text{La}_{0.01}(\text{Zr}_z\text{Ti}_{1-z})\text{O}_3$ ceramics.....	55

Figure 4.15 The hysteresis behavior in $\text{Pb}_{0.94}\text{Sr}_{0.05}\text{La}_{0.01}(\text{Zr}_z\text{Ti}_{1-z})\text{O}_3$ ceramics.....	56
Figure 4.16 Variations of coercive field and remnant polarization with Zr/Ti ratio in $\text{Pb}_{0.94}\text{Sr}_{0.05}\text{La}_{0.01}(\text{Zr}_z\text{Ti}_{1-z})\text{O}_3$ ceramics.	57
Figure 4.17 SEM micrographs of $\text{Pb}_{0.99-x}\text{Sr}_x\text{La}_{0.01}(\text{Zr}_{0.54}\text{Ti}_{0.46})\text{O}_3$ ceramics modified with various levels of Sr addition: (a) undoped, (b) $x=0.02$, (c) $x=0.04$, and (d) $x=0.05$	59
Figure 4.18 The XRD patterns of the $\text{Pb}_{0.99-x}\text{Sr}_x\text{La}_{0.01}(\text{Zr}_{0.54}\text{Ti}_{0.46})\text{O}_3$ ceramics. The values of x indicate the Sr content in the PSLZT.	60
Figure 4.19 Relative proportions of tetragonal and rhombohedral modifications in the $\text{Pb}_{0.99-x}\text{Sr}_x\text{La}_{0.01}(\text{Zr}_{0.54}\text{Ti}_{0.46})\text{O}_3$ ceramics with variable Sr content.....	61
Figure 4.20 Variations in the dielectric and piezoelectric properties of $\text{Pb}_{0.99-x}\text{Sr}_x\text{La}_{0.01}(\text{Zr}_{0.54}\text{Ti}_{0.46})\text{O}_3$ ceramics.....	62
Figure 4.21 The hysteresis behavior in $\text{Pb}_{0.99-x}\text{Sr}_x\text{La}_{0.01}(\text{Zr}_{0.54}\text{Ti}_{0.46})\text{O}_3$ ceramics. .	63
Figure 4.22 Variations of coercive field and remnant polarization with Zr/Ti ratio in $\text{Pb}_{0.99-x}\text{Sr}_x\text{La}_{0.01}(\text{Zr}_{0.54}\text{Ti}_{0.46})\text{O}_3$ ceramics.....	64
Figure 4.23 The change in the dielectric constant of the $\text{Pb}_{0.99-x}\text{Sr}_x\text{La}_{0.01}(\text{Zr}_{0.54}\text{Ti}_{0.46})\text{O}_3$ ceramics with temperature.....	65
Figure 5.1 Phase diagram of PZT doped with Mn and/or F showing the range of MPB region [57].	72
Figure 5.2 The system $\text{Pb}(\text{Mg}_{1/3}\text{Nb}_{2/3})\text{O}_3$ - PbTiO_3 - PbZrO_3 at room temperature [2].	75
Figure 5.3 The phase diagram of the PbTiO_3 - PbZrO_3 - $\text{Pb}(\text{Mn}_{1/3}\text{Sb}_{2/3})\text{O}_3$ system at room temperature [84].	78
Figure 5.4 The XRD pattern of 0.97[PSLZT] - 0.03[PMnN] powder.	83

Figure 5.5 SEM micrographs of PSLZT samples doped with (a) 0.01, (b) 0.05, (c) 0.07 and (d) 0.10 mole PMnN.	85
Figure 5.6 The XRD patterns of (1-x)[PSLZT]-(x)[PMnN] samples. The values of x in the figure indicate the PMnN content in the PSLZT-PMnN.	87
Figure 5.7 Relative proportions of tetragonal and rhombohedral modifications in [PSLZT] – [PMnN] ceramics with varying PMnN content.	88
Figure 5.8 Variation of piezoelectric and dielectric properties as a function of PMnN doping.....	90
Figure 5.9 Variation of mechanical quality factor and loss tangent value as a function of PMnN doping.....	91
Figure 5.10 Ferroelectric hysteresis loops of (1-x)[PSLZT]-(x)[PMnN] ceramics.	93
Figure 5.11 The change in the dielectric constant (1-x)[PSLZT]-(x)[PMnN] ceramics with temperature.....	94
Figure 5.12 The XRD patterns of 0.97[Pb _{0.94} Sr _{0.05} La _{0.01} (Zr _x Ti _{1-x}) _{0.9975} O ₃]-0.03[Pb(Mn _{1/3} Nb _{2/3})O ₃] samples. The values of x in the figure indicate the Zr content in the 0.97[PSLZT]-0.03[PMnN].	96
Figure 5.13 Relative proportions of tetragonal and rhombohedral modifications in 0.97[PSLZT]-0.03[PMnN] ceramics with varying Zr/Ti ratio.....	97
Figure 5.14 Variation of piezoelectric strain coefficient, dielectric constant and coupling factor as a function of Zr/Ti ratio in 0.97[PSLZT]-0.03[PMnN] ceramics.	98
Figure 5.15 Variation of mechanical quality factor and loss tangent as a function of Zr/Ti ratio in 0.97[PSLZT]-0.03[PMnN] ceramics.	99

Figure 5.16 The change in the dielectric constant of $0.97[\text{Pb}_{0.94}\text{Sr}_{0.05}\text{La}_{0.01}]$	100
Figure 5.17 SEM micrographs of PSLZT-PMnN-PMS samples:	102
Figure 5.18 XRD patterns of $0.97[\text{PSLZT}]-(0.03-y)[\text{PMnN}]-y[\text{PMS}]$ samples sintered at $1240\text{ }^\circ\text{C}$ for 2h. The values of y in the figure indicate the PMS content in the PSLZT-PMnN-PMS.	103
Figure 5.19 Variations of relative contents of tetragonal and rhombohedral phases with the amount of PMS doping.	104
Figure 5.20 Variation of piezoelectric strain coefficient, dielectric constant and coupling factor as a function of PMS additions.	106
Figure 5.21 Variation of mechanical quality factor and loss tangent as a function of PMS additions.	107
Figure 5.22 Ferroelectric hysteresis loops of $0.97[\text{PSLZT}]-(0.03-y)[\text{PMnN}]-y[\text{PMS}]$ ceramics.	108
Figure 5.23 Variation of dielectric constant of $0.97[\text{PSLZT}]-(0.03-y)[\text{PMnN}]-y[\text{PMS}]$ ceramics with temperature.	109
Figure 6.1 (a) Structure of the stator of metal tube motor and (b) assembly of the motor [98].	115
Figure 6.2 The wobbling and clock-wise motions obtained by driving plate X [100].	116
Figure 6.3 The dimensions of the stator of the metal tube motor [100].	117
Figure 6.4 (a) Ultrasonic motor parts, (b) Assembled motor and (c) Stator bonded with a ceramic plate.	118
Figure 6.5 Impedance spectrum of the piezoelectric ceramic plate.	119
Figure 6.6 Impedance spectrum of the plate-bonded-stator.	120

Figure 6.7 The schematic of the driving and characterization systems for ultrasonic motor.	121
Figure 6.8 Speed-frequency characteristic of USM for different operating voltages.	122
Figure 6.9 Speed-time characteristic of USM driven at 120 V _{pp}	123
Figure 6.10 Speed of the motor as a function of driving frequency for ceramic plates of different compositions.	125
Figure 6.11 Load characteristics of the ultrasonic motor for composition number (a) 1, (b) 2, (c) 3, (d) 4, (e) 5 and (f) 6 given in Table 6.1.	126
Figure 6.12 The dependency of no-load speed of the ultrasonic motor to the piezoelectric strain coefficient of ceramic plate.	128
Figure 6.13 The variation of decrease in the speed of ultrasonic motor with mechanical quality factor of ceramic plate.	129

CHAPTER 1

INTRODUCTION

Lead zirconate titanate (PZT) based ceramic materials are widely used as hard-drive devices like transducers and actuators in a wide range of application areas. Ultrasonic motor (USM) application is a specific field in which piezoelectric ceramics show an increasing importance. An ultrasonic motor is an actuator with a drive source of mechanical vibrations in the ultrasonic range. Piezoelectric ceramics which mechanically vibrate with an applied ac electric field are used in ultrasonic motors as the vibrational source to provide the ultrasonic waves [1].

Piezoelectricity is the generation of an electrical charge under applied mechanical pressure on the material or vice versa which means the development of deformation (strain) of the material when subjected to an applied electric field. Lead zirconate-lead titanate (PZT) based compositions are the most successful and commonly used piezoelectric ceramics in the electronics industry. Lead zirconate-titanate, $\text{Pb}(\text{Zr}_x\text{Ti}_{1-x})\text{O}_3$, has the perovskite structure with ABO_3 formula where A indicates the divalent (Pb^{2+}) and B indicates the tetravalent (Zr^{4+} , Ti^{4+}) cation. The composition, microstructure and the structural alterations are the primary factors that affect the physical and electrical properties of PZT ceramics. PZT ceramics exhibit their optimum electrical properties in the vicinity of morphotropic phase boundary (MPB) where the Zr/Ti ratio is approximately 53/47 [2]. MPB is the boundary between PbTiO_3 and PbZrO_3 phases, considering the $\text{Pb}(\text{Zr},\text{Ti})\text{O}_3$ solid solution, and is nearly independent of temperature. The isovalent and nonisovalent (aliovalent) substituents at the A and/or B sites can modify the piezoelectric properties of PZT [2].

One of the most important properties in hard-drive applications is the mechanical quality factor, Q_m , which is defined as the reciprocal of the internal friction in a vibrating piezoelectric element. A low Q_m indicates fatigue and tendency of degradation in piezoelectric properties. Therefore, a high Q_m value is necessary for piezoelectric materials to be used in cyclic motion (e.g. ultrasonic motors) [3].

A piezoelectric ceramic must be operated at its resonance frequency in order to have an efficient conversion of electrical energy to mechanical energy. The piezoelectric element exhibits the maximum displacement at this specific frequency. The internal energy losses in a vibrating piezoelectric element due to the dissipated heat and the internal friction affect the value of Q_m . The dissipated heat in the body causes an increase in the temperature of the ceramic which in turn results in the degradation of piezoelectric and dielectric properties [2, 3]. K. Nagata et al. [4] determined that the temperature rise in a piezoelectric transformer under operation became lower as the mechanical quality factor of the ceramic increased as shown in Figure 1.1.

The most characteristic property of a piezoelectric ceramic, piezoelectric strain coefficient, d_{33} , is the mechanical strain generated by the material per unit electric field applied to it. Materials with high d coefficients are desirable in motional or vibrational devices [3].

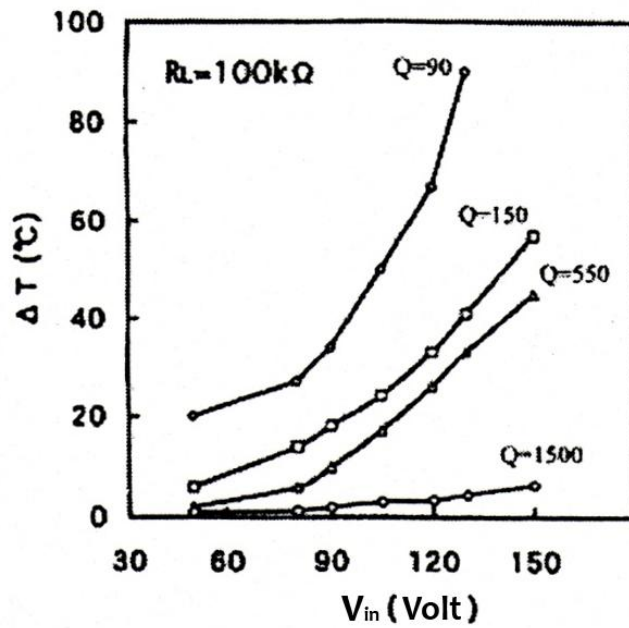


Figure 1.1 Temperature rise in a vibrating piezoelectric body [4].

Piezoelectric ceramic materials transform the mechanical energy to electrical energy and vice versa. The measure of the effectiveness of this conversion is called as the electromechanical coupling coefficient. The relation between the converted energies is expressed as:

$$k^2 = \frac{\text{stored mechanical energy}}{\text{supplied electrical energy}} = \frac{\text{stored electrical energy}}{\text{supplied mechanical energy}} \quad (1-1)$$

“k” is generally smaller than 0.7 for piezoelectrics and the maximum value of k could reach to unity [3]. The planar coupling factor, k_p , is defined as the coupling between an electric field parallel to the poling direction of the ceramic and radial mechanical vibrations for a thin disc of piezoceramic.

In piezoelectric ceramics, an increase in d accompanies with a decrease in Q_m which is mainly due to the domain structure of ferroelectric ceramics. Ferroelectrics are a subgroup of piezoelectrics which have also a spontaneous polarization. Additionally, the direction of the spontaneous polarization can be oriented in inverse direction by an applied electric field. The regions in ferroelectric crystals in which all the electric dipoles are oriented in the same direction are called as domains. A ferroelectric ceramic possess many domains which are separated by interfaces called domain walls.

An increase in wall mobility results in an observed reduction in mechanical quality factor and increase in piezoelectric coefficients and coupling factors. Piezoelectric ceramic materials with these properties are called as “soft” piezoceramics. On the other hand, decrease in wall mobility and stabilization of domains lead to high Q_m piezoceramics, but attended with low piezoelectric constant and coupling coefficient which are the characteristics of “hard” ceramics.

Piezoelectric ceramics used in high-power devices, such as transformers, actuators and ultrasonic motors, are operated at their resonant frequencies in order to convert electrical energy to mechanical energy and vice versa. Therefore, ceramics with improved electrical properties like mechanical quality factor ($Q_m > 1000$), planar electromechanical coupling factor ($k_p > 0.5$), piezoelectric strain constant ($d_{33} > 200$ pC/N) and also low dielectric loss ($\tan \delta$) are needed to meet the demands for these types of high power electromechanical applications [5-7].

In this regard, this study has two major goals:

- Developing piezoelectric lead zirconate titanate (PZT)-based ceramic materials that possess appropriate piezoelectric properties (i.e., high d_{33} , Q_m and k_p) for ultrasonic motor applications by altering composition and processing conditions.

➤ Constructing a piezoelectric (ultrasonic) motor by using the developed ceramics and characterization of its performance in terms of speed, torque and efficiency.

The thesis dissertation consists of seven parts. In chapter two, a literature review is presented on PZT materials to layout the theoretical background. In consecutive chapters, the details on the studies concerning the effects of doping PZT with Sr, La, Mn, Nb or Sb are presented. The chapter on piezoelectric motor is devoted to the performance results of an ultrasonic motor utilizing the piezoelectric ceramics developed during this study. Final chapter of the thesis gives conclusions of the study.

CHAPTER 2

THEORETICAL BACKGROUND

2.1 Piezoelectricity

Piezoelectricity is the ability of certain group of crystals to develop an electrical polarization under the application of a mechanical stress. The magnitude of the electric charge produced on the surface of the material is proportional to the applied mechanical stress. This phenomenon, discovered by P. and J. Curie in 1880, is called as the direct piezoelectric effect. Piezoelectric materials also show the opposite effect, called converse effect, which is defined as the generation of geometric deformation (strain) by the application of an electric field [2].

The descriptions of the aforementioned piezoelectric effects are given by the basic equations,

$$D = dT + \epsilon^X E \quad (\text{direct effect}) \quad (2-1)$$

$$S = s^E T + dE \quad (\text{converse effect}) \quad (2-2)$$

where D is the dielectric displacement, T is the stress, E is the electric field, S is the strain, d is the piezoelectric coefficient which is numerically equal in both equations, ϵ^X is the dielectric constant at constant stress which means the piezoelectric element is mechanically unconstrained, and s^E is the material compliance (inverse of modulus of elasticity) at constant electric field which means the electrodes on the elements are shorted together. Piezoceramics with high d

coefficients are needed for vibrational devices, such as ultrasonic echo sounders, and underwater microphones.

The crystal lattice should have no center of symmetry in order the piezoelectric phenomenon to occur in a material. 21 of the 32 crystal classes or point groups do not possess a centre of symmetry and 20 of them are piezoelectric, as shown in Figure 2.1. The only exception, (432) point group, in the cubic system possesses symmetry elements which in turn lead to no piezoelectric effect [9]. 10 out of these 20 piezoelectric crystal classes contain a unique polar axis along which they are spontaneously polarized. If the temperature of the crystal is changed, a change in polarization is induced which leads to the term pyroelectricity. The ferroelectrics are a subgroup of pyroelectrics. They have also a spontaneous polarization and the direction of the spontaneous polarization can be reversed by an applied electric field [8].

The application of stress to a crystal causes a deformation which in turn results in a displacement of the positive and negative charges within the piezoelectric crystal. The application of a stress in centrosymmetric crystals does not change the positions of the center of positive and negative charges. But in acentric crystals, the positive and negative charges are taken apart if an external stress is applied, and so dipoles are developed in the crystal. The polarization developed in a piezoelectric crystal is dependent on the orientation of the stress applied to the crystal.

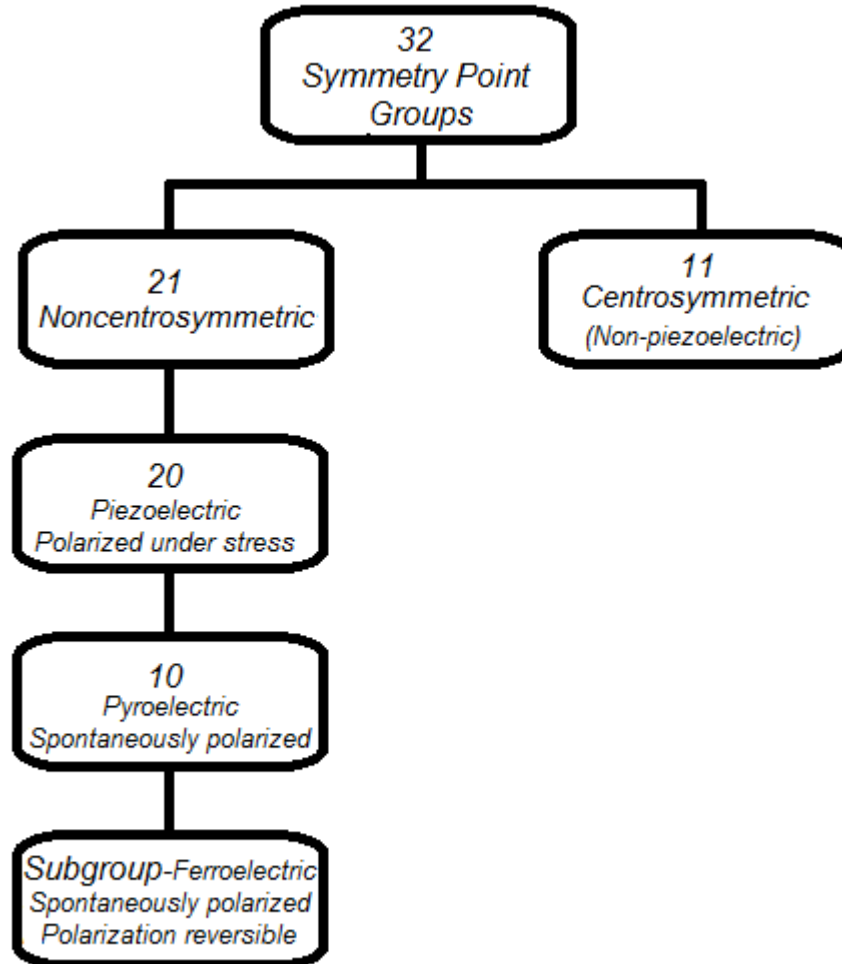


Figure 2.1 Relationship of piezoelectrics and subdivisions with symmetry groups
(Reproduced from [8]).

The visualization of the directional nature of the piezoelectric effect is possible by considering the effect of tensile stress on a two-dimensional unit cell as shown in Figure 2.2. If there is no external stress acting on the unit cell as shown in Figure 2.2a, then the centers of positive charge coincide. But, if a tensile stress is applied in the direction shown in Figure 2.2b, the centers of positive and negative charge are drawn apart. This provides the formation of a net polarization and piezoelectricity is observed. On the other hand, no piezoelectricity is observed since the centers of positive and negative charges are not separated when a tensile stress is applied in the direction shown in Figure 2.2c [10].

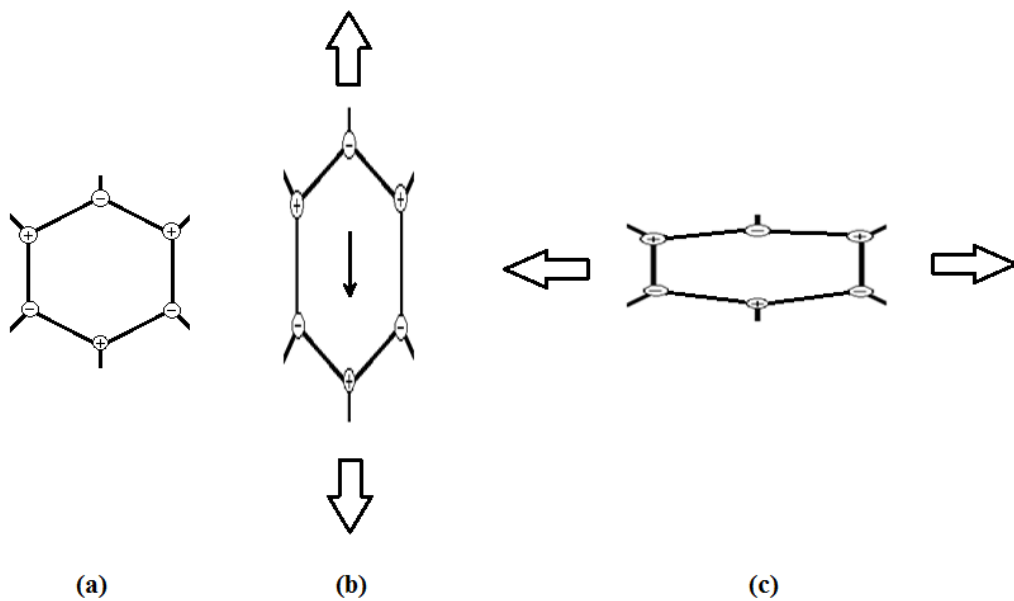


Figure 2.2 Schematic of a two dimensional unit cell showing the directional dependency of piezoelectricity (Reproduced from [10]).

Among piezoelectric ceramics, like barium titanate, lead niobate, lead titanate, etc, PZT is the most widely used one. PZT ceramics exhibit excellent piezoelectric characteristics and thus they are suitable for wider spectrum of technological applications. A large spectrum of lead zirconate titanate based ceramic materials was produced by chemical modifications which led to the optimization of electromechanical properties for different applications. The studies on the compositional modifications of the base PZT showed that the piezoelectric properties of these ceramics could be enhanced by the use additives [11-15].

A conventional piezoelectric ceramic is formed of perovskite crystals. Each crystal consists of a tetravalent metal ion, usually titanium or zirconium, in a lattice of larger, divalent metal ions, usually lead or barium, and O^{2-} ions as shown in Figure 2.3. If the crystal has tetragonal or rhombohedral symmetry, then it has a dipole moment which is shown in Figure 2.3b [16].

Figure 2.3a shows that each perovskite crystal possesses a simple cubic symmetry with no dipole moment above a specific temperature. This temperature is called as the *Curie temperature*. As can be seen in Figure 2.3b, each crystal has tetragonal or rhombohedral symmetry and thus a dipole moment at temperatures below the Curie temperature.

Neighboring dipoles form regions of local orientation called *domains*. This orientation provides a net dipole moment to the domain, and as a result a net polarization is obtained for this domain. Since the polarization direction among the adjoining domains is random, the ceramic element has no overall polarization as shown in Figure 2.4a.

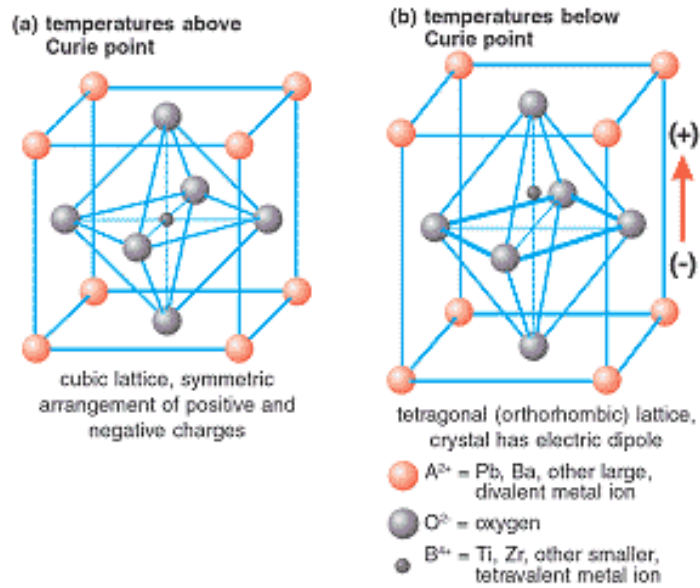


Figure 2.3 Crystal structure of a traditional piezoelectric ceramic [16].

The domains in a ceramic element can be oriented in a certain direction by applying a strong, direct current electric field to the ceramic element at a temperature slightly below the Curie temperature. Domains align nearly parallel to the direction of applied electric field during poling treatment. The domains that are not aligned with the applied electric field are expended by the domains oriented parallel to the field as shown in Figure 2.4b. As a result the ceramic element lengthens in that direction. Most of the dipoles keep their configuration of near alignment even if the electric field is removed as shown in Figure 2.4c. The element now has a permanent polarization, called remanent polarization (P_r), and is permanently elongated.

A compression or tension stress on a poled piezoelectric ceramic alters the dipole moment and creates a voltage between the parallel surfaces of the element. Compression along the direction of polarization generates voltage of the same polarity as the poling voltage which is visualized in Figure 2.5b. Tension stress perpendicular to the direction of polarization also leads to the same result.

Compression perpendicular to the polarization direction or tension along that direction results in the generation of a voltage with polarity opposite that of the poling voltage as shown in Figure 2.5c. The direct piezoelectric effect is also known as the generator action. The main application areas in which this behavior is used are fuel-igniting devices, solid state batteries, and force-sensing devices. The voltage and stress values are linearly proportional up to a certain stress value. The same is also valid for applied voltage and generated strain.

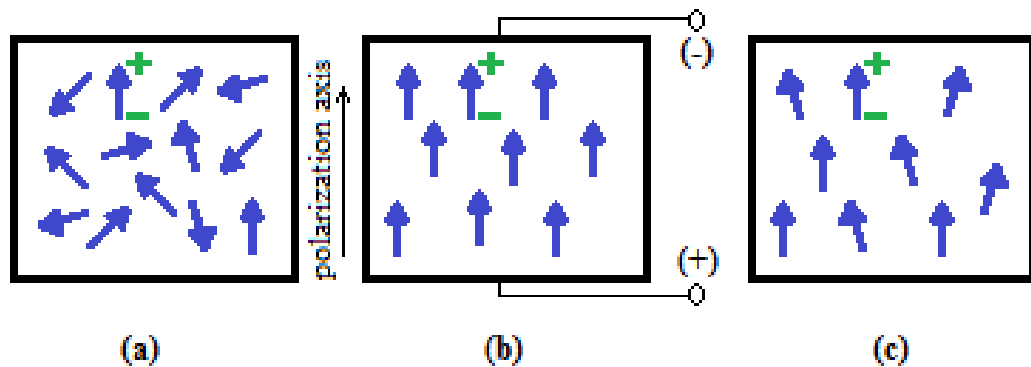


Figure 2.4 Poling of a piezoelectric ceramic.

If the ceramic element is exposed to a voltage of the same polarity as the poling voltage in the direction of the poling, it will lengthen as shown in Figure 2.5d. On the other hand, when a voltage of opposite polarity is applied to the ceramic, this time the element will shorten and become broader as shown in Figure 2.5e. If the element is exposed to an alternating voltage, then the element will lengthen and shorten continually. This is the converse piezoelectric effect, also known as motor action, in which electrical energy is converted into mechanical energy. The principle is utilized in sound generating devices, **ultrasonic motors**, and many other applications [16].

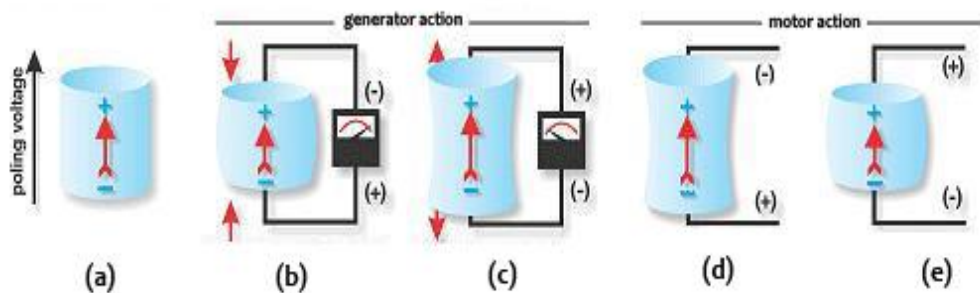


Figure 2.5 Direct and inverse behaviors of a piezoelectric element [16].

2.2 The Dielectric and Piezoelectric Parameters of Importance

The electrical properties of piezoelectrics are tensor quantities since they have directional nature and they depend on the magnitude and the direction of the applied stress or electric field. As a result, the coefficients describing the electromechanical properties are defined by two subscripts (ij), which indicate the direction of two quantities and by a superscript, which indicates that a quantity is kept constant [2]. For example, in the direct effect, an applied stress in the direction 3 (j) generates a voltage on the planes normal to direction 3 (i). Figure 2.6 shows the axes and directions of possible deformations.

2.2.1 Dielectric Constant, K

The relative dielectric constant is defined as the ratio between the electrical charge accumulated on an electroded slab of material brought to a given voltage and the charge accumulated on a set of identical electrodes separated by vacuum. It is usually referred as the dielectric constant, K , and is dimensionless [2].

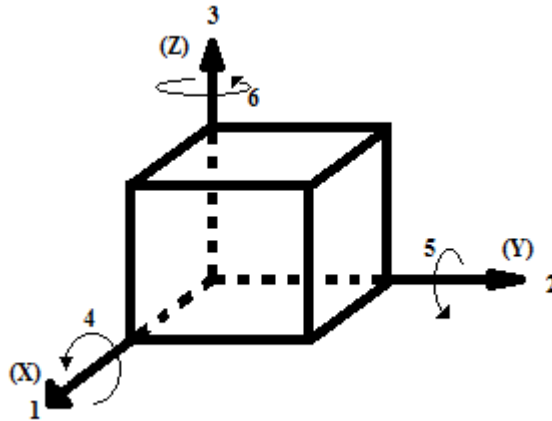


Figure 2.6 Designations of directions.

The measurement of the relative dielectric constant may be done at constant (zero) stress which is called as the free dielectric constant and is denoted by the superscript T. It may also be measured at constant (zero) strain and is then called the clamped dielectric constant, denoted by the superscript S [2].

2.2.2 Loss Tangent, $\tan \delta$

Loss tangent ($\tan \delta$) is another important dielectric property indicating the dielectric loss of a material driven by an alternating current. If the applied current on a dielectric material is AC, then the charge accumulated on the material has both real and imaginary components as a result of either resistive leakage or dielectric absorption. The dielectric loss is expressed as the ratio of imaginary component to the real component. This is also called as dissipation factor, and is usually referred to as loss tangent, $\tan \delta$ in the literature [2].

2.2.3 Piezoelectric Strain Coefficient, d

Piezoelectric strain coefficient relates the electrical polarization in a material with the applied mechanical stress for the direct effect. For the converse effect, it relates the mechanical strain generated by the material with the electric field applied to it.

This electromechanical parameter is also defined as the proportionality constant between dielectric displacement and mechanical stress or mechanical strain and electric field. Materials with high piezoelectric strain coefficients are desirable motional or vibrational devices [2].

d_{33} : induced polarization in the direction-3 per unit applied stress in the direction-3 / induced strain in the direction-3 per unit applied electric field in the direction-3.

$$d = \frac{D}{T} = \frac{S}{E} \quad (2-3)$$

2.2.4 Electromechanical Coupling Factor, k

The electromechanical coupling factor is the measure of the fraction of the electrical energy converted into mechanical and vice versa. The relation of energy conversion can be expressed as:

$$k^2 = \frac{\text{stored mechanical energy}}{\text{supplied electrical energy}} = \frac{\text{stored electrical energy}}{\text{supplied mechanical energy}} \quad (2-4)$$

“ k ” is usually smaller than 0.7 for piezoelectric ceramics [2]. The remainder can be stored in the material elastically, dielectrically or dissipated but also the unconverted energy can be, in some instances, recovered. The planar coupling

factor, k_p , is the coupling between an electric field along the poling direction of the ceramic element (direction 3) and mechanical effects that cause radial vibrations, relative to the direction of polarization (direction 1 and 2) for a thin disc of piezoceramic. [16].

2.2.5 Mechanical Quality Factor, Q_m

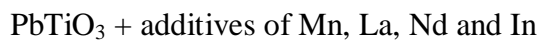
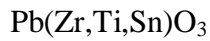
The dimensionless measure of the mechanical response to vibration by a piezoelectric body is defined as the mechanical quality factor, Q_m . It is the ratio of strain in phase with stress to strain out of phase with stress. The energy losses in the ceramic body during vibration due to internal friction and dissipated heat affect the value of Q_m . The heat is dissipated in a vibrating ceramic element due to the friction during the domain wall motion which makes the temperature of the ceramic rise and results in the degradation of piezoelectric properties.

The higher the mechanical quality factor, the higher the maximum deflection a vibrating body possesses at its fundamental resonance. Hence, a piezoelectric ceramic with high Q_m value is desirable in devices utilizing vibration [2].

2.3 Materials

Piezoelectric ceramics have been manufactured from a number of compositions which include barium titanate, barium strontium titanate, lead zirconate-lead titanate, bismuth titanate, sodium potassium niobate, lead magnesium niobate, etc. Barium titanate is the main constituent in the ceramic capacitor applications but its usage for electromechanical applications has been taken over by PZT based materials. Because PZT compositions exhibit higher electromechanical coupling coefficients; have higher Curie temperatures, can easily be poled, are relatively easy to sinter; and form solid solutions with many chemical compositions [1].

Usually full solid solubility can be obtained between piezoelectric end members, such as BaTiO₃, SrTiO₃, PbTiO₃ and PbZrO₃, due to their similar crystal structure and valences. Therefore, a remarkably wide range of piezoelectric properties can be achieved. Some of the major families of ceramics based on PZT compositions are:



High dielectric and piezoelectric parameters of PZT based ceramics are sensitive to the type and amount of additives and to the Zr/Ti ratio in the vicinity of the MPB. This is usually due to both the intrinsic and extrinsic effects, intrinsic one being the unit cell distortion and extrinsic effect being the movement of domain walls.

In order to improve the piezoelectric properties of the base PZT ceramic material for certain applications, PZT ceramics are always used with dopants. Excellent electromechanical properties could be achieved in lead-based piezoelectric solid solutions [17, 18].

These modifications can be done on A and/or B site of the ABO₃ lattice depending on the ionic radii and the solubility of the dopant. The substitutions can be isovalent or nonisovalent; that is determined by the ionic charge of the dopant. The effect of doping is a complex matter, but following generalizations can be made.

Sr²⁺ (isovalent): is an element that can be substituted into the A site of the perovskite in PZT to replace lead. Sr decreases the Curie point and increases the room temperature dielectric constant and the piezoelectric strain coefficient. It was also reported that Sr does not change the dissipation factor very much but it slightly raises the coupling factor along the phase boundary. MPB moves towards the

rhombohedral site and grain growth is inhibited with increasing Sr substitution into PZT.

Donor Dopants: Those with higher valence than that of the ions they replace are compensated by cation vacancies. Typical donor dopants are La^{3+} and Sb^{3+} on A-site, and Nb^{5+} and Sb^{5+} on B-site. For each, La^{3+} or Nb^{5+} introduced into the lattice, one Pb vacancy occurs. The whole family of A-site vacancy compositions has increased dielectric constants, low mechanical quality factors, low coercive field and relatively square hysteresis fields, increased electrical volume resistivity and high piezoelectric coupling factor.

Acceptor Dopants: Dopant of lower charge than that of the replaced ions are compensated by oxygen vacancies. In this case either A or B site of the lattice is substituted with a lower valence element. Typical acceptor cations are Na^+ on A-site, and Mn^{2+} , Fe^{3+} , and Cr^{3+} on B-site. This type of substitution results in ceramics with lower dielectric constant and electrical resistivity, high Q_m , high coercive field; O-site vacancies inhibit domain wall motion effectively and high Q_m could be attained. [2, 9].

CHAPTER 3

GENERAL EXPERIMENTAL PROCEDURE

3.1 Method

Ceramic powders used in the experiments were prepared by processing the constituent oxides through a standard thermochemical treatment known as the mixed oxide route. Sample ceramics were produced by pressing the powders into thin discs and then by sintering them under specified heat treatment schedules. The constitution and microstructure of the ceramics were characterized by XRD and SEM analyses. The dielectric and piezoelectric properties were measured on the electroded and poled samples.

3.2 Preparation of Ceramic Powders

Powders of modified PZT ceramic compositions were prepared by the mixed oxide route. High purity powders of PbO, ZrO₂, TiO₂, SrCO₃, La₂O₃, MnCO₃, Nb₂O₅ and Sb₂O₃ were used in forming the desired compositions. The sources of these raw-materials were as follows: PbO (Merck 5658), ZrO₂ (SEPR CS10), TiO₂ (Merck 808), SrCO₃ (Merck 7861), La₂O₃ (Merck 11222), MnCO₃ (Strem Chem. 93-2533), Nb₂O₅ (Merck 6868), Sb₂O₃ (Merck 7835).

All of these powders had a certified purity in excess of 99 weight percent (wt%). In order to prepare modified PZT compositions, the powders were weighed in accordance with the molar ratios of unit formula and each powder batch was

blended thoroughly in an agate mortar with pestle in a medium of ethanol. The dried mixture was compacted as a slug in a hardened steel die and then calcined at 820 °C for 2 h. The product was ball milled for 4 h; it was dried and then given a second calcination at 850 °C for 2 h. The final slug was crushed and ball milled in a plastic vial for 16 h. All millings were done with stabilized zirconia balls in a medium of ethanol. The average particle size of the powder obtained by this process, determined with a Malvern Mastersizer 2000 laser particle size analyzer, was about 1µm. As shown in Figure 3.1, the powder was heated to 600 °C and kept there for 1 h to allow for the combustion of plastics introduced from the plastic bottle during milling.

3.3 Sintering of Ceramic Samples

Green ceramic discs, each measuring 15 mm in diameter and 1 mm in thickness, were prepared from the PZT based powders plasticized by 3 wt% PEG addition. The discs were compacted by uniaxial pressing in a hardened tool steel die under a load of 150 MPa. Before sintering, the organic additive in green discs was removed by heating them at 600 °C for 30 min.

Sintering experiments were conducted in a muffle furnace equipped with Honeywell UDC-2000 type temperature controller. The discs were sintered by soaking at 1240 °C for 2 h in a closed saggar assembly which contained PZT bedding to inhibit PbO evaporation from the ceramic samples. All heating and cooling rates were maintained as 4 °C /min in line with the suggestions made by Mohiddon and Yadav [19]. The appearance of ceramic samples manufactured for measurements is shown in Figure 3.2.

Powders of **PbO, ZrO₂, TiO₂** (and **SrCO₃, La₂O₃, MnCO₃, Nb₂O₅ and Sb₂O₃**)

Weighing and mixing in mortar and pestle in alcohol



PELLET PRESSING (Uniaxial Pressing, 32 mm die)



CALCINATION #1 (in closed alumina crucible, 820 °C, 2 h)



GRINDING #1 (with ZrO₂ balls, 4 h)



Plastic Removal (600 °C, 1 h)



PELLET PRESSING ((Uniaxial Pressing, 15 mm die)



CALCINATION #2 (in closed alumina crucible, 850 °C, 2 h)



GRINDING #2 (with ZrO₂ balls, 16 h)



Drying (Oven, 100 °C, Overnight)



Plastic Removal (600 °C, 1 h)



Modified PZT Powder

Figure 3.1 Production of PZT-based powder by the mixed oxide route.

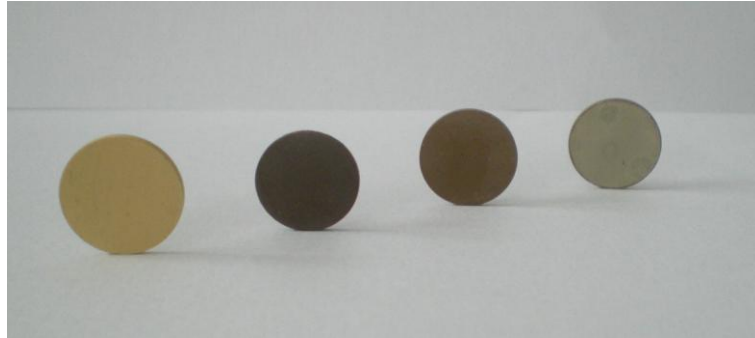


Figure 3.2 PZT-based ceramics prepared for measurements.

3.4 Ceramic Characterization

3.4.1 Phase Analysis and Microstructure

A PZT-based ceramic with a proper Zr/Ti ratio exhibits the rhombohedral and tetragonal phases. This is because the composition is in the morphotropic phase boundary (MPB) range (Figure 3.3). MPB is defined as the Zr/Ti ratio in PZT which causes a sudden structural change from tetragonal to rhombohedral symmetry and the location of which is almost independent of temperature [9]. The optimum piezoelectric properties of PZT ceramics can be obtained near the MPB. It is a result of 14 possible directions for polarization arising from 6 in tetragonal and 8 in rhombohedral structures. MPB depends on the changes in compositions like Zr/Ti ratio and amounts of dopants [1].

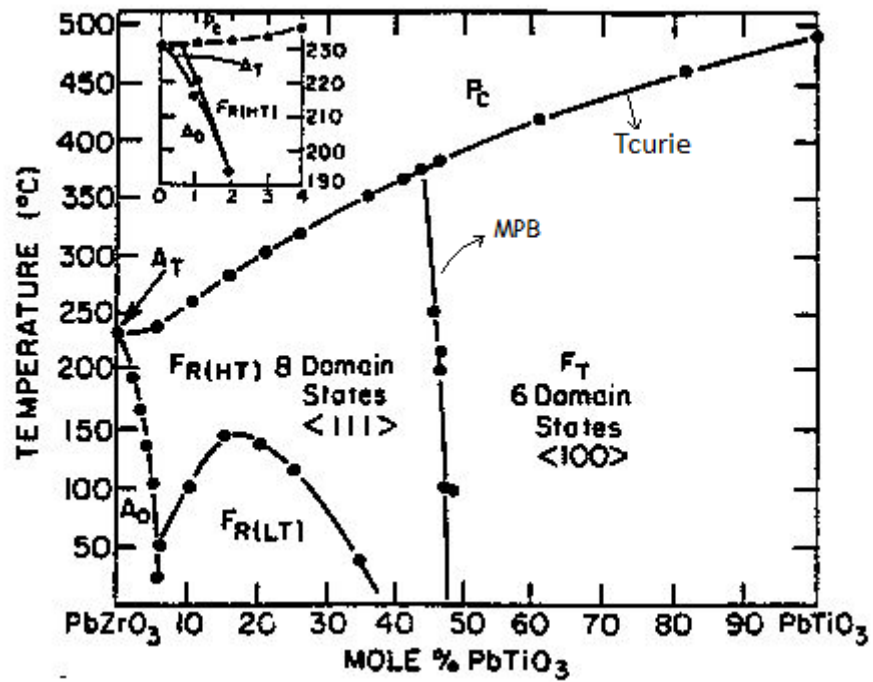


Figure 3.3 Phase diagram of PbZrO_3 - PbTiO_3 system [20].

The phases present in the PZT-based powder and sintered ceramics were determined by an X-ray diffractometer Rigaku D/max2200/PC using $\text{Cu-K}\alpha$ radiation. The x-ray diffraction study was operated under an accelerating voltage of 40 kV and a current of 40 mA. The diffraction data were collected over the 2θ ranging from 20° to 60° with a step size of 0.02° . Using these XRD patterns, lattice parameters and theoretical densities were calculated. These values along with the experimental density values are given in the Appendix B.

The microstructural studies were conducted mainly on polished sections under FEI Nova Nano 430 FEG and JEOL JSM 6400 scanning electron microscopes (SEM). The polished surfaces were given a thermal etch at 1000°C for 1 h in enclosures containing PZT bedding to compensate for PbO loss. Preceding the SEM work, the sample surfaces were sputtered with gold. The average grain size was calculated on

the SEM micrographs by the usual linear intercept method [21]. The extent of porosity in the ceramics was also ascertained from examination of their fracture surfaces under SEM.

3.4.2 Sintered Density

The density of sintered ceramics was measured by the liquid displacement technique based on Archimedes principle. At the start of the density measurement, the dry weight W_{dry} of the samples, lapped on an emery paper, were determined. Then they were immersed in xylene for 2 days to allow the penetration of liquid into possible pore channels. The weighing process was carried out while the samples were inside the liquid and taken outside the liquid; so the suspended weight (W_{sus}) and the saturated weight (W_{sat}) of each sample were determined. Sintered density, $\rho_{sintered}$, of a sample was calculated as follows:

$$\rho_s = \frac{W_{dry} \times \rho_{xylene}}{W_{sat} - W_{sus}} \quad (3-1)$$

where $\rho_{xylene} = 0.861 \text{ g/cm}^3$.

3.4.3 Measurement of Dielectric and Piezoelectric Parameters

Before the measurement of dielectric and piezoelectric parameters, ceramic discs with ~1 mm thickness were lapped on 1200 grit emery paper so that clean and smooth surfaces were obtained. Diameter and thickness were measured and the samples were electroded with silver paste. The surface was metalized by firing the paste at 700 °C and 30 min. Electroded ceramic discs were poled in silicon oil bath at 120 °C for 30 min under a maximum DC electric field of 3kV/mm. During the poling process, the electric field was increased gradually with 250 V increments, allowing 10 min at each voltage. The dielectric and piezoelectric properties of the

poled discs were evaluated according to the IRE standards [22]. The reliability of the data was checked by conducting measurements on duplicate samples, the experimental uncertainty was confined to $\pm 4\%$ of the reported values.

3.4.3.1 Measurement of the Dielectric Constant

The capacitances of the poled ceramics were measured in HP 4194A Impedance/Gain Phase Analyzer. During this measurement the frequency was maintained at 1 kHz. The capacitance values of the samples were used to calculate their dielectric constants from the following relationship:

$$K^T = \frac{C^T \times t}{\epsilon_o \times A} \quad (3-2)$$

where A is the cross-sectional area of the sample in m^2 , t is thickness in m and C^T is the material capacitance in Farads(F), ϵ_o is the dielectric permittivity of vacuum, 8.85×10^{-12} F/m. The dielectric constant calculated at 1 kHz is called the “free dielectric constant” and is designated by the symbol K^T .

3.4.3.2 Measurement of Piezoelectric Parameters

3.4.3.2.1 *Electromechanical Coupling Factor*

The electromechanical coupling coefficient of the poled ceramics was determined from the measurement of the resonant and anti-resonant frequencies of the analog circuit. The resonant, f_r and anti-resonant, f_a , frequencies were determined from the impedance spectra of the piezoelectric ceramics. The impedance spectrum for each poled ceramic disc was obtained in the form of an impedance-frequency plot by operating the HP 4149-A Impedance/Gain Phase Analyzer in the impedance mode. The frequencies of the peaks in the first harmonic are the fundamental resonant and anti-resonant frequencies of the ceramic element.

The planar coupling coefficient, k_p is related to the resonant frequency, f_r and anti-resonant frequency, f_a by the following relationship [14]:

$$k_p = \left[\frac{f_a - f_r}{0.395f_r + 0.574(f_a - f_r)} \right]^{1/2} \quad (3-3)$$

3.4.3.2.2 Mechanical Quality Factor

Mechanical quality factor, Q_m was calculated by using the values of the impedance spectrum parameters in Equation (3-4).

$$Q_m = \frac{f_a^2}{2\pi |Z_m| C f_r (f_a^2 - f_r^2)} \quad (3-4)$$

where f_a is the antiresonant frequency, f_r the resonant frequency, Z_m the resonant impedance and C the capacitance at 1 kHz which were measured using HP 4194-A Impedance/Gain Phase Analyzer [23].

3.4.3.2.3 Piezoelectric Strain Constant

The axial piezoelectric strain constant, d_{33} is the ratio of strain in the z -direction to the electric field applied in the same direction. Piezoelectric strain coefficient can be determined utilizing either one of the direct or the converse piezoelectric effects. In the former, a known stress is applied to the ceramic and the resulting electric charge is measured. The applied stress can be static or dynamic. In commercially available piezometers a cyclic stress is applied to the piezoelectric element and the charge generated is converted to piezoelectric strain constant. In this study a Berlincourt Piezo d_{33} Meter was used to measure the d_{33} -values. Prior to

measurements, the equipment was calibrated with several standard piezoelectric elements of known d_{33} values.

3.5 Particle Size

The particle size distribution of the starting powder synthesized by mixed-oxide technique was determined by laser scattering with a Mastersizer 2000 (Malvern Inst.) laser particle size analyzer at R&D Training and Measure Center at Central Laboratory, METU. Figure 3.4 shows the particle size distribution of the $0.97[\text{Pb}_{0.94}\text{Sr}_{0.05}\text{La}_{0.01}(\text{Zr}_{0.53}\text{Ti}_{0.47})_{0.9975}\text{O}_3]-0.024[\text{Pb}(\text{Mn}_{1/3}\text{Nb}_{2/3})\text{O}_3]-0.006[\text{Pb}(\text{Mn}_{1/3}\text{Sb}_{2/3})\text{O}_3]$ powder ball-milled for 20h. The particle size distribution was narrow and the $d(0.1)$, $d(0.5)$ and $d(0.9)$ values were $0.456\mu\text{m}$, $1.055\mu\text{m}$ and $2.755\mu\text{m}$, respectively. The peak in the distribution at $\sim 9\mu\text{m}$ is a result of agglomeration of particles although the precipitation of particles in suspension was tried to be hindered using an ultrasonic bath.

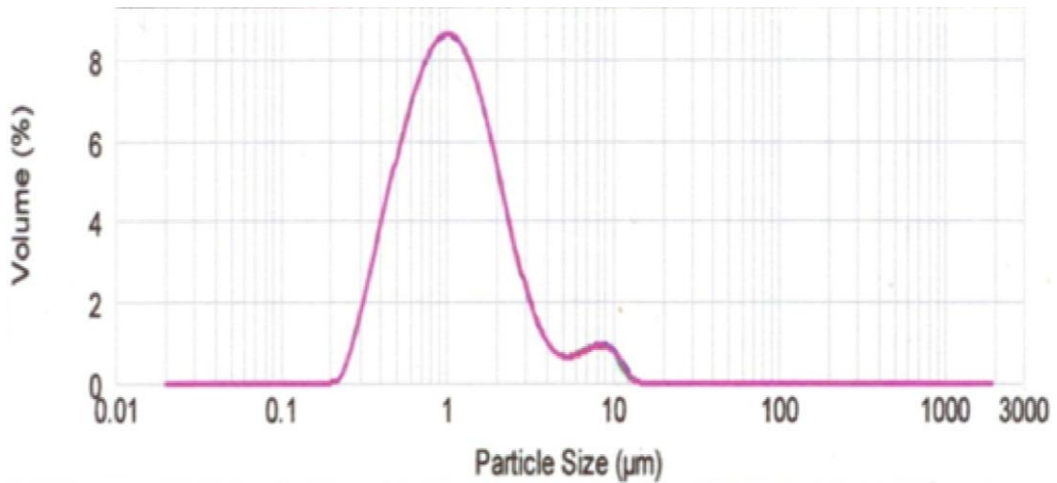


Figure 3.4 Fractional particle size distribution of ball-milled modified PZT powder.

3.6 Stoichiometry

Chemical elemental analysis of the sintered ceramics was carried out in order to determine the stoichiometry using inductively coupled plasma - optical emission spectrometry (ICP-OES) technique.

The ceramic samples in this study were prepared by means of solid-state reaction. This preparation method requires the use of high temperatures. Under these conditions, the calcined and sintered material can lose oxygen and/or lead [24]. Because the chemical stoichiometry strongly influences the dielectric and piezoelectric properties of these materials, the chemical composition has to be controlled.

In order to carry out stoichiometry and element distribution determination, inductively coupled plasma - optical emission spectrometry (ICP-OES, Perkin Elmer Optima 4300DV) technique was used at R&D Training and Measure Center at Central Laboratory, METU. The sintered ceramic samples $0.97[\text{Pb}_{0.94}\text{Sr}_{0.05}\text{La}_{0.01}(\text{Zr}_{0.53}\text{Ti}_{0.47})_{0.9975}\text{O}_3]-0.024[\text{Pb}(\text{Mn}_{1/3}\text{Nb}_{2/3})\text{O}_3]-0.006[\text{Pb}(\text{Mn}_{1/3}\text{Sb}_{2/3})\text{O}_3]$ were pulverized and digested by microwave-assistance in a 5 ml HCl+0.5 ml HF acid solution for 100 mg of sample [25]. Two specimens were prepared and parallel measurements were carried out for each element analyzed.

The results are listed in Table 3.1. In contrast to the claim made in literature [25], Pb could not be taken up totally by the acid solution, therefore this element was left outside the scope of analysis. The weight percentages of elements determined by analyses were in good agreement with the expected values considering the $\pm 2\%$ error tolerance in ICP-OES technique.

Table 3.1 ICP-OES analysis of modified PZT samples sintered at 1240 °C for 2h.

Element	Expected (wt%)	ICP Results	
		Sample-1 (wt%)	Sample-2 (wt%)
Zr	14.678	14.19±0.08	14.09±0.10
Ti	6.8299	6.44±0.04	6.41±0.04
Sr	1.3704	1.36±0.03	1.34±0.01
Nb	0.4842	0.47±0.005	0.482±0.005
La	0.4345	0.418±0.003	0.422±0.001
Sb	0.1543	0.157±0.004	0.1603±0.011
Mn	0.1081	0.1001±0.0001	0.1018±0.0006
O	15.015	15.002±0.09	15.011±0.10

3.7 Curie Temperature (T_c)

Ferroelectric crystals in a piezoceramic have polar axes and exhibit a spontaneous polarization below a specific temperature called the Curie temperature. The non-polar phase above this temperature is known as the paraelectric phase (P_c) which is shown in Figure 3.3. The line indicating the transition between the P_c phase and tetragonal (F_T) or rhombohedral (F_R) phases shows the Curie temperature of the compositions between $PbZrO_3$ and $PbTiO_3$. The spontaneous polarization reaches to a maximum at temperatures well below the Curie temperature and decreases to zero as the Curie temperature is approached [6].

Piezoelectrics utilized in high-power applications are operated close to their resonant frequencies which in turn causes heating of the ceramic element due to

internal frictions during vibration. If the temperature throughout the ceramic element increases close to Curie temperature then the piezoelectric and dielectric properties will be deteriorated. Therefore, a high Curie temperature is desirable for this kind of piezoelectric materials.

The dielectric permittivity of the material exhibits a peak value at the Curie temperature. In order to determine the Curie temperature of ceramics produced in this study, the dielectric response was measured at the frequency of 1 kHz using HP4194A Impedance Analyzer in the temperature range from 50 °C to 400 °C. The measurements were done by placing the samples in a small pot furnace in which the data on permittivity were taken upon cooling the ceramics from high temperature at a rate of 3 °C/min. Capacitance were converted to dielectric constant using the sample geometry and permittivity of air. The free dielectric constant K^T was determined using the Equation (3-2).

3.8 Hysteresis Loops

Ferroelectric materials exhibit polar axes which provide spontaneous polarization in the as-produced material and the orientation of this polarization can be reversed by an external field. Hysteresis loop, which is a plot of polarization versus electric field, is among the important properties of a ferroelectric ceramic. It describes the dynamic nonlinear polarization-switching behavior as a function of field.

General insight into the ferroelectric behavior of the ceramics could be gained from measurement of the major hysteresis loop at room temperature. Figure 3.5 illustrates a typical hysteresis loop. The application of an electric field to a virgin ferroelectric electroded disc produces very little effect at first. But dipoles in the ferroelectric crystallites are switched as the field becomes sufficiently high. Further increase in the applied field causes the polarization to change slightly and to approach saturation. If the electric field is reduced to zero, The material posses a net permanent polarization known as remnant polarization, P_r . As the applied field

is reversed, polarization is first reached to zero and then changes sign as the field produces saturation polarization in the opposite direction. As a result, the hysteresis loop is obtained. The field at which the polarization equals to zero is called the coercive field, E_c . The area of the loop indicates the energy which is dissipated as heat within the sample. Such a hysteresis loop is a good evidence of ferroelectricity [3].

The charge field hysteresis of the samples was used to determine the remnant polarization and coercive field values. Remnant polarization is a true measure of the degree of ferroelectricity and the coercive field value shows the materials resistance to depoling.

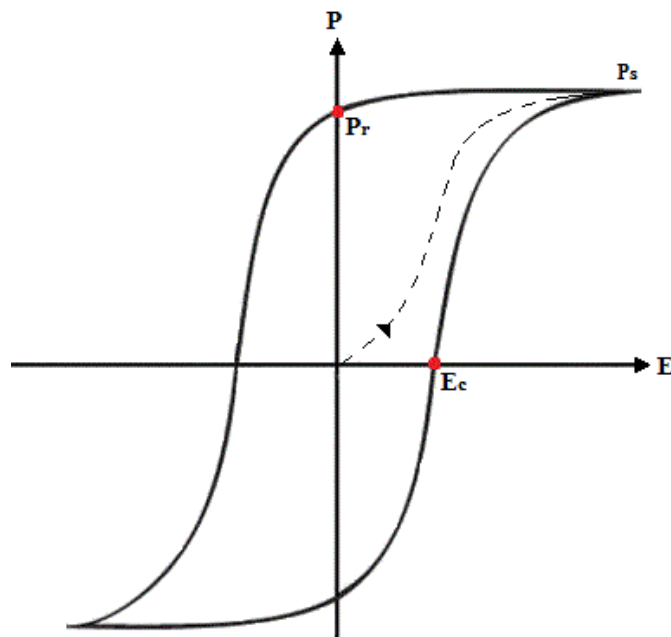


Figure 3.5 Hysteresis loop for a ferroelectric crystal.

The polarization (P) versus electric field (E) was measured using a modified Sawyer-Tower circuit at room temperature as shown in Figure 3.6 [26]. The hysteresis loop was displayed by an oscilloscope in which the voltage across the resistance R_2 is measured at X axis. On the other hand, at Y axis the voltage induced across the capacitor C_y is measured. The magnitude on the X axis is proportional to the field on the sample. Electric field was obtained by dividing the values on X axis to the sample thickness. Since the charge accumulated on the material is equal to the product of capacitance and the induced voltage, the charge accumulated across the sample could be obtained by using the measured voltage if the capacitance of the capacitor C_y was known. Once the charge accumulated was known, then the polarization could be calculated by dividing the charge to the surface area of the sample. The small resistance in R_2 makes sure the voltage across the oscilloscope is small and detectable.

The samples denoted by C_s were submerged into silicon oil to obtain a uniform temperature and to prevent arcing. The AC power was supplied using a high voltage amplifier. The remnant polarization (P_r) and the coercive field (E_c) values were evaluated by measuring the electrical polarization values at zero electric field and electric field values at zero polarization, respectively.

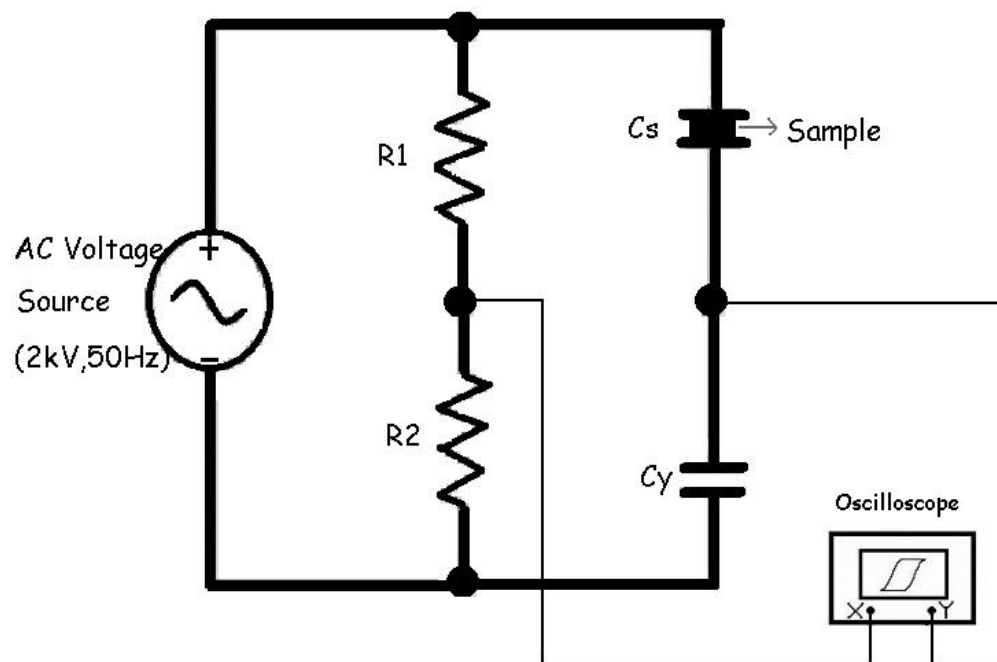


Figure 3.6 Modified Sawyer-Tower circuit.

CHAPTER 4

PSZT-PSLZT CERAMICS

4.1 Introduction

Piezoelectric ceramics based on lead-zirconate-titanate (PZT) are widely used for numerous applications in the microelectronics industry. In order to tailor the physical properties required in specific applications, PZT ceramics are usually doped with small amounts of other oxides. The compositions neighboring the morphotropic phase boundary (MPB) exhibit enhanced piezoelectric activity; therefore the Zr/Ti ratio in the ceramic has also been given an important consideration in the production of PZT ceramics. The effects of Zr/Ti ratio and those of different additives on the structural and electrical properties of PZT ceramics were investigated extensively in various earlier studies [2, 27-35].

Present study is concerned with the dual incorporation of Sr and La into PZT ceramics. Sr is an isovalent additive substituting Pb on the A site in the perovskite structure. Kulcsar [36] was the first to note that PZT ceramics produced with Sr additions exhibited improved dielectric permittivity, ϵ , and larger piezoelectric strain constant, d_{31} , with slight increase in the planar coupling factor, k_p . These effects were attributed to the straining of the PZT lattice due to the smaller size of Sr as compared to that of the parent Pb [2].

Following the findings of Kulcsar [36], Sr has entered into the formulation of a large number of PZT ceramics, including both the soft and the hard types [37-40].

The ceramic with composition $\text{Pb}_{0.95}\text{Sr}_{0.05}\text{Zr}_{0.53}\text{Ti}_{0.47}\text{O}_3$ or $\text{Pb}_{0.94}\text{Sr}_{0.06}\text{Zr}_{0.53}\text{Ti}_{0.47}\text{O}_3$ has been denoted as the basis for the commercial PZT4 [39, 40]. Lal et al. [41] verified that the improvement in the electromechanical properties of this MPB type PSZT ceramic was linked with the distortions in the lattices of the coexisting tetragonal and rhombohedral phases. Bedoya et al. [42] showed that PSZT ceramics with 6 atomic percent (at%) Sr exhibited favorable depoling characteristics, typical of a hard PZT. Such ceramics are favored generally in high power applications which require low dielectric loss, $\tan \delta$, and high mechanical quality factor, Q_m [43].

The size of the La^{3+} ion (0.136nm) is compatible with that of Pb^{2+} (0.149nm) [44]. Therefore, La^{3+} can replace Pb^{2+} in the perovskite lattice resulting in excess charge which is compensated by vacancies distributed mainly over the A-site cationic positions of PZT [45-47]. The PLZT ceramics with compositions rich in Zr display high photostrictive effect which makes these materials interesting for electrooptic applications. The notable composition developed for this purpose was a hot-pressed transparent PLZT denoted as 9/65/35, the ratio standing for the atomic percentages of La/Zr/Ti [48]. In a more recent publication, Galassi et al. [49] reported that electrostrictive, piezoelectric and ferroelectric properties of the 9/65/35 type PLZT ceramics were highly sensitive to the practices adapted during calcination and sintering stages.

PLZT ceramics with Zr/Ti ratio closer to the MPB region of the PZT system have been the subject of intensive dielectric and piezoelectric investigations. In the ceramic $\text{Pb}(\text{Zr}_{0.54}\text{Ti}_{0.46})\text{O}_3$ large improvements were obtained in dielectric permittivity and piezoelectric strain coefficient by 1 or 2 wt% addition of La_2O_3 [50]. Tawfik [51] showed that 0.1 or 0.2 mole percent (mole%) La_2O_3 addition to the same PZT ceramic resulted in increased compliance and lower resonant frequencies of transducers due, probably, to the freedom attained by the domain walls with smaller ionic size of La^{3+} . Hammer and Hoffman [52] observed that in the PLZT the MPB has shifted to higher Zr/Ti ratio implying that the tetragonal phase attained greater stability, which was argued as the cause of higher dielectric

permittivity. The method of powder preparation has profound influence on the properties of PZT ceramics. Until now, the highest piezoelectric strain constant reported in the literature for a MPB type pure PLZT ceramic was achieved in the composition $\text{Pb}_{0.97}\text{La}_{0.03}(\text{Zr}_{0.53}\text{Ti}_{0.47})\text{O}_3$; the value attained was $d_{33}=455$ pC/N and the powders of this ceramic was produced by a mechanochemical technique [53].

The electromechanical properties of PZT ceramics may be improved significantly with proper combination of multiple dopants. Kulcsar [50] observed that dielectric permittivity and the radial piezoelectric strain coefficient were enhanced upon incremental additions of La_2O_3 into the base ceramic $\text{Pb}_{0.95}\text{Sr}_{0.05}(\text{Zr}_{0.54}\text{Ti}_{0.46})\text{O}_3$. However, the results were rather inconsistent and the synergy emanating from dual doping was not clear. Mehta et al. [54] examined the structural changes in $\text{Pb}_{0.94}\text{Sr}_x\text{La}_y(\text{Zr}_{0.52}\text{Ti}_{0.48})\text{O}_3$ in terms of the variation in the tetragonality index as a function of co-doping. No data was provided on electromechanical properties. Ramam and Lopez [55] investigated the effect of Sr additions on the dielectric and piezoelectric properties of PLZTN ceramics containing 1.2 at% La and 0.75 at% Nb. Although the roles of dopant couples (Sr, La) and (Sr, Nb) could not be resolved, the results showed that small substitutions of Sr (≤ 1.5 at%) caused large enhancements in ϵ and d_{33} . Despite the data provided recently by Ramam and Chandramouli [56] on the effects of limited substitutions of Sr into a PZT which contained La and Mn as co-dopants, the information on electromechanical properties of such ceramics remained rather scarce. Therefore, the focus of the present study was to examine in detail the effects of (Sr, La) co-doping on the dielectric and piezoelectric properties of PZT ceramics and the changes in the associated microstructures.

4.2 Compositions Studied

PZT based piezoelectric ceramics obtained by doping with various levels of Sr^{2+} and La^{3+} , and designated as PSZT or PSLZT, were prepared by the mixed-oxide method. High purity powders of PbO , SrCO_3 , La_2O_3 , TiO_2 (Merck) and ZrO_2 (SEPR-CS10) were used to prepare the desired compositions. The oxide

constituents were weighed in accordance with the molecular formula $\text{Pb}_{1-x-y}\text{Sr}_x\text{La}_y(\text{Zr}_z\text{Ti}_{1-z})_{1-(y/4)}\text{O}_3$ ($x=0.0$ to 0.05 , $y=0.0$ to 0.05 , and $z=0.5$ to 0.6). This formulation was preferred due to the enhanced sinterability stemming from the slight excess of PbO over the A-site formula despite the fact that the charge neutrality condition is met by forming vacancies on both the A and B sites of the perovskite lattice [46, 47].

The effects of Sr^{2+} and La^{3+} additions, and that of the Zr/Ti ratio on microstructure, on phase constitution, and on the dielectric and piezoelectric properties were investigated. Structural and electrical characterization studies were performed according to the procedures given in Section 3.4.

4.3 Results and Discussion

4.3.1 PSZT Ceramics

The PSZT ceramics were based on PZT having 5 at% Sr. The ceramics were produced with Zr/Ti ratio ranging between 50/50 to 60/40. The data related to various physical properties are summarized in Table 4.1. The porosity in the PSZT ceramics was rather small; the values of %TD which is an indicator of the degree of densification achieved in the sintering process were in excess of 96% of the theoretical.

The average grain size in the PSZT ceramics, evaluated from micrographs similar to those shown in Figure 4.1, revealed that the change in the Zr/Ti ratio had little effect on the size of the polycrystals; the average grain size in all PSZT ceramics was about $4.4 \mu\text{m}$. A PZT ceramic with composition $\text{Pb}(\text{Zr}_{0.53}\text{Ti}_{0.47})\text{O}_3$ was produced under the same sintering conditions of the PSZT group samples. The SEM micrograph of this ceramic is presented in Figure 4.1 for comparison. The average grain size in the ceramic without Sr was $2.5 \mu\text{m}$, indicating the fact that Sr had a significant role in the grain growth during firing.

Table 4.1 Physical and electrical properties of $\text{Pb}_{0.95}\text{Sr}_{0.05}(\text{Zr}_z\text{Ti}_{1-z})\text{O}_3$ ceramics.

z	0.50	0.52	0.54	0.56	0.58	0.60
d_{33} (pC/N)	250	305	305	259	207	192
k_p	0.36	0.48	0.44	0.41	0.33	0.36
Q_m	750	440	345	325	316	310
K^T	1118	1350	1138	640	573	596
$\tan \delta$ (%)	0.49	0.42	0.44	0.99	1.19	1.20
Density (%TD)	96.87 (± 0.07)	96.50 (± 0.04)	96.94 (± 0.07)	97.12 (± 0.09)	96.87 (± 0.06)	96.62 (± 0.10)
Average Grain Size (μm)	4.45 (± 0.03)	4.45 (± 0.03)	4.51 (± 0.04)	4.42 (± 0.03)	4.40 (± 0.02)	4.43 (± 0.04)
Open/Closed Porosity (vol%)	0.73/ 2.40	0.81/ 2.69	0.62/ 2.44	0.60/ 2.28	0.75/ 2.38	0.77/ 2.61

Figure 4.2 shows the XRD patterns of PSZT ceramics with different Zr/Ti ratio. All of the samples had pure perovskite structure. The variations in the morphology of the peaks in the XRD patterns shown in Figure 4.2 indicated that, for the present study, the MPB in the PSZT ceramics covered a wide range of Zr/Ti ratios. The overlapping triplet peaks from the (200)T, (200)R, and (002)T planes of the perovskite in the 2θ range 43° to 46° were deconvoluted using the Lorentzian profile function by a computer program, Peakfit v4.0, and the relative volume fractions of rhombohedral and tetragonal phases, %R and %T, were estimated from the intensities $I_{(200)R}$, $I_{(200)T}$, and $I_{(002)T}$ through the following relationships [52]:

$$\%R = \frac{I_{(200)R}}{I_{(200)T} + I_{(200)R} + I_{(002)T}}, \quad \%T = 100 - \%R \quad (4-1)$$

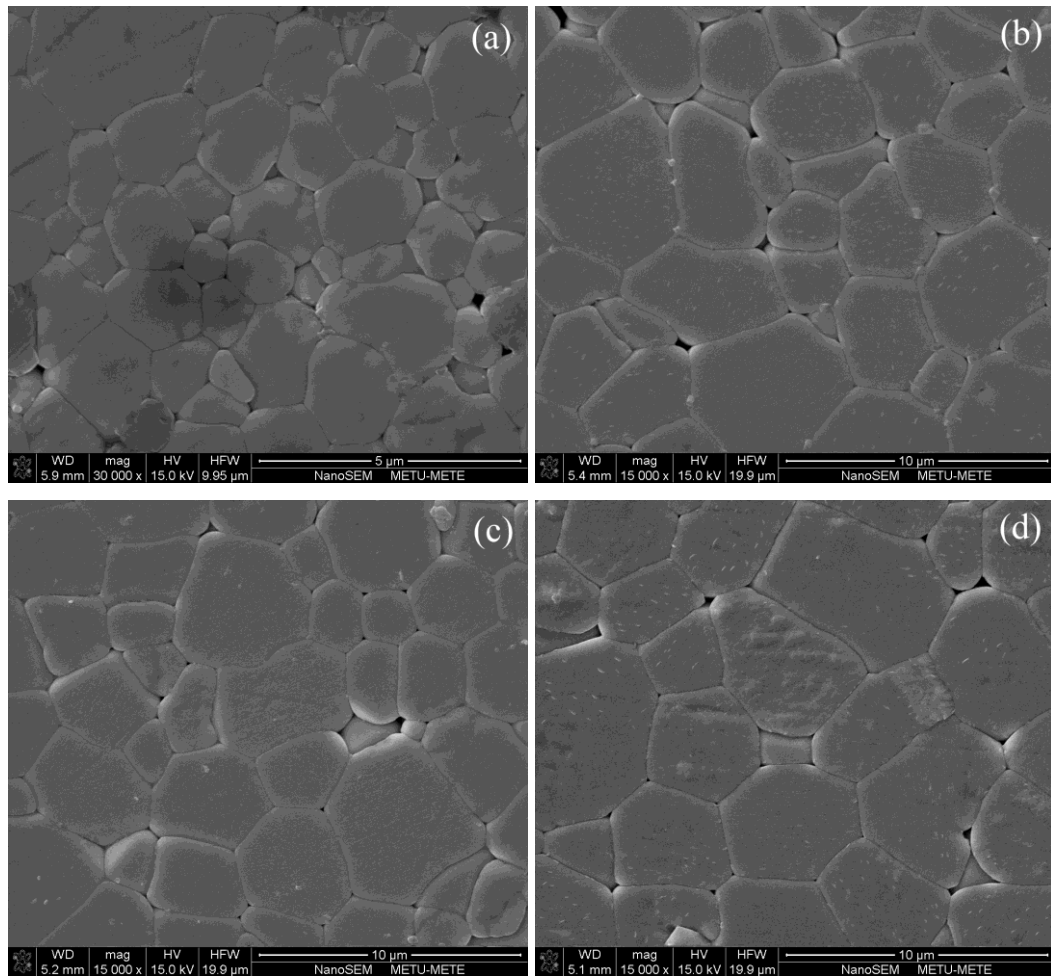


Figure 4.1 SEM micrographs of $\text{Pb}_{0.95}\text{Sr}_{0.05}(\text{Zr}_z\text{Ti}_{1-z})\text{O}_3$ ceramics having variable Zr/Ti ratio: (a) PZT without Sr, (b) $z=0.52$, (c), $z=0.56$, and (d) $z=0.60$.

The calculations on the relative proportions of the T and R phases in PSZT ceramics in the composition range $\text{Zr}/\text{Ti} = 50/50$ to $\text{Zr}/\text{Ti} = 60/40$ resulted in the quantitative distribution shown in Figure 4.3. T and R modifications coexisted in the composition interval extending from $\text{Zr}/\text{Ti}=52/48$ to $\text{Zr}/\text{Ti}=58/42$. In earlier studies on undoped PZT ceramics the T+R field was located from $\text{Zr}/\text{Ti}=48/52$ up to $\text{Zr}/\text{Ti}=55/45$ [57, 58]. The differences in the location and the width of the MPB

were related to the compositional fluctuations arising from powder preparation practices which may lead to micro-heterogeneity in the distribution of cations in the perovskite lattice [58, 59]. The proportion of the T phase in the ceramic $\text{Pb}_{0.94}\text{Sr}_{0.06}(\text{Zr}_{0.53}\text{Ti}_{0.47})\text{O}_3$ determined by Bedoya et al. [42] was 69 volume percent (vol%). The lower proportion of the T phase attained in their work should be attributed to the lower sintering temperature.

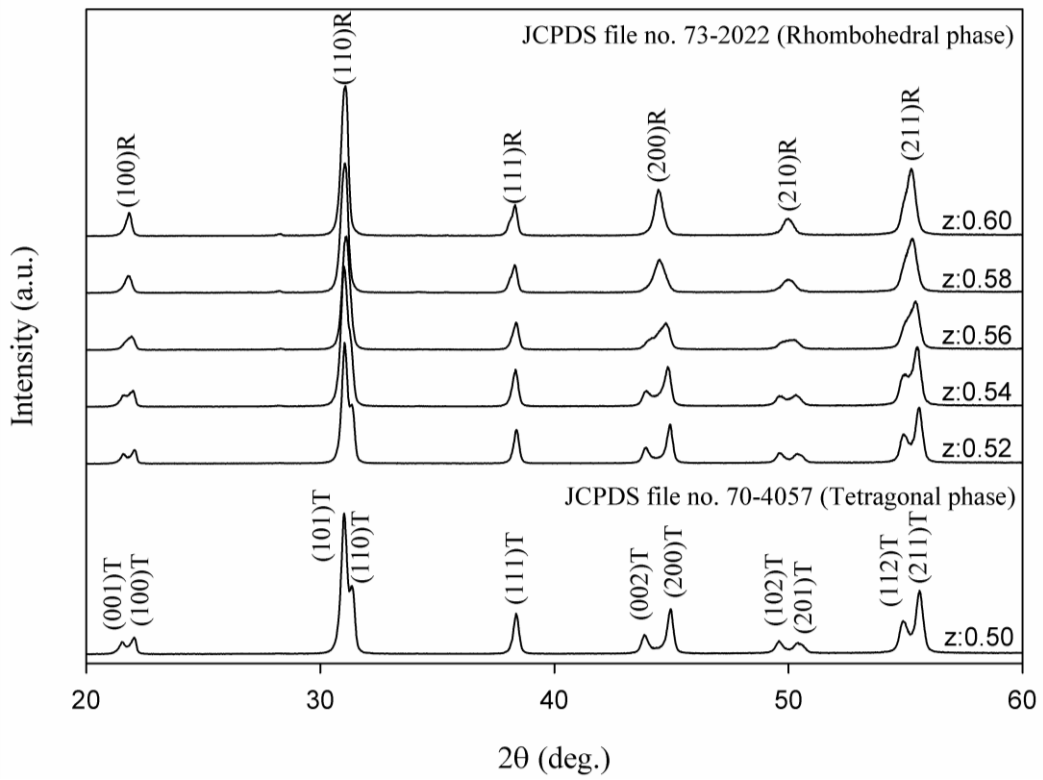


Figure 4.2 The XRD patterns of the $\text{Pb}_{0.95}\text{Sr}_{0.05}(\text{Zr}_z\text{Ti}_{1-z})\text{O}_3$ ceramics. The values of z in the figure indicate the Zr content in the PSZT.

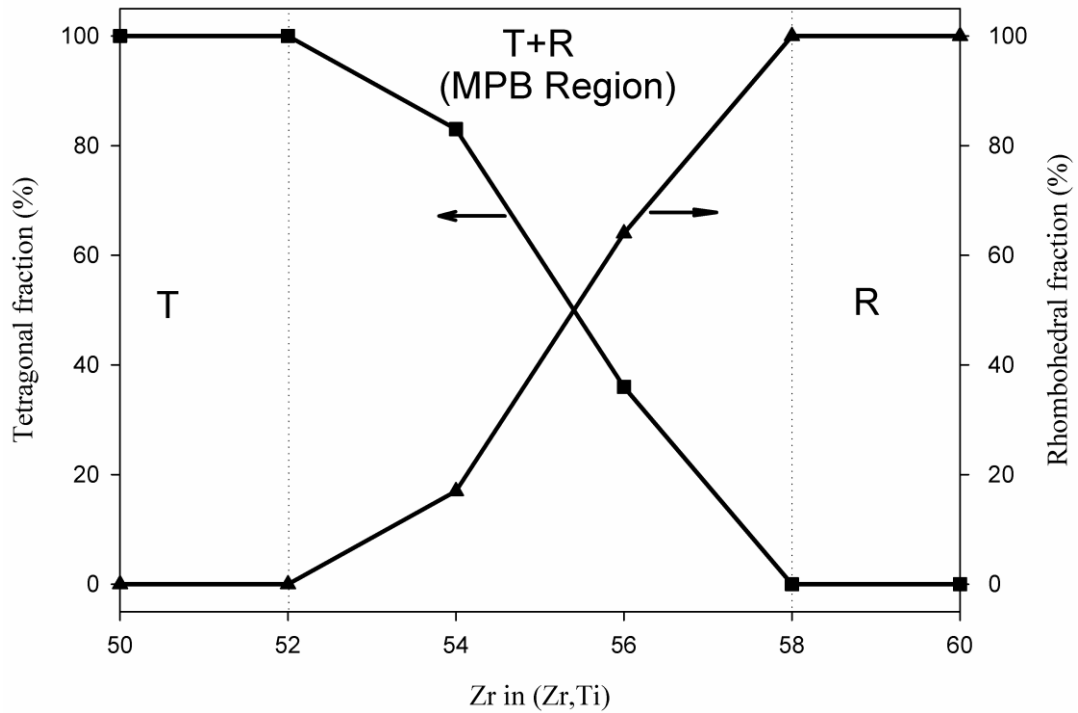


Figure 4.3 Relative proportions of tetragonal and rhombohedral modifications in the $\text{Pb}_{0.95}\text{Sr}_{0.05}(\text{Zr}_z\text{Ti}_{1-z})\text{O}_3$ ceramics.

In contrast to the situation observed on grain size, the piezoelectric and dielectric properties were highly sensitive to the Zr/Ti ratio. The piezoelectric strain coefficient d_{33} , the electromechanical coupling coefficient k_p , and the dielectric constant K^T , displayed in Figure 4.4, exhibited visible maxima in the interval of the Zr/Ti ratios corresponding to the MPB region of the PSZT system examined. The maxima in these parameters were due to the coexistence of the tetragonal (T) and the rhombohedral (R) phases which lead to high levels of electromechanical response. The enhanced piezoelectric activity within the transition MPB region has been attributed to the presence of a large number of energetically equivalent states allowing a high degree of alignment of ferroelectric dipoles and enhanced polarizability of the ceramic [2, 57, 60].

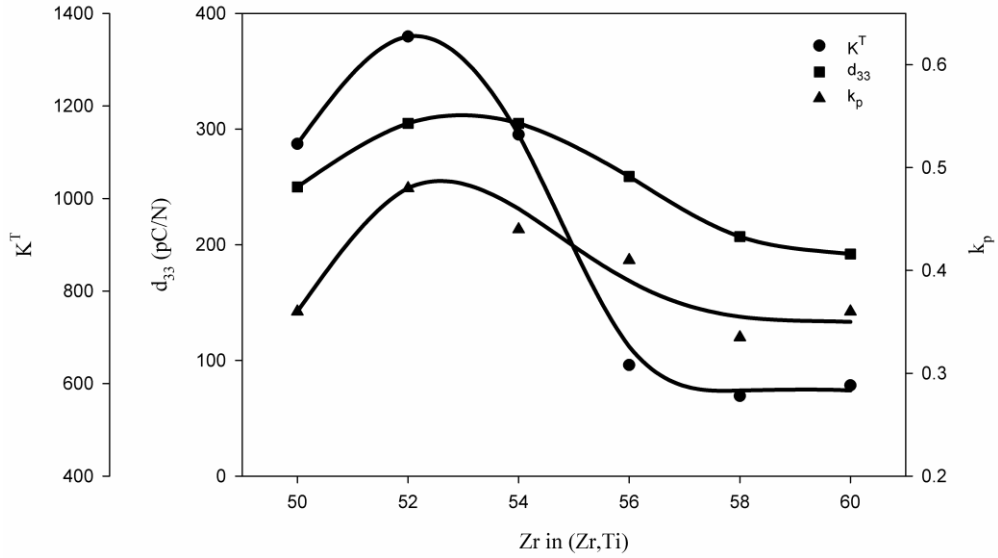


Figure 4.4 Variations in the dielectric and piezoelectric properties of $\text{Pb}_{0.95}\text{Sr}_{0.05}(\text{Zr}_z\text{Ti}_{1-z})\text{O}_3$ ceramics.

Lal et al. [41] made similar measurements on $\text{Pb}_{0.94}\text{Sr}_{0.06}(\text{Zr}_z\text{Ti}_{1-z})\text{O}_3$ ceramics. Their powders were produced by spray drying nitrate solutions of the constituents. As a result of ideal mixing on atomic scale, the properties K^T , d_{33} , and k_p exhibited sharp peaks at the MPB which was located at 53/47 ratio of Zr/Ti. Despite this difference, the results of the present study, in terms of peak values of these variables are in good agreement with those of Lal et al. [41]. Their values at MPB were $K^T = 1360$, $d_{33} = 305$, $k_p = 0.53$, and $\tan \delta = 0.34\%$.

The higher degree of tetragonal distortion at low Zr/Ti ratio within the MPB indicated that such ceramics would have higher internal stresses leading to the increase in the population of domains per unit volume. Thus the ceramics with high $(c/a)_T$ ratio would have harder polarization characteristics due to the more difficult

nature of domain orientation and hindered domain wall mobility. This is reflected in the variation of Q_m and $\tan \delta$ with respect to Zr/Ti ratio, depicted by the curves in Figure 4.5. In the Zr-poor side of the composition spectrum, the Q_m values were higher and $\tan \delta$ values were lower, typical of hard PZT ceramics. As the PSZT composition moved towards higher Zr, the Q_m was lowered and $\tan \delta$ was increased due to the enhanced mobility of the domain walls.

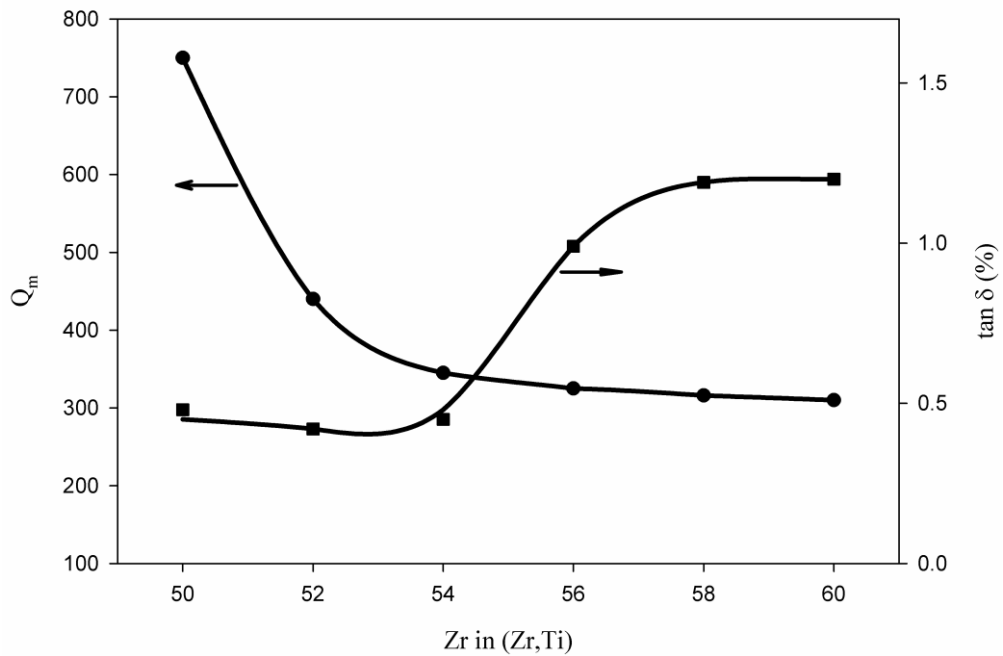


Figure 4.5 Variations in Q_m and $\tan \delta$ with Zr/Ti ratio in $\text{Pb}_{0.95}\text{Sr}_{0.05}(\text{Zr}_x\text{Ti}_{1-x})\text{O}_3$ ceramics.

4.3.2 PSLZT Ceramics

4.3.2.1 $\text{Pb}_{0.95-y}\text{Sr}_{0.05}\text{La}_y(\text{Zr}_{0.54}\text{Ti}_{0.46})\text{O}_3$ Ceramics

The ceramic $\text{Pb}_{0.95}\text{Sr}_{0.05}\text{Zr}_{0.54}\text{Ti}_{0.46}\text{O}_3$ which exhibited a high d_{33} was modified by partial substitution of La^{3+} ions for Pb^{2+} with increasing levels of La from 0.5 up to 5 at% replacement in the molecular formula of the PSLZT. The data on the piezoelectric and dielectric properties of these ceramics are given in Table 4.2.

Table 4.2 Physical and electrical properties of $\text{Pb}_{0.95-y}\text{Sr}_{0.05}\text{La}_y(\text{Zr}_{0.54}\text{Ti}_{0.46})\text{O}_3$ ceramics.

y	0.005	0.01	0.02	0.03	0.04	0.05
d_{33} (pC/N)	490	640	535	490	430	425
k_p	0.51	0.56	0.52	0.50	0.46	0.42
Q_m	92	70	78	76	76	71
K^T	1347	1800	1963	1944	1850	1460
$\tan \delta$ (%)	1.40	1.55	1.55	1.65	1.77	1.86
Density (%TD)	97.80 (± 0.06)	98.29 (± 0.07)	98.78 (± 0.06)	98.78 (± 0.08)	97.38 (± 0.06)	96.63 (± 0.04)
Average Grain Size (μm)	4.02 (± 0.03)	3.62 (± 0.04)	2.93 (± 0.04)	2.52 (± 0.03)	2.21 (± 0.03)	1.75 (± 0.02)
Open/Closed Porosity (vol%)	0.82/ 1.38	0.63/ 1.08	0.48/ 0.74	0.50/ 0.72	1.01/ 1.61	0.99/ 2.38

The densification behavior was rather complex; at low levels of La, up to 3 at%, the ceramics attained higher densities than the base PSZT, but the densification became increasingly poor above 3 at% La. At all levels of La, however, the amount of porosity was quite lower than that reported by Hammer and Hoffmann [52] probably due to the higher sintering temperature applied in the present work. The SEM micrographs shown in Figure 4.6 revealed that average grain size decreased continuously with increased La substitution, supporting the findings of the earlier studies in which the grain size decreased sharply towards 2 μm and even lower when the doping level in the PLZT ceramics exceeded 1 at% La [52, 61].

The reduction in the grain size with increasing La substitution in PLZT ceramics has been explained by the solid solution impurity drag mechanism in which the La ion concentration gradient present at grain boundaries was claimed to cause blocking of grain boundary mobility leading to substantially slower grain growth rate [62].

The XRD patterns of the $\text{Pb}_{0.95-y}\text{Sr}_{0.05}\text{La}_y(\text{Zr}_{0.54}\text{Ti}_{0.46})\text{O}_3$ ceramics are shown in Figure 4.7. At all levels of La addition, the perovskite PSLZT consisted of a mixture of T and R phases, with T being the dominant modification as seen in Figure 4.8. Obviously, in this group of PSLZT ceramics, La additions did not destroy the stability of the T phase. This observation is somehow different than the findings of Hammer and Hoffmann [52]. According to their XRD work on the PLZT solid solutions with Zr/Ti ratio of 53/47, the T phase content showed fluctuations with varying levels of La addition; at low La contents (<0.2 at%), the T phase proportion rose sharply to 83 vol%, verifying the results of the present study, then the proportion dropped to about 67 vol% up to 3 at% La, and then increased back to 83 vol% T when La content became 6 at% and higher. The greater stability obtained in the relative amount of the T phase in this work may be linked with the coexistence of Sr and La.

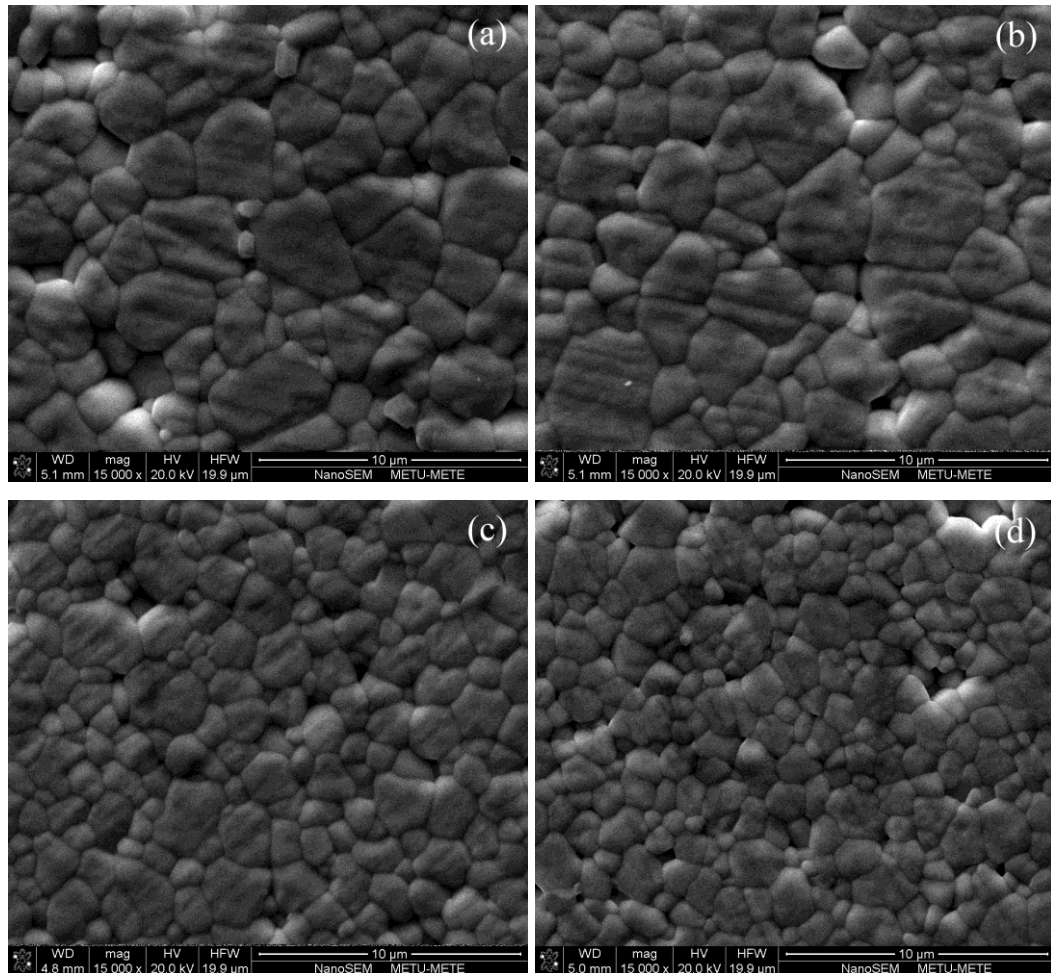


Figure 4.6 SEM micrographs of $\text{Pb}_{0.95-y}\text{Sr}_{0.05}\text{La}_y(\text{Zr}_{0.54}\text{Ti}_{0.46})\text{O}_3$ ceramics with increasing La content: (a) $y=0.01$, (b) $y=0.03$, (c) $y=0.04$, and (d) $y=0.05$.

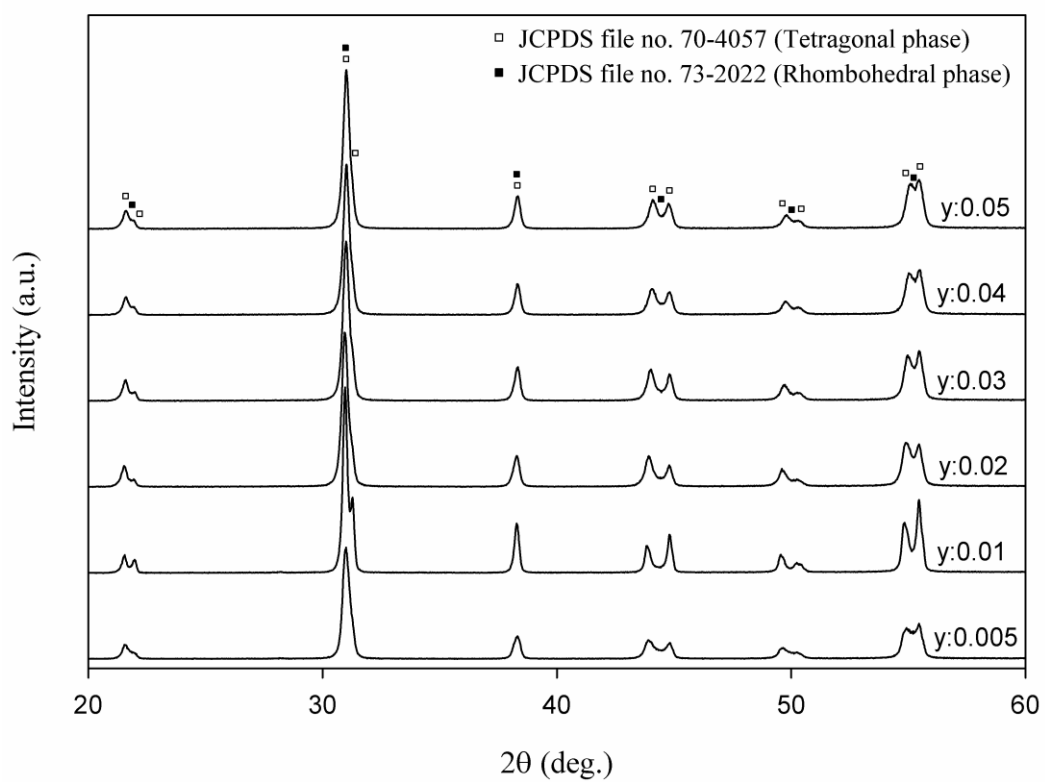


Figure 4.7 The XRD patterns of the $\text{Pb}_{0.95-y}\text{Sr}_{0.05}\text{La}_y(\text{Zr}_{0.54}\text{Ti}_{0.46})\text{O}_3$ ceramics. The values of y in the figure indicate the La content in the PSLZT.

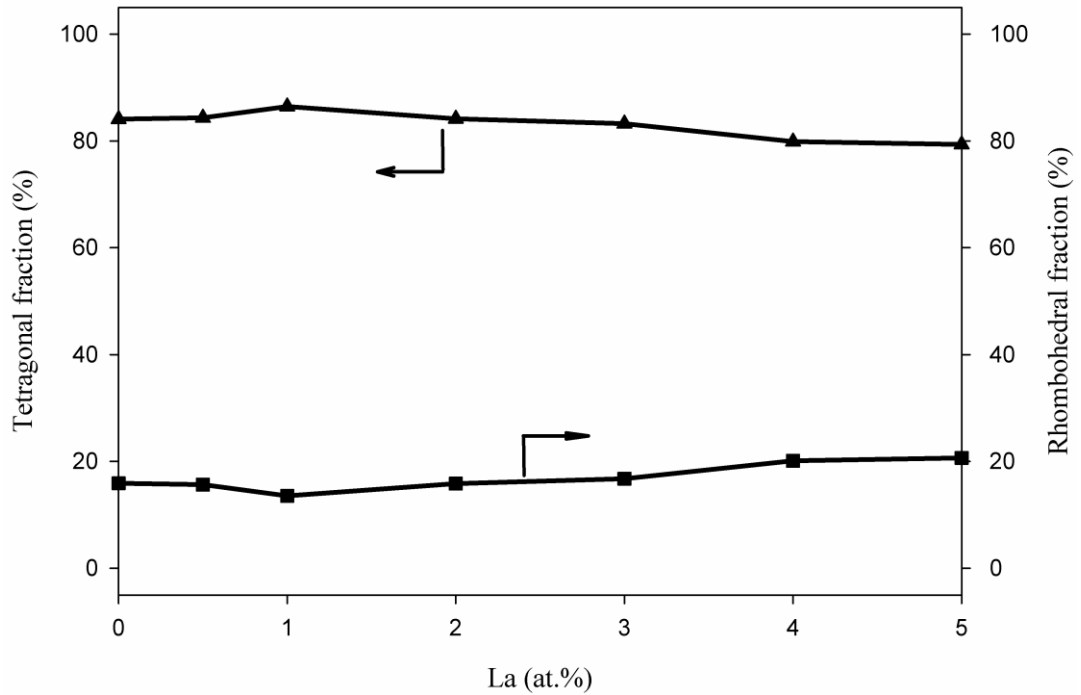


Figure 4.8 Relative proportions of tetragonal and rhombohedral modifications in the $\text{Pb}_{0.95-y}\text{Sr}_{0.05}\text{La}_y(\text{Zr}_{0.54}\text{Ti}_{0.46})\text{O}_3$ ceramics as a function of La doping.

The variations in the piezoelectric properties of $\text{Pb}_{0.95-y}\text{Sr}_{0.05}\text{La}_y(\text{Zr}_{0.54}\text{Ti}_{0.46})\text{O}_3$ ceramics with La content are shown in Figure 4.9. A small amount of La substitution in the base PSZT caused a large increase in the piezoelectric strain coefficient d_{33} which exhibited a peak value of 640 pC/N at 1 at% La. d_{33} of 640 pC/N is the highest level of d_{33} ever reported in PSLZT [55,56]. Additions of La beyond this limit moved the composition away from the MPB and resulted in reduced d_{33} values. The same trend was observed in k_p and K^T . The curve for K^T exhibited a rather diffuse pattern which may be attributed to the gradual reduction of coupling, caused by increased La substitution, between $(\text{Zr},\text{Ti})\text{O}_6$ octahedra and the A site occupants [63].

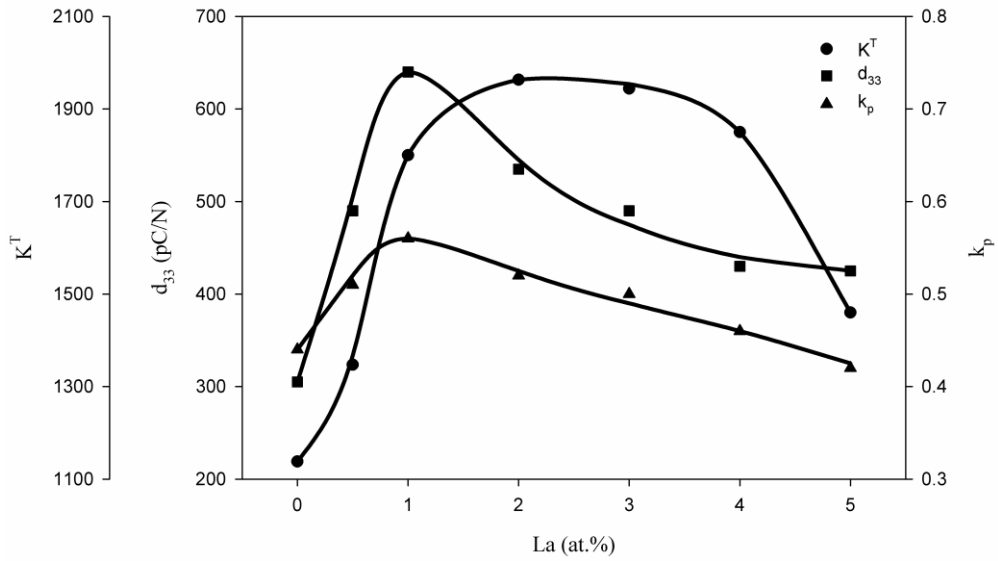


Figure 4.9 Variations in the dielectric and piezoelectric properties of $\text{Pb}_{0.95-y}\text{Sr}_{0.05}\text{La}_y(\text{Zr}_{0.54}\text{Ti}_{0.46})\text{O}_3$ ceramics with increasing La substitution.

The complex behavior observed for d_{33} , k_p , and K^T in Figure 4.9 was attributed to the competition between the vacancy effect and the grain growth inhibition brought by La, both being manifested in the movement of domain walls. In the PSLZT ceramics of interest, the T phase is dominant which means that the 180° domains and 90° domains belonging to this modification are of importance. During the poling process, virtually all 180° domains are oriented along the poling direction; therefore the 90° domains gain further significance. At low levels of La, the vacancies introduced by doping facilitate the rotation of 90° domains and promote the motion of the 90° domain walls leading to enhancement in electromechanical properties. On the other hand, additions of La cause reduction in the grain size which implies that the domain size is also reduced [61]. Furthermore, the sintered density starts declining at La levels above 3 at%. Under these conditions, the domains get clamped gradually by increasing La substitution due to the pinning

action of grain boundaries and the dominance of space charge effects [64]. Hence, reductions in the electromechanical properties are observed when La doping is increased beyond a certain value.

The addition of La made the PSZT ceramic a soft piezoelectric as seen in Figure 4.10. The material assumed lossy characteristics upon the smallest La substitution. The trends in Q_m and $\tan \delta$ were very much similar to those observed by Pdungsap et al. [65].

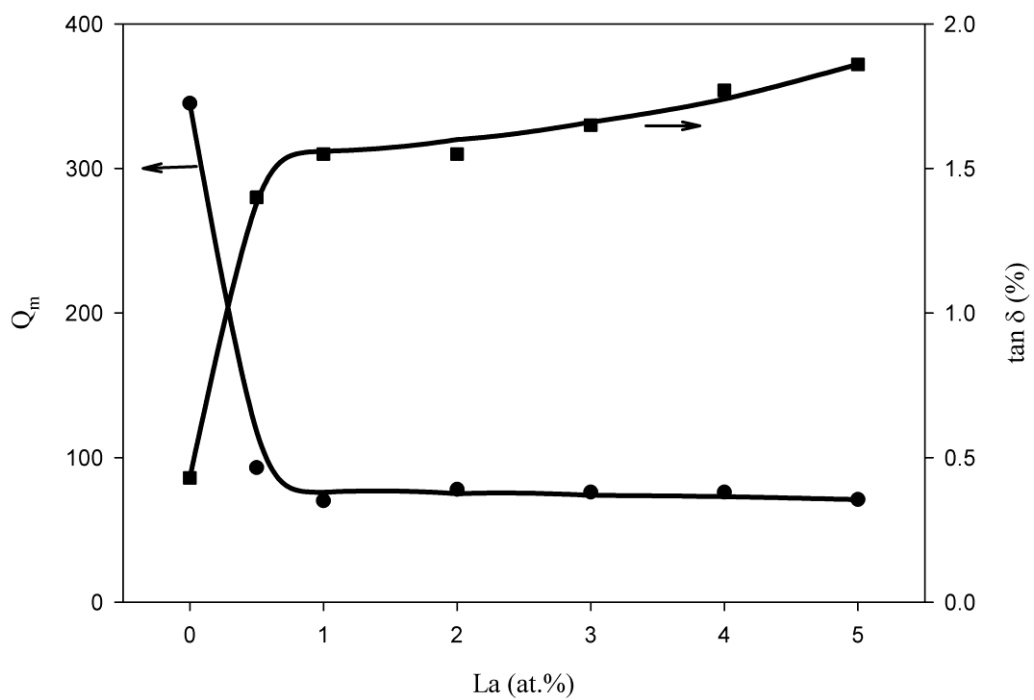


Figure 4.10 Variations in Q_m and $\tan \delta$ with La content in $Pb_{0.95-y}Sr_{0.05}La_y(Zr_{0.54}Ti_{0.46})O_3$ ceramics.

4.3.2.2 $\text{Pb}_{0.94}\text{Sr}_{0.05}\text{La}_{0.01}(\text{Zr}_{1-z}\text{Ti}_z)\text{O}_3$ Ceramics

The data on physical properties of PSLZT ceramics with 1 at% La and 5 at% Sr, but variable Zr content are given in Table 4.3. Based on comparison with x-ray densities, the ceramics densified to better than 97% of the theoretical. SEM micrographs from thermally etched surfaces revealed limited porosity. The average grain size was not affected much by the Zr/Ti ratio. However, the size distribution, as seen in the SEM micrographs of Figure 4.11, was rather wide; small grains filling the interstices among the larger ones may be the reason for better densification.

Table 4.3 Physical and electrical properties of $\text{Pb}_{0.94}\text{Sr}_{0.05}\text{La}_{0.01}(\text{Zr}_z\text{Ti}_{1-z})\text{O}_3$ ceramics.

z	0.50	0.52	0.54	0.56	0.58	0.60
d_{33} (pC/N)	393	480	640	560	427	380
k_p	0.39	0.42	0.56	0.53	0.42	0.40
Q_m	96	83	70	84	99	115
K^T	972	1475	1800	1138	608	487
$\tan \delta$ (%)	1.15	1.46	1.55	1.89	2.22	2.34
Density (%TD)	98.12 (±0.09)	97.98 (±0.06)	98.29 (±0.07)	98.36 (±0.05)	97.23 (±0.05)	97.48 (±0.07)
Average Grain Size (μm)	3.31 (±0.04)	3.44 (±0.02)	3.62 (±0.04)	3.64 (±0.03)	3.64 (±0.03)	3.70 (±0.04)
Open/Closed Porosity (vol%)	0.78/ 1.10	0.94/ 1.08	0.63/ 1.08	0.63/ 1.01	0.82/ 1.95	0.97/ 1.55

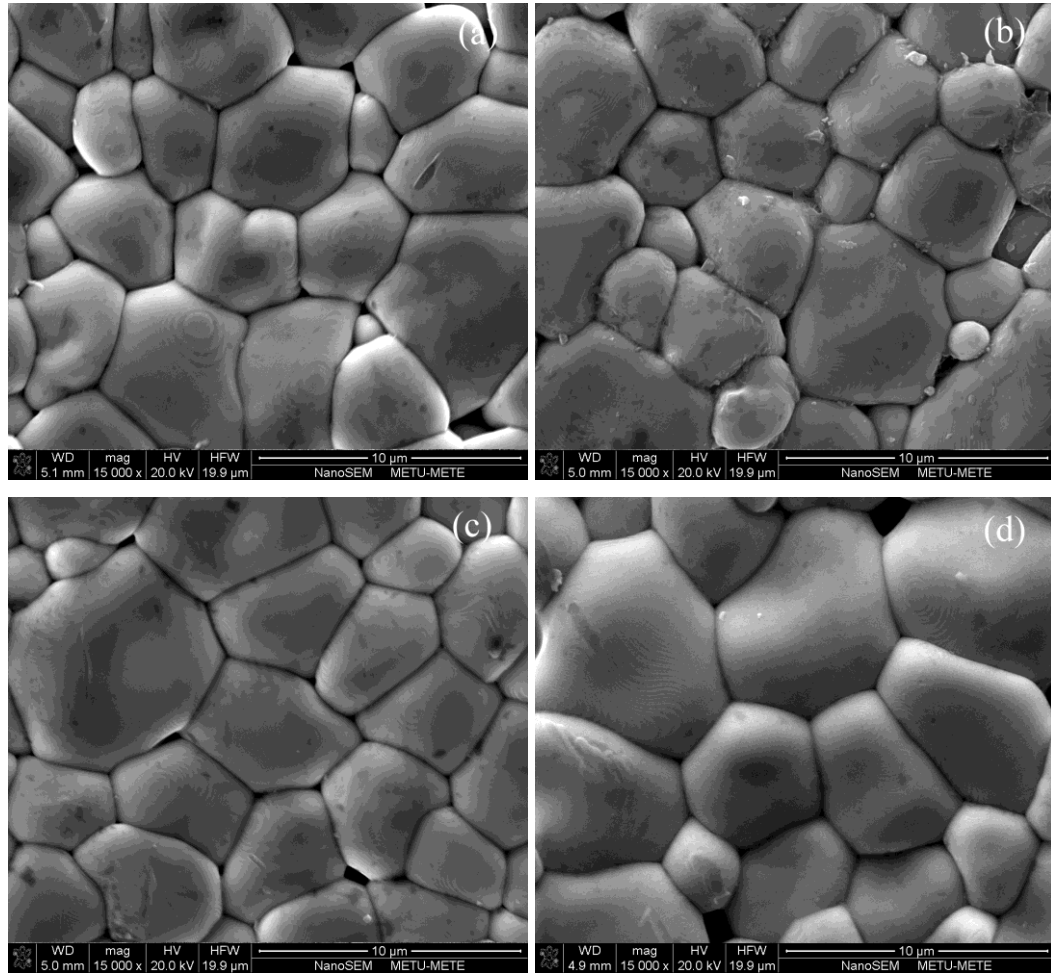


Figure 4.11 SEM micrographs of $\text{Pb}_{0.94}\text{Sr}_{0.05}\text{La}_{0.01}(\text{Zr}_z\text{Ti}_{1-z})\text{O}_3$ ceramics with Zr content of (a) $z=0.52$, (b) $z=0.54$, (c) $z=0.58$, (d) $z=0.60$.

Figure 4.12 shows XRD patterns of the $\text{Pb}_{0.94}\text{Sr}_{0.05}\text{La}_{0.01}(\text{Zr}_z\text{Ti}_{1-z})\text{O}_3$ ceramics. The patterns revealed the co-existence of T and R modifications. The proportions of T and R phases in the MPB are displayed in Figure 4.13. Compared to the distribution in the PSZT system observed in Figure 4.3, the width of the MPB, as well as its limits and the midpoint were not affected noticeably by presence of La.

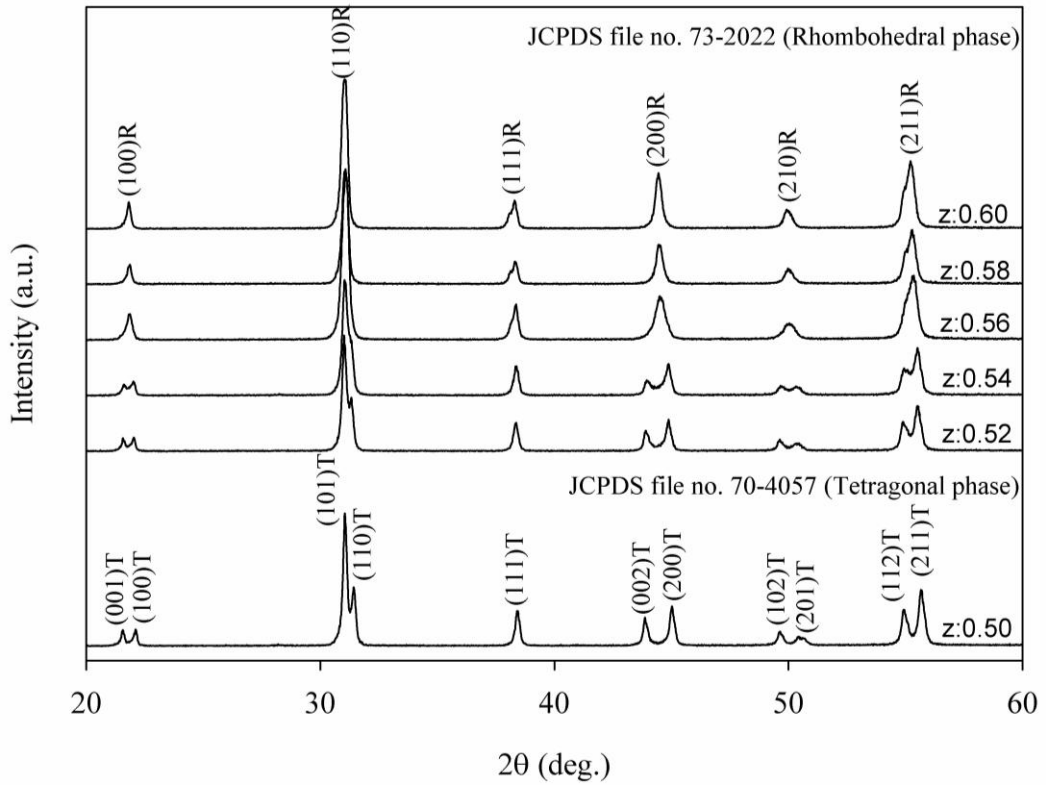


Figure 4.12 The XRD patterns of the $\text{Pb}_{0.94}\text{Sr}_{0.05}\text{La}_{0.01}(\text{Zr}_z\text{Ti}_{1-z})\text{O}_3$ ceramics. The values of z in the figure indicate the Zr content in the PSLZT.

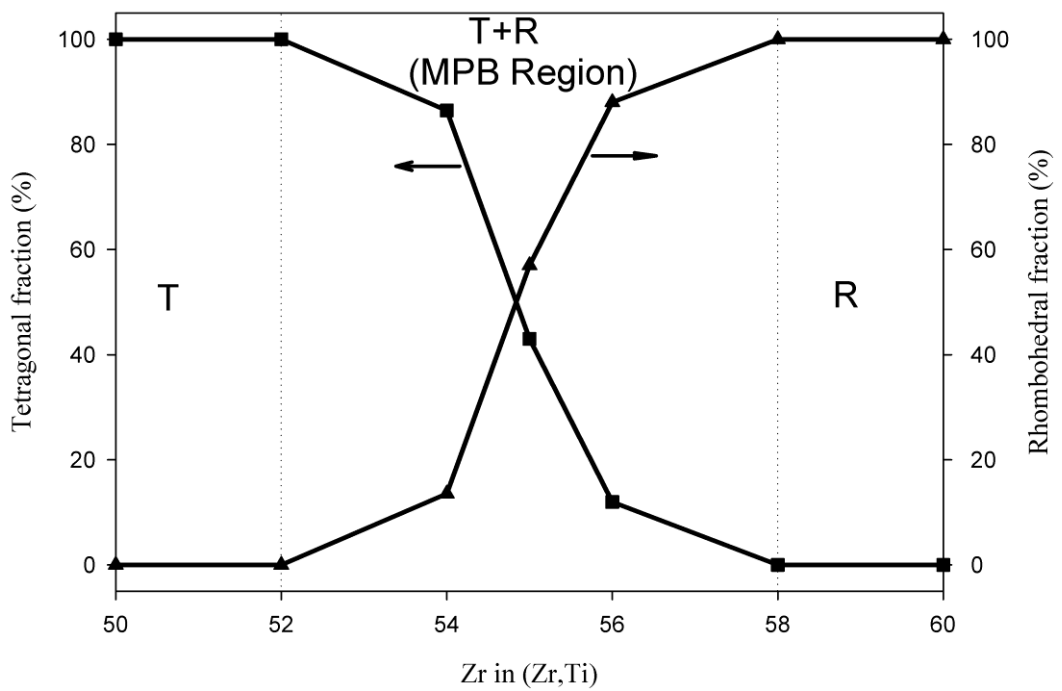


Figure 4.13 Relative proportions of tetragonal and rhombohedral modifications in the $\text{Pb}_{0.94}\text{Sr}_{0.05}\text{La}_{0.01}(\text{Zr}_z\text{Ti}_{1-z})\text{O}_3$ ceramics.

The dielectric and piezoelectric properties of the $\text{Pb}_{0.94}\text{Sr}_{0.05}\text{La}_{0.01}(\text{Zr}_z\text{Ti}_{1-z})\text{O}_3$ group ceramics, displayed in Figure 4.14, exhibited changes typical of MPB compositions. The curves for d_{33} and k_p had sharp peaks at Zr/Ti ratio of 54/46. The discussion offered in the Section 4.3.1 is also valid for the electromechanical properties displayed in Figure 4.14.

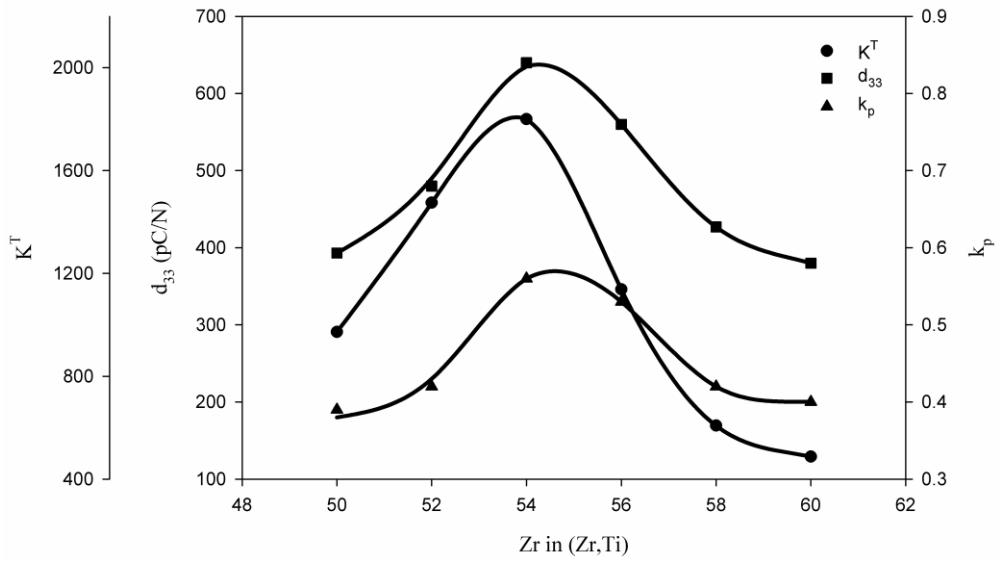


Figure 4.14 Variations in the dielectric and piezoelectric properties of $\text{Pb}_{0.94}\text{Sr}_{0.05}\text{La}_{0.01}(\text{Zr}_z\text{Ti}_{1-z})\text{O}_3$ ceramics.

Hysteresis behavior of the $\text{Pb}_{0.94}\text{Sr}_{0.05}\text{La}_{0.01}(\text{Zr}_z\text{Ti}_{1-z})\text{O}_3$ ceramics are displayed by the polarization curves as shown in Figure 4.15. The PSLZT ceramics could be polarized rather easily. In all samples the coercive field, E_c , was equal to or smaller than 1 kV/mm, comparable to the magnitude of E_c reported earlier for PLZT ceramics [61]. The ceramics with lower Zr/Ti ratio exhibited loops of ferroelectrically harder PZT ceramics owing to the dominance of the T phase [66]. As shown in Figure 4.16, the increase in the Zr/Ti ratio resulted in higher remanance and lower coercive field. The area occupied by the hysteresis loop, which is a measure of polarization energy, became increasingly smaller as the Zr content was increased. These features are correlated with the increased proportion of the rhombohedral phase in PZT compositions having relatively higher Zr [67].

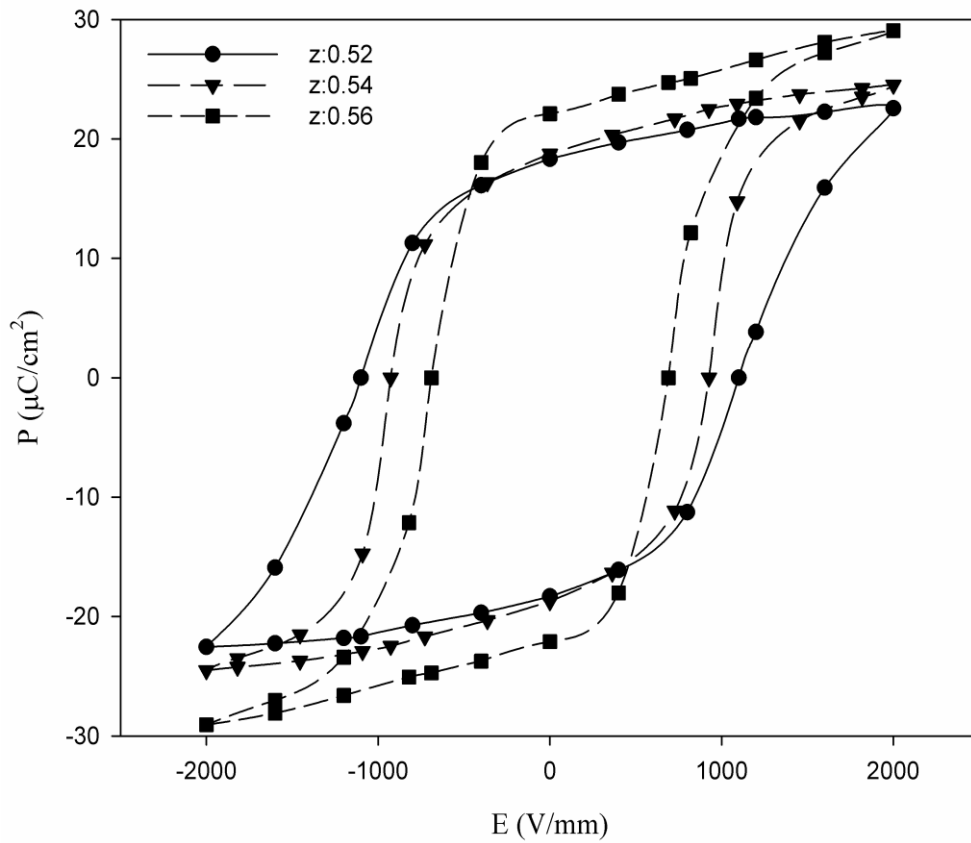


Figure 4.15 The hysteresis behavior in $\text{Pb}_{0.94}\text{Sr}_{0.05}\text{La}_{0.01}(\text{Zr}_z\text{Ti}_{1-z})\text{O}_3$ ceramics.

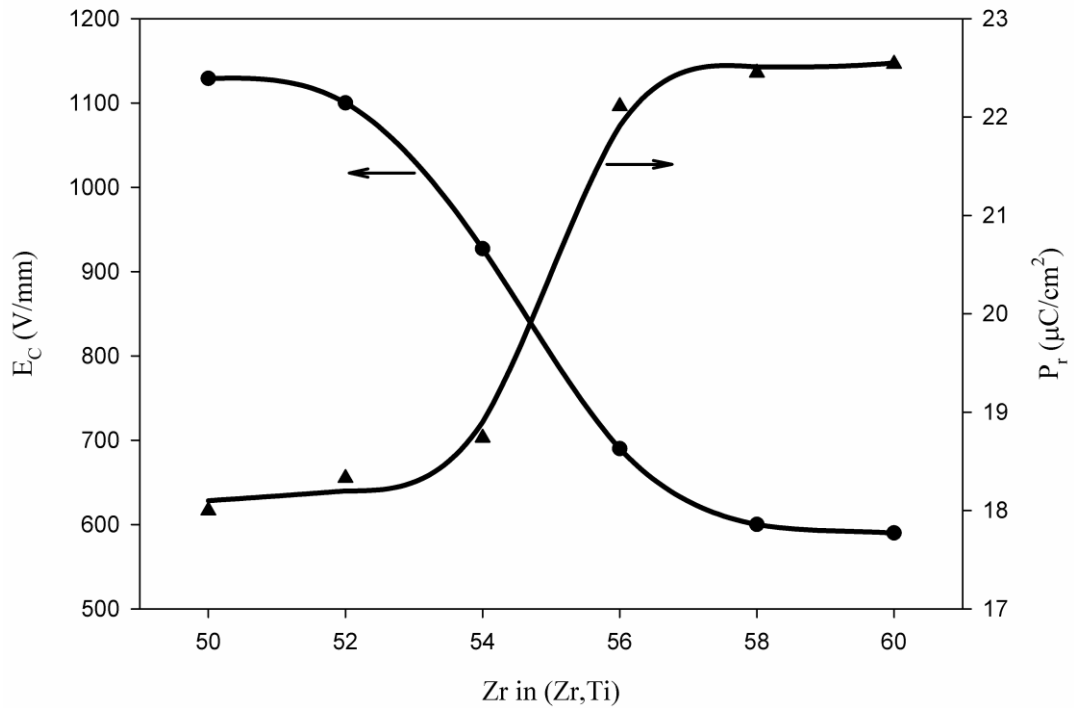


Figure 4.16 Variations of coercive field and remnant polarization with Zr/Ti ratio in $\text{Pb}_{0.94}\text{Sr}_{0.05}\text{La}_{0.01}(\text{Zr}_z\text{Ti}_{1-z})\text{O}_3$ ceramics.

4.3.2.3 $\text{Pb}_{0.99-x}\text{Sr}_x\text{La}_{0.01}(\text{Zr}_{0.54}\text{Ti}_{0.46})\text{O}_3$ Ceramics

The effect of Sr content on the dielectric and piezoelectric properties of $\text{Pb}_{0.99-x}\text{Sr}_x\text{La}_{0.01}(\text{Zr}_{0.54}\text{Ti}_{0.46})\text{O}_3$ ceramics was studied by changing the Sr-content from 0 to 5 at%. Various physical properties measured are listed in Table 4.4. The densification was improved with increasing Sr substitution in PLZT. Sr was instrumental in grain growth as evidenced by the SEM micrographs shown in Figure 4.17. The average grain size in the PSLZT ceramic doped with 5 at% Sr increased to 3.62 μm as opposed to 1.4 μm in the version without Sr.

Table 4.4 Physical and electrical properties of $\text{Pb}_{0.99-x}\text{Sr}_x\text{La}_{0.01}(\text{Zr}_{0.54}\text{Ti}_{0.46})\text{O}_3$ ceramics.

x	0.00	0.01	0.02	0.03	0.04	0.05
d_{33} (pC/N)	260	400	505	610	625	640
k_p	0.40	0.48	0.49	0.52	0.54	0.56
Q_m	55	58	63	60	67	70
K^T	810	895	1020	1240	1520	1800
$\tan \delta$ (%)	1.60	1.64	1.48	1.50	1.55	1.55
Density (%TD)	94.06 (± 0.07)	95.62 (± 0.05)	96.25 (± 0.07)	96.89 (± 0.08)	97.83 (± 0.07)	98.29 (± 0.07)
Average Grain Size (μm)	1.40 (± 0.05)	1.60 (± 0.05)	2.00 (± 0.04)	2.75 (± 0.06)	3.25 (± 0.06)	3.62 (± 0.04)
Open/Closed Porosity (vol%)	1.15/ 4.79	1.02/ 3.36	1.03/ 2.72	0.89/ 2.22	0.81/ 1.26	0.63/ 1.08

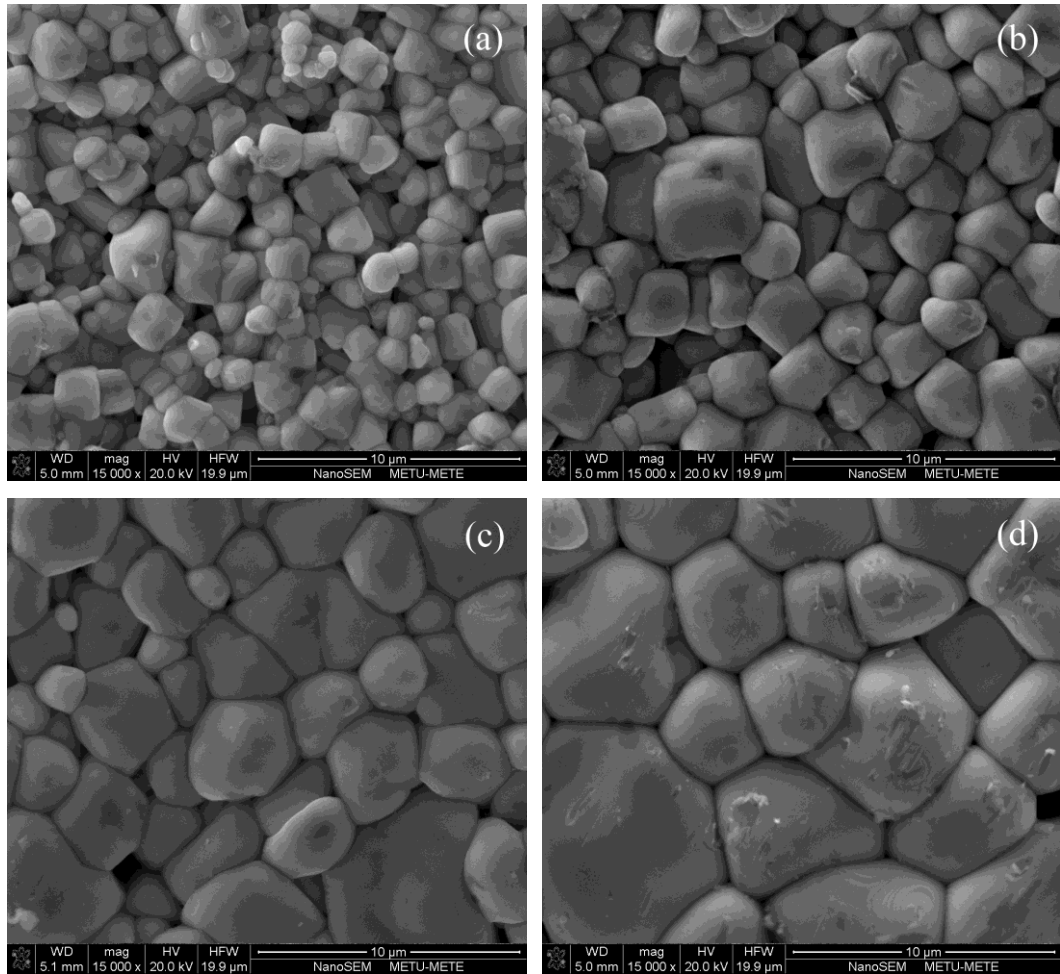


Figure 4.17 SEM micrographs of $\text{Pb}_{0.99-x}\text{Sr}_x\text{La}_{0.01}(\text{Zr}_{0.54}\text{Ti}_{0.46})\text{O}_3$ ceramics modified with various levels of Sr addition: (a) undoped, (b) $x=0.02$, (c) $x=0.04$, and (d) $x=0.05$.

The XRD patterns shown in Figure 4.18, and the fractions of T and R phases given in Figure 4.19 revealed that the tetragonal phase formation was favored at all levels of Sr substitution. The proportion of the T phase increased steadily from 55 vol% in the Sr-free PLZT ceramic to 83 vol% as Sr was raised to 5 at%.

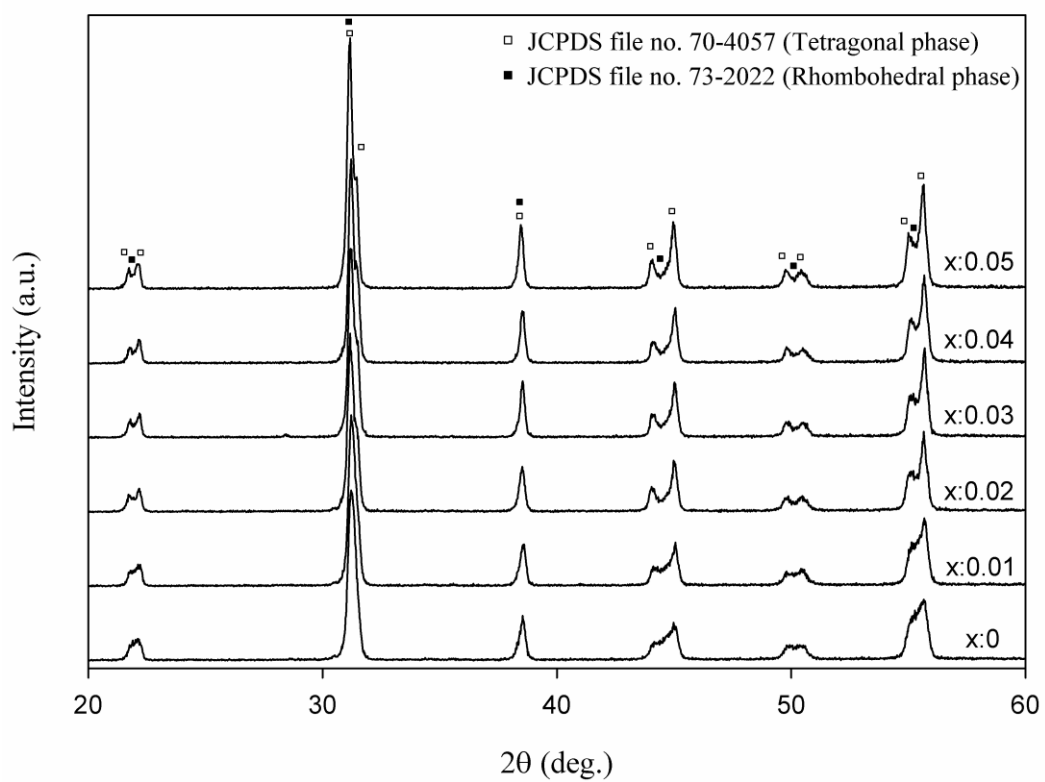


Figure 4.18 The XRD patterns of the $\text{Pb}_{0.99-x}\text{Sr}_x\text{La}_{0.01}(\text{Zr}_{0.54}\text{Ti}_{0.46})\text{O}_3$ ceramics. The values of x indicate the Sr content in the PSLZT.

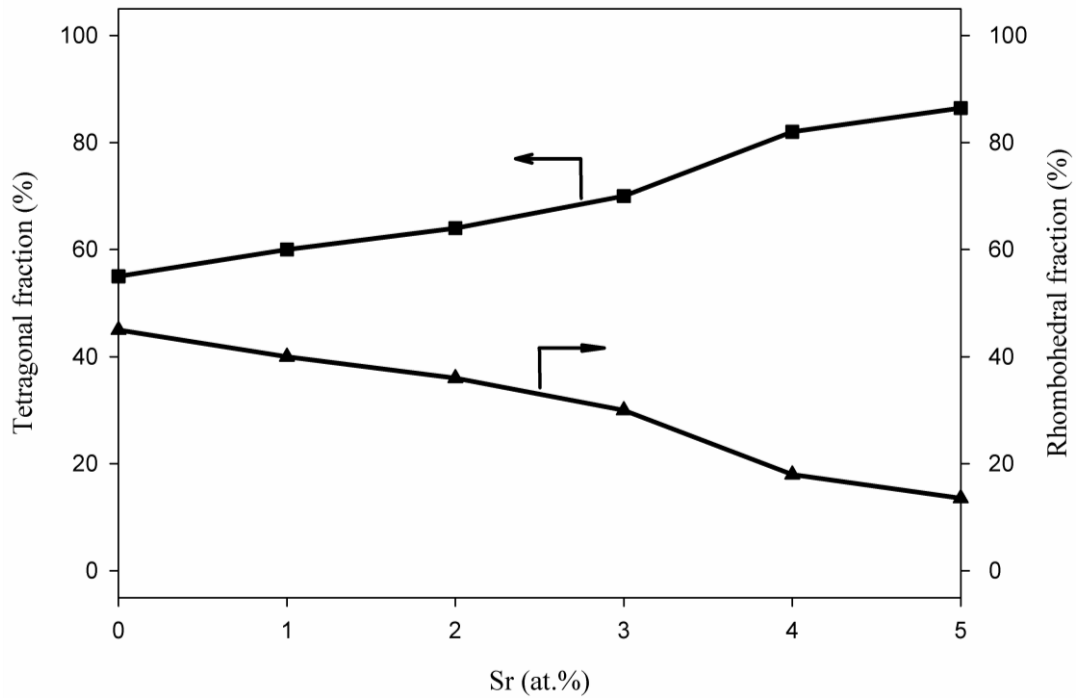


Figure 4.19 Relative proportions of tetragonal and rhombohedral modifications in the $\text{Pb}_{0.99-x}\text{Sr}_x\text{La}_{0.01}(\text{Zr}_{0.54}\text{Ti}_{0.46})\text{O}_3$ ceramics with variable Sr content.

Figure 4.20 shows the changes in the dielectric and piezoelectric properties of the $\text{Pb}_{0.99-x}\text{Sr}_x\text{La}_{0.01}(\text{Zr}_{0.54}\text{Ti}_{0.46})\text{O}_3$ ceramics. With increasing Sr substitution the dielectric constant K^T exhibited a continuous rise, indicating a steady enhancement in polarization due to the elimination of the effect of compression of the 180° domains in the T phase [66]. The effect of Sr on the piezoelectric strain coefficient was more striking; the parameter d_{33} was a modest 260 pC/N at zero Sr but it raised to 610 pC/N with 3 at% replacement of Pb with Sr. Seemingly, however, the piezoelectric activity reached near saturation at 3 at% Sr addition. Planar coupling coefficient showed steady improvement with Sr, but the loss tangent was not affected drastically from the presence of Sr in PLZT.

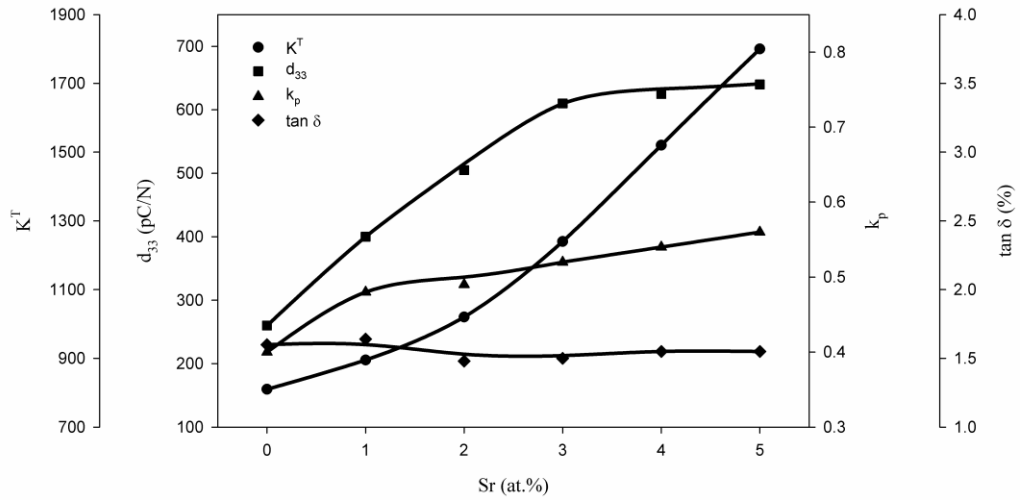


Figure 4.20 Variations in the dielectric and piezoelectric properties of $\text{Pb}_{0.99-x}\text{Sr}_x\text{La}_{0.01}(\text{Zr}_{0.54}\text{Ti}_{0.46})\text{O}_3$ ceramics.

The deflection in the d_{33} curve at 3 at% Sr substitution is reflected in the dynamic polarization behavior of the PSZLT ceramics as depicted by the hysteresis curves shown in Figure 4.21. The ceramics having less than 3 at% Sr displayed lower remanance and lower coercivity. Those with 3 at% and more Sr had evidently higher polarization energy.

The hysteresis loops could be classified under two major groups. The loops of the ceramics with low Sr were round in shape; these samples had smaller grain size and they exhibited lower electromechanical coupling. The ceramics having $\text{Sr} \geq 3\text{at}\%$ had square-like hysteresis loops; they had higher k_p , and their remanance was also higher due to the increased freedom of domains emanating from removal of the clamping effect on domains which is associated with larger grain size.

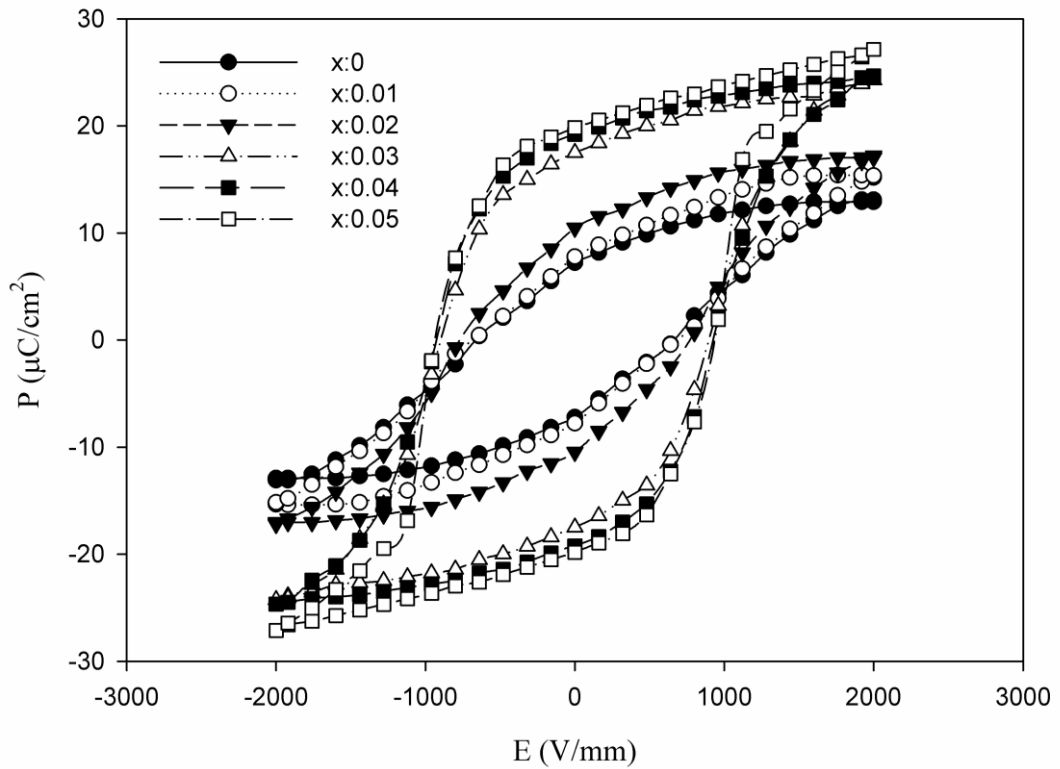


Figure 4.21 The hysteresis behavior in $\text{Pb}_{0.99-x}\text{Sr}_x\text{La}_{0.01}(\text{Zr}_{0.54}\text{Ti}_{0.46})\text{O}_3$ ceramics.

The coercive field and remanance values in the low Sr group could be compared with the data provided by Nasar et al. [68] on the $\text{Pb}(\text{Zr}_{0.53}\text{Ti}_{0.47})\text{O}_3$ ceramics doped with up to 1.5 at% Sr. Their results for the ceramic with 1.5 at% Sr were $E_c = 780$ V/mm, and $P_r = 8.9 \mu\text{C}/\text{cm}^2$. The values determined for the low-Sr group ceramics of this study, shown in Figure 4.22, were quite comparable; $E_c = 720$ V/mm, and $P_r = 8.5 \mu\text{C}/\text{cm}^2$.

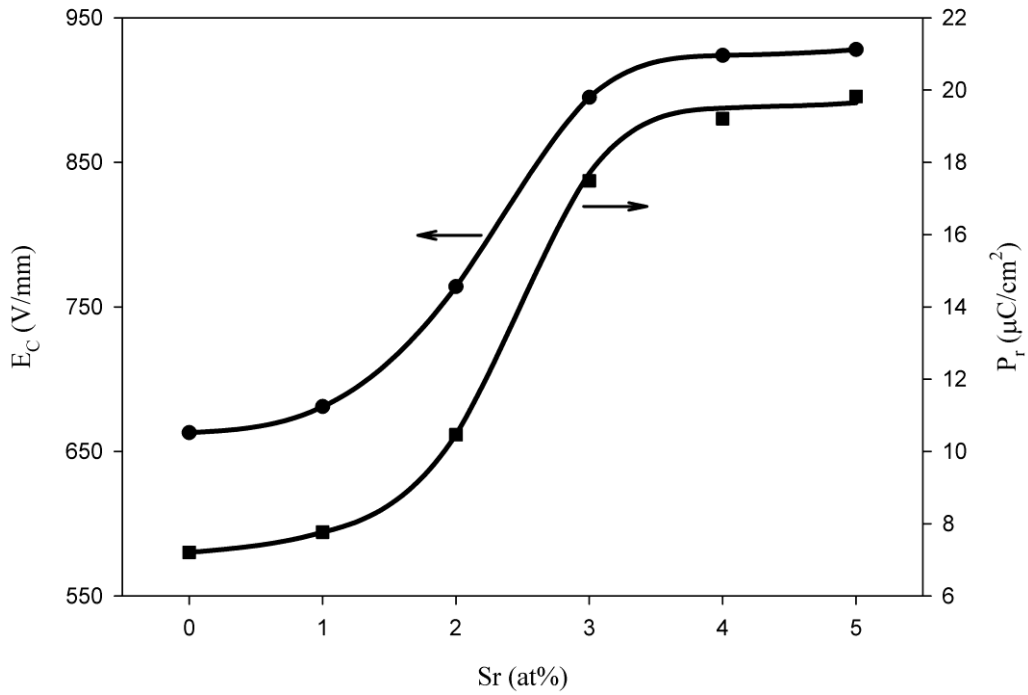


Figure 4.22 Variations of coercive field and remnant polarization with Zr/Ti ratio in $\text{Pb}_{0.99-x}\text{Sr}_x\text{La}_{0.01}(\text{Zr}_{0.54}\text{Ti}_{0.46})\text{O}_3$ ceramics.

Temperature dependence of the dielectric constant of the $\text{Pb}_{0.99-x}\text{Sr}_x\text{La}_{0.01}(\text{Zr}_{0.54}\text{Ti}_{0.46})\text{O}_3$ ceramics is displayed by the curves in Figure 4.23. The shrinkage or elongation of crystal lattice can shift the Curie temperature of perovskites. If the unit cell dimensions are forced to shrink then the Curie temperature decreases. As a result of shrinkage in the a_T axis given in Table B.4, there was a continuous decrease in the Curie temperature (T_C) with increasing Sr addition. Since The Curie temperature of the undoped $\text{Pb}(\text{Zr}_{0.54}\text{Ti}_{0.46})\text{O}_3$ ceramic was reported as 385 °C [36]. La addition at 1 at% level caused a large decrease in the Curie temperature of this ceramic; the T_C was measured as 339 °C. The PSLZT ceramic with 1 at% La and 5 at% Sr had a T_C of 272 °C. Since Sr and La exhibit similar straining effects on the perovskite lattice the drop in T_C was consistent with studies reported in the literature [36, 53]. The trend of lower T_C in the presence of

Sr has been observed in other PZT families [69, 70]; the effect has been correlated with the ease of transformation from T phase to R modification at lower temperatures due to the smaller size of the dopants [70].

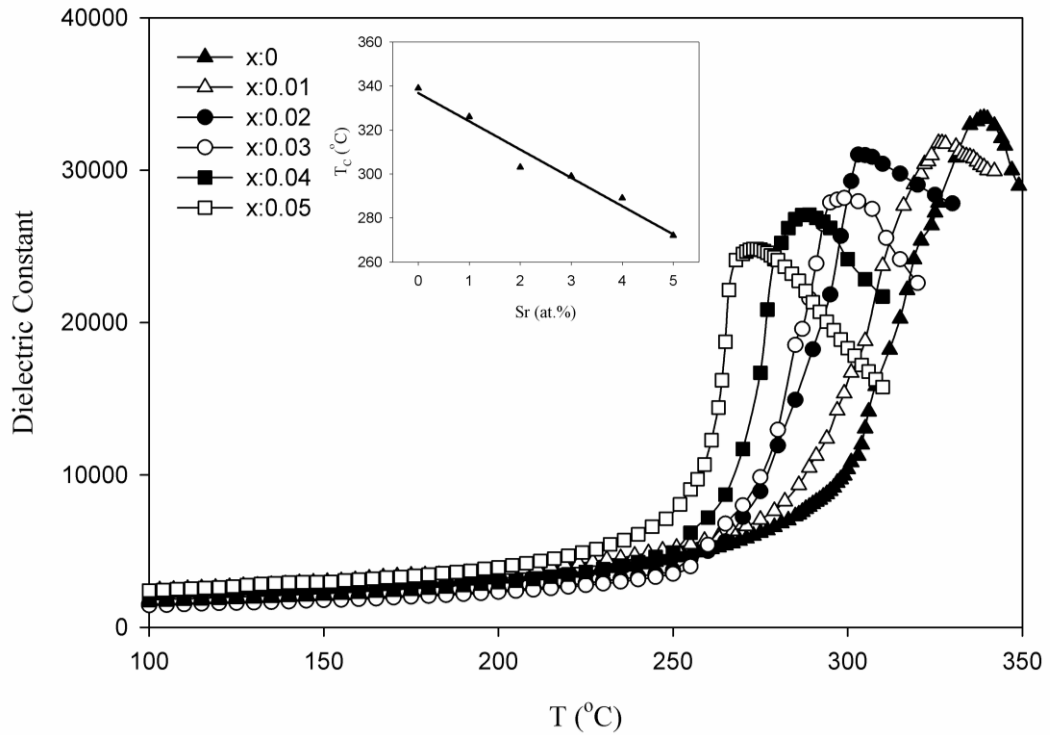


Figure 4.23 The change in the dielectric constant of the $\text{Pb}_{0.99-x}\text{Sr}_x\text{La}_{0.01}(\text{Zr}_{0.54}\text{Ti}_{0.46})\text{O}_3$ ceramics with temperature.

4.4 Conclusions of the PSZT – PSLZT Ceramics

1. PZT ceramics modified with simultaneous additions of Sr and La were produced in pure perovskite structure through conventional ceramic processing techniques. The incorporation of Sr^{2+} into the PZT lattice stabilized the tetragonal symmetry

over the rhombohedral one and enhanced the grain growth during sintering. Although La had similar effect on the stability of the tetragonal phase it had the tendency of decreasing the grain size. In the co-doped ceramics, satisfactory densification could be attained due to effective development of the microstructure consisting of a mixture of large and small grains.

2. The overall weight loss in the PSLZT discs during sintering was typically less than 0.4% indicating that the small excess of PbO due to B-site formulation was nullified during sintering, and also no PbO was gained from the bedding. Consequently, in the SEM micrographs, there was no evidence of PbO as a second phase.

3. PSLZT ceramics prepared in this study were essentially soft in nature. Sr had a dominant role in the improvement of the piezoelectric moduli and the dielectric constant. The Sr-La co-doping may be used to manufacture bulk PZT ceramics with tailorable properties.

4. Combination of Sr and La as co-dopants had great implications on the dielectric and piezoelectric properties of the PZT ceramics. A remarkably high strain constant d_{33} of 640 pC/N was attained in the PSLZT ceramic containing 1 at% La and 5 at% Sr, the Zr/Ti ratio being the one on the MPB. The Curie temperature of this particular ceramic was 272 °C.

CHAPTER 5

PSLZT CERAMICS MODIFIED BY Mn, Nb AND Sb

5.1 Introduction

PZT based ceramics have been studied extensively for many years. However, their usage in high-power/hard-drive devices such as ultrasonic motors and ultrasonic transformers was studied actively only in the last decade. In such applications, these ceramic materials are driven near their resonance frequencies in order to obtain high mechanical vibration. Therefore, it is necessary for these piezoelectric ceramics to combine a high mechanical quality factor, $Q_m > 1000$, with high piezoelectric constant, $d_{33} > 200$ pC/N, and high electromechanical coupling coefficient, $k_p > 0.5$ [5, 71].

For high-power applications, high Q_m is the most important requirement. Since Q_m is the indicator of internal friction and heat dissipation in the piezoelectric [3]. Low Q_m ceramics will heat faster as a result of energy loss; this alters the resonance frequency, which will be detrimental to piezoelectric properties. Hence, for high-power applications ceramics that exhibit high Q_m and low dielectric loss, $\tan \delta$, are desirable. Furthermore, piezoelectric ceramics utilized in the ultrasonic motors are required to have high transformation efficiency, i.e. their electromechanical coupling factor k_p must be also high. In addition, the piezoelectric ceramic should have high d_{33} since it is the indicator of the extent of piezoelectric activity. Many ternary and quaternary piezoelectric solid solutions have been manufactured by chemical modifications in the base PZT composition in order to satisfy the requirements of high power applications. [6, 13, 23, 70].

In order to obtain high Q_m ceramics, usually acceptor dopants are used which are incorporated mainly to the B-site of the ABO_3 structure of PZT. Common acceptor dopants include cations such as Cr^{3+} , Mn^{3+} , Al^{3+} , and Fe^{3+} [2, 29, 37, 38, 71-73]. Acceptors, also known as hardeners, lead to the formation of oxygen vacancies when they enter to the B-site to substitute for Ti^{4+} and Zr^{4+} and provide fine grained materials. The increase in Q_m has been linked to the reduced domain wall mobility due to finer domain size. As a disadvantage, however, the acceptors lower the piezoelectric constant, electromechanical coupling factor and generally deteriorate the dielectric parameters [3].

The dielectric and piezoelectric properties of PZT ceramics that have been modified in composition for attaining high Q_m are listed in Table 5.1; that represents a summary of the references available in the literature on high Q_m ceramics. The noteworthy feature of the table is that with modifications in chemical composition and using proper processing conditions, PZT ceramics can be manufactured with Q_m values reaching 2600.

One of the objectives of this thesis investigation was to develop high Q_m ceramics from a base PSLZT which exhibited an unusually high d_{33} . For this purpose, the PSLZT ceramics of the present study were modified by manganese, niobium, and antimony in order to obtain high Q_m materials. In the following, a review of previous literature related to the use of the specified modifier elements will be presented in order to highlight their role in PZT.

Table 5.1 PZT-based ceramic compositions developed for high power applications.

Reference	Base Composition	Additive(s)	Q_m	d_{33} (pC/N)	k_p	K^T	$\tan \delta$ (%)
C.K.Liang et al. [38]	$Pb_{0.97}Sr_{0.03}[Zr_{0.458}Ti_{0.452}(Mn_{1/3}Nb_{2/3})_{0.09}]O_3$	0.1 wt% Cr_2O_3	2000	x	0.58	1200	x
E.Boucher et al. [57]	$[Pb_{0.89}(Ba,Sr)_{0.11}][(Zr_{0.7}Ti_{0.3})_{0.99}Mn_{0.01}]O_3$	1.0 at% F	2000	125	0.58	350	x
H.Chen et al. [6]	$Pb_{0.98}Sr_{0.02}(Mg_{1/3}Nb_{2/3})_{0.06}(Mn_{1/3}Nb_{2/3})_{0.06}(Zr_{0.48}Ti_{0.52})_{0.88}O_3$	0.2 wt. CeO_2	2379	307	0.55	1200	0.5
S.Priya et al. [81]	$0.9(Pb_{0.94}Sr_{0.06})(Zr_{0.57}Ti_{0.43})O_3-0.1Pb(Mn_{1/3}Nb_{2/3})O_3$	x	1644	154	0.44	501	0.6
B.S.Li et al. [82]	$Pb[Zr_{0.499}Ti_{0.461}Mn_{0.05/3}Nb_{0.1/3}]O_3$	x	1300	x	0.55	x	x
C.Chen et al. [83]	$0.93Pb(Zr_{0.503}Ti_{0.497})O_3-0.07Pb(Mn_{1/3}Nb_{2/3})O_3$	x	2050	x	0.61	x	x
Z.G.Zhu et al. [88]	$Pb_{0.98}Sr_{0.02}(Mn_{1/3}Sb_{2/3})_yZr_zTi_{1-y-z}O_3$ ($0 < y < 0.10$, $0.4 < z < 0.5$)	x	1620	348	0.57	1370	0.62
D.Liang et al. [7]	$0.93Pb(Zr_{0.5}Ti_{0.5})O_3-0.07Pb(Mn_{1/3}Sb_{2/3})O_3$	x	1520	230	0.66	675	0.52
L.Sun et al. [70]	$Pb_{0.96}Sr_{0.02}Ba_{0.02}[(Zr_{0.455}Ti_{0.445})(Zn_{1/3}Nb_{2/3})_{0.03}(Sn_{1/3}Nb_{2/3})_{0.03}(Mn_{1/3}Sb_{2/3})_{0.04}]O_3$	1.0 wt% Pb_3O_4	1671	285	0.52	1294	0.4
S.J.Yoon et al. [67]	$0.02Pb(Y_{2/3}W_{1/3})O_3-0.98Pb(Zr_{0.52}Ti_{0.48})O_3$	0.7 wt% MnO_2	1000	240	0.55	800	1.2
C.Galassi et al. [35]	$[Pb(Li_{0.25}Nb_{0.75})]_{0.06}[Pb(Mg_{0.33}Nb_{0.67})]_{0.06}[Pb(Zr_{0.50}Ti_{0.50})]_{0.88}O_3$	0.7 wt% MnO_2	2132	148.7	0.54	447	x

Table 5.1 (Continued)

Reference	Base Composition	Additive(s)	Q_m	d_{33} (pC/N)	k_p	K^T	$\tan \delta$ (%)
J.H.Yoo et al. [89]	$Pb(Ni_{1/2}W_{1/2})_{0.02}(Mn_{1/3}Nb_{2/3})_{0.07}(Zr_{0.49}Ti_{0.51})_{0.91}O_3$	0.5 wt% PbO + 0.3 wt% Fe ₂ O ₃ + 0.25 wt% CeO ₂	1886	x	0.50	1302	x
G.Feng et al. [90]	$0.80Pb(Zr_{0.5}Ti_{0.5})O_3 - 0.20Pb(Zn_{1/3}Nb_{1/3})O_3$	1.0 wt% WO ₃	1178	314	0.62	1200	0.425
H.W.Chung et al. [91]	$0.96Pb(Zr_{0.52}Ti_{0.48})O_3-0.04Pb(Mn_{0.32},W_{0.36},Sb_{0.16},Nb_{0.16})O_3$	x	2344	x	0.56	755	x
S.Zhao et al. [23]	$0.88Pb(Zr_{0.5}Ti_{0.5})O_3 - 0.06Pb(Sn_{1/3}Nb_{2/3})O_3$ - $0.06Pb(Zn_{1/3}Nb_{2/3})O_3$	0.5 wt% MnO ₂ + 0.5 wt% Sb ₂ O ₃ + 0.5 wt% Cr ₂ O ₃	2614	314	0.58	1665	0.4
H.L.Du et al. [92]	$(Pb_{0.95}Sr_{0.05})[(Mn_{1/3}Sb_{2/3})_{0.06}(Ni_{1/2}W_{1/2})_{0.02}(Zr_{1/2}Ti_{1/2})_{0.92}]O_3$	1 mole% ex. PbO + 0.2 wt% MnO ₂ + 0.25 wt% CeO ₂	1275	380	0.61	2138	0.58
Y.Hou et al. [93]	$(Pb_{0.95}Sr_{0.05})((Zn_{1/3}Nb_{2/3})_{0.20}(Zr_{0.50}Ti_{0.50})_{0.80})O_3$	0.5 wt% MnO ₂	1360	325	0.62	1240	0.2
C.Y.Chen et al. [94]	$0.07Pb(Mn_{1/3}Nb_{2/3})O_3-0.468PbZrO_3-0.462PbTiO_3$	0.3 wt% 2CaO.Fe ₂ O ₃	2150	x	0.53	x	0.25
J.H.Yoo et al. [13]	$Pb_{0.94}Ba_{0.06}(Zr_{0.52}Ti_{0.48})_{0.925}(Mn_{1/3}Nb_{2/3})_{0.075}O_3$	0.25 mole% CeO ₂	1792	x	0.52	767	x
C.S.Kim et al. [95]	$0.96PbZr_{0.52}Ti_{0.48}O_3-0.04Pb(Mn_{0.32},W_{0.36},Sb_{0.16},Nb_{0.16})O_3$	x	2344	x	0.56	755	x
R.Zhang et al. [96]	$0.90Pb(Zr_{0.51}Ti_{0.49})O_3 - 0.07Pb(Mn_{1/3}Nb_{2/3})O_3$ - $0.03Pb(Ni_{1/2}W_{1/2})O_3$	0.1 wt% CeO ₂	1405	388	0.60	2140	0.59

5.1.1 Manganese

According to the research reported in literature, when manganese is added into PZT as a modifier it is usually introduced in the form of MnO_2 in which Mn is in the form of Mn^{4+} ion [73]. During calcination and sintering stages Mn^{4+} is reduced partially into Mn^{2+} and Mn^{3+} in proportions depending on the prevailing oxygen partial pressure in the environment. Thus, in PZT the manganese may be present in 2^+ , 3^+ , and 4^+ states of valency. Boucher et al. [57] made an analytical study on the coexistence of Mn^{2+} , Mn^{3+} , and Mn^{4+} ions in the PZT through ESR. The ESR spectra displayed Mn^{2+} and Mn^{4+} conclusively. Since Mn^{3+} has even number of 3d electrons it could not be detected by ESR but its presence was ascertained by mass balance calculations on Mn. These calculations, carried over a range of Zr/Ti ratios, indicated that the proportion of Mn^{3+} was maximized at the MPB.

In an earlier work published in 2000, He and Li [73] had also studied the state of valency of Mn in an MPB type PZT through ESR methods. Their spectra showed the presence of the Mn^{2+} ion only but none of Mn^{4+} . The presence of the Mn^{3+} ion could be ascertained visually from the darker color of the ceramic as opposed to the pale PZT which has Mn^{2+} only. When the observations of He and Li [73] are combined with those of Boucher et al. [57], it may be concluded that the relative abundance of Mn^{4+} type manganese cation is highly sensitive to the Zr/Ti ratio of the PZT ceramic in hand. With compositions near or at MPB all Mn^{4+} fraction is converted into Mn^{3+} due probably to the combination reaction $\text{Mn}^{2+} + \text{Mn}^{4+} \rightarrow 2\text{Mn}^{3+}$.

The size of the Mn^{3+} ion is 66 nm [74]. Therefore it can fit into the Zr/Ti positions in the octahedral cage of the perovskite, making Mn^{3+} an acceptor dopant. The size of the Mn^{2+} ion in 8-fold coordination within perovskite structure is 110 nm, therefore it can place Pb on the A site of the PZT [43]. On the other hand, in 6-fold coordination the size of Mn^{2+} is 82 nm [74]. Hence it may partly occupy the B site positions as well. The effect of manganese on PZT properties is found to be concentration dependent. Rema and Kumar [43] noted that when the concentration

of manganese was kept below 0.1 at% it entered into the A site as Mn^{2+} and caused a dipole moment whose effect was to increase moderately the Curie temperature, T_c , and to decrease slightly the d_{33} of the ceramic. Above 0.1 at% addition, up to 0.4 at%, Mn appeared as Mn^{3+} acting as acceptor. Therefore within this additive range the Q_m of the ceramic increased steadily due to the pinning of the domain walls by oxygen vacancies. Interestingly, in the same additive range, the ceramic $\text{Pb}_{0.94}\text{Sr}_{0.06}(\text{Zr}_{0.53}\text{Ti}_{0.47})_{1-(3/4)x}\text{Mn}_x\text{O}_3$ exhibited enhanced d_{33} values; the maximum attained at 0.004 mole Mn^{3+} addition was $d_{33}=450$ pC/N [43].

The role of manganese is unique in combining the “soft” and “hard” piezoelectric characteristics in the same PZT. Boucher et al. [57] showed that small amounts of Mn additions modified the conventional subsolidus phase diagram of the PZT system greatly. The new diagram, reproduced in Figure 5.1, revealed that the MPB in the PZT system became an area consisting of the mixture of tetragonal and rhombohedral phases. The coexistence of T and R was spread over the composition interval ranging from 48 mole% PZ to 55 mole% PZ.

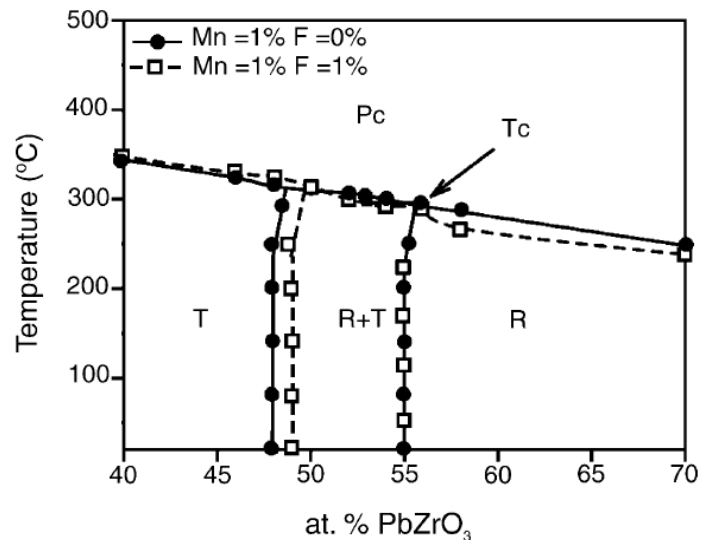


Figure 5.1 Phase diagram of PZT doped with Mn and/or F showing the range of MPB region [57].

The reason why the PZT doped with Mn^{3+} exhibited soft piezoelectric behavior in addition to the hard characteristics was explained with the Jahn-Teller distortion in the MnO_6 octahedra [43]. While at one hand the Mn^{3+} acceptor creates oxygen vacancies that pin the domain walls which increase the Q_m , on the other hand, the J-T distortion brings about the gradual change from tetragonal to rhombohedral symmetry increasing the dielectric and electromechanical characteristics through enhanced domain wall mobility.

The views on the solubility limit of Mn^{3+} in the perovskite lattice are rather conflicting. Rema and Kumar [43] placed the limit at 0.4 at% Mn; they argued that above this level the manganese separated into a second phase, resulting in deterioration of dielectric and piezoelectric characteristics. In contrast, He and Li [73] claimed that up to 1.5 at% Mn^{3+} could be incorporated in the B site of the perovskite leading to high Q_m ; beyond this level it accumulated at the grain boundaries giving rise to the decrease in piezoelectric properties.

5.1.2 Antimony

Two oxides of antimony, Sb_2O_3 and Sb_2O_5 , have found use as dopants in the development of electronic ceramics for applications involving semi-conductivity and piezoelectricity. The size of the Sb^{3+} ion is 245 pm and that of Sb^{5+} is 62 pm [74]. Sb^{3+} is too large to fit into the B site cationic positions of PZT, therefore no study is found in the literature concerning the acceptor action of this ion. Sb^{3+} is also too large to fit into the A site, but, surprisingly a publication was released by Rai and Sharma [75] on its use in a PZT as a donor dopant. The base ceramic was a PLZT with a molecular composition of $\text{Pb}_{0.9}\text{La}_{0.1}(\text{Zr}_{0.55}\text{Ti}_{0.45})_{0.975}\text{O}_3$. Sb^{3+} was introduced as a partial substitute for La^{3+} in quantities up to 7 at% in the PZT. The notable effects of the Sb^{3+} involvement were increase in the dielectric permittivity and increase of the Curie temperature of the PLZT ceramic. No data were provided on the piezoelectric properties.

The Sb^{5+} ion may be introduced into the B site of the PZT ceramics either alone or in combination with Nb and/or Mn. In common practice the Mn-Nb, Mn-Sb, and Mn-Nb-Sb additions are made in the form of niobate or antimonite combinations which will be discussed in the following.

5.1.3 Niobates and Antimonates

An outstanding PZT group of ceramics is typified by compensating valence substitutions made in accordance with the stoichiometry $\sum X_A V_A + \sum X_B V_B = 6$ where X is concentration and V is the valency of ions entering the A and B positions of perovskite [2]. Notable piezoelectric ceramic products having compensating dopants occupying only the B site positions in perovskite are solid solutions of $\text{Pb}(\text{Zr,Ti})\text{O}_3$ with compounds such as $\text{Pb}(\text{Mg}_{1/3}\text{Nb}_{2/3})\text{O}_3$, $\text{Pb}(\text{Zn}_{1/3}\text{Nb}_{2/3})\text{O}_3$, $\text{Pb}(\text{Fe}_{1/2}\text{Nb}_{1/2})\text{O}_3$, $\text{Pb}(\text{Y}_{2/3}\text{W}_{1/3})\text{O}_3$, and $\text{Pb}(\text{Ni}_{1/2}\text{W}_{1/2})\text{O}_3$.

The compound $\text{Pb}(\text{Mg}_{1/3}\text{Nb}_{2/3})\text{O}_3$, which is called lead-magnesium niobate and denoted with the acronym PMN, is the basis of the niobate chemistry in PZT technology. This compound, synthesized first in late 1950's, has later proved to be an excellent dielectric material. High dielectric constants and broad maxima observed in the dielectric spectrum around the ferroelectric transition temperature are two important features of PMN. With an increase in applied frequency the magnitude of the dielectric permittivity maximum decreases and the transition temperature increases. The materials having these characteristics are classified as relaxor dielectrics [76, 77].

PMN based ceramics are capable to generate large strains up to 0.1 percent under moderate electric fields due to the large dielectric permittivities of these materials which are several times higher than that of PZT ceramics. Their thermal expansion coefficients are smaller by a factor of 10 than the PZT group materials. With these superior properties over PZT, PMN group ceramics have become materials of

choice for actuator applications such as medical transducers, optical equipment, precision machinery, and piezoelectric motors [78].

Like PZT, PMN crystallizes in the perovskite structure. Therefore PMN can form solid solutions with PT, PZ, and PZT. As shown in the PMN-PT-PZ system in Figure 5.2, PMN and PT have a MPB similar to the one in the PZT system [2]. This boundary extends into the ternary upon additions of PZ. Likewise, the MPB of the PZT system extends into the ternary with additions of PMN. With proper processing, extraordinarily high dielectric and piezoelectric properties can be obtained in the PMN-PT or PMN-PZT group systems having compositions along MPB. A good example is the PMN-PT ceramics in which d_{33} values as high as 830 pC/N could be attained upon 5 at% La addition [79].

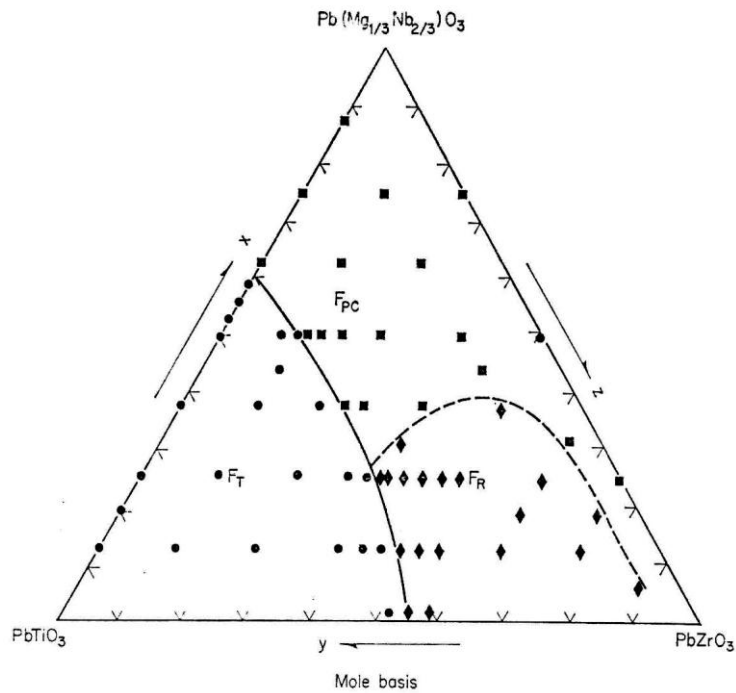


Figure 5.2 The system $\text{Pb}(\text{Mg}_{1/3}\text{Nb}_{2/3})\text{O}_3\text{-PbTiO}_3\text{-PbZrO}_3$ at room temperature [2].

In the past two decades the population of the PMN type perovskites that could be used for modifying the properties of PZT ceramics have enlarged extensively. Examples of newer PMN type compounds are niobates such as $\text{Pb}(\text{Mn}_{1/3}\text{Nb}_{2/3})\text{O}_3$, $\text{Pb}(\text{Zn}_{1/3}\text{Nb}_{2/3})\text{O}_3$, $\text{Pb}(\text{Ni}_{1/3}\text{Nb}_{2/3})\text{O}_3$, and $\text{Pb}(\text{Sn}_{1/3}\text{Nb}_{2/3})\text{O}_3$. In contrast to the abundance of niobates only a single antimonate compound has been used in the alloying process of PZT. The antimonate equivalent of the PMN is PMS which is represented by the molecular formula $\text{Pb}(\text{Mn}_{1/3}\text{Sb}_{2/3})\text{O}_3$.

The kind of ceramics in which high Q_m values are obtainable with the use of niobates and/or antimonates were listed in Table 5.1. Although the exact mechanism of enhancement in piezoelectric properties has not been completely understood, the factors related to domain structure, domain wall motion, degree of poling, and proximity of chemical composition to MPB definitely play role in them [3]. In the present study, the compensating valence substitutions in the form of $\text{Pb}(\text{Mn}_{1/3}\text{Nb}_{2/3})\text{O}_3$ (PMnN) and $\text{Pb}(\text{Mn}_{1/3}\text{Sb}_{2/3})\text{O}_3$ (PMS) were of particular interest. Therefore literature relevant to these was examined with greater attention.

The first report on a Rosen type piezoelectric transformer made from a PZT-PMnN material was published by Ise et al. [80]. The authors claimed that very high resonant velocities could be attained by using PZT-PMnN type ceramics. Although some details of sintering procedure related to ceramic manufacture were provided in their publication, no information was given on the chemical composition of their ceramics.

Chen and coworkers [6] showed that tetragonal PZT ceramics ($\text{Zr}/\text{Ti}=0.50/0.50$) modified by combined additions of PMN and PMnN could attain Q_m values reaching 2400 and $d_{33} = 307$ pC/N which made them good candidates for ultrasonic motors. In search of a ceramic for piezoelectric transformer with a low coefficient of temperature dependence in resonant frequency (TCF), Priya et al. [81] worked on a PSZT system doped with 10 mole% PMnN. They showed that a ceramic with Zr/Ti ratio of 51/49 had $Q_m= 800$ and $d_{33} = 274$ pC/N with reasonable TCF. Their

Q_m would reach 1600 by increasing the Zr/Ti ratio to 57/43 in which case the d_{33} would fall down to 154 pC/N and the TCF became exceedingly high.

Li et al. [82] prepared PZT ceramics with 4 mole% PMnN from fine particle size powders obtained through sort of an attrition milling. The PZT had a composition close to the MPB, i.e., Zr/Ti = 52/48. The firing temperature was varied in the range 1070 to 1280 °C. The data on d_{33} were not disclosed. The Q_m of the ceramic fluctuated between 1000 to 1500 displaying no systematic dependence on sintering temperature. Recently, Chen and coworkers [83] studied the effect of sintering temperature on the Q_m characteristics of a PZT-PMnN ceramic. The Zr/Ti ratio of their PZT component was 50/50 and the ceramic was doped with 7 mole% PMnN. The Q_m increased steadily from 800 to 2100 as the sintering temperature was raised from 1050 to 1250 °C. Again, no data was given for d_{33} .

While PMnN crystallizes as a perovskite, PMS is a ferroelectric compound basically with pyrochlore structure. However, the phase diagram of the PT-PZ-PMS system, shown in Figure 5.3 reveals that the PZT can form perovskite solid solutions with PMS up to about 20 mole% PMS addition without the appearance of the pyrochlore phase. This diagram, reproduced from the work of Takahashi et al. [84], was the basis of their work in developing transducers for piezoelectric devices durable at high vibration levels. Although the entire piezoelectric characterization was not made, they showed that PMS additions up to 10 mole% level improved the mechanical dissipation behavior of the PZT-PMS ceramics working under high drive conditions.

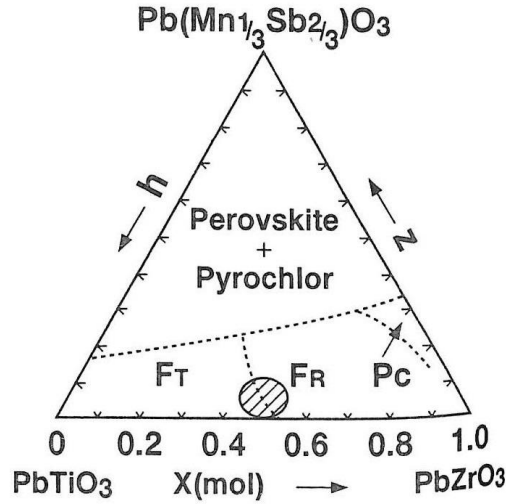


Figure 5.3 The phase diagram of the PbTiO_3 - PbZrO_3 - $\text{Pb}(\text{Mn}_{1/3}\text{Sb}_{2/3})\text{O}_3$ system at room temperature [84].

Lee et al. [85] worked on PZT ceramics alloyed with 10 mole% PMS. The PZT had a Zr/Ti ratio of 52/48. The PZT-PMS ceramics fired at 1250 °C for 2 h had the following piezoelectric properties: $d_{33} = 350$ pC/N, $Q_m = 1300$, and $k_p = 0.54$. Long et al. [12] investigated the piezoelectric properties of PSZT-PMS ceramics with compositions designated as $\text{Pb}_{0.98}\text{Sr}_{0.02}(\text{Zr}_{0.5}\text{Ti}_{0.5})_{1-x}(\text{Mn}_{1/3}\text{Sb}_{2/3})_x\text{O}_3$. Their ceramics also had an extraneous 0.2 wt% CeO_2 addition for unspecified reasons. The proportion of PMS component was increased up to 10 mole%. The piezoelectric properties were maximized at 5 mole% PMS with $d_{33} = 405$, $Q_m = 1220$, $k_p = 0.62$. A small amount of Nb addition to this ceramic, 0.1 mole%, raised the d_{33} to 450 pC/N without a substantial loss in Q_m .

The effects of rare-earth substitutions in PZT-PMS ceramics were studied by Yoon et al. [86] and later by Gao et al. [87]. Yoon et al. [86] selected a tetragonal PZT with Zr/Ti ratio of 47/53 and alloyed it with 5 mole% PMS. The ceramic was doped on the B site with Lu which has the smallest ionic size in the rare earth family. The sintering was done at 1200 °C for 1 h. The Lu-free PZT-PMS had a

Q_m of 1933 and a d_{33} of 251 pC/N. Lu addition deteriorated the Q_m , the value dropped sharply to 714 when 2 at% Lu was added.

In contrast to the findings of Yoon and coworkers [86], Gao et al. [87] observed that rare earth additions in the form of Yb, Eu, or Ce enhanced the Q_m of the PZT-PMS ceramics. The improvement was better with increasing cation size of the rare earth. The base composition of their ceramics was $0.90\text{Pb}(\text{Zr}_{0.52}\text{Ti}_{0.48})\text{O}_3$ - $0.10\text{Pb}(\text{Mn}_{1/3}\text{Sb}_{2/3})\text{O}_3$. The ceramic was modified by adding the rare earths Yb^{3+} , Eu^{3+} , or Ce^{4+} without any effort for charge compensation. Hence, vacancies were probably created on the Pb site of the perovskite. The Q_m of the base ceramic was 1150, it increased to 1250 with 2 at% Yb^{3+} addition, and to 1650 with 2 at% Ce^{4+} addition.

The piezoelectric properties of PSZT-PMS ceramics were investigated by Zhu et al. [88]. The ceramic was a combination of $\text{Pb}_{0.98}\text{Sr}_{0.02}(\text{Zr}_x\text{Ti}_{1-x})\text{O}_3$ with up to 10 mole% PMS addition. The Zr/Ti ratio of the PSZT was confined to $0.4 < x < 0.5$ which meant that the structure was tetragonal. For a ceramic of undisclosed Zr/Ti ratio, the dielectric and piezoelectric properties were maximized in a sintering regime involving a soak at 1240 °C for 2 h. The values reported were $d_{33} = 374$ pC/N, $Q_m = 1250$, $K^T = 1550$, and $\tan \delta = 0.40\%$.

The effect of sintering temperature on the properties of PZT-PMS ceramics were investigated recently by Hong-liang et al. [7]. The base PZT had a Zr/Ti ratio of 0.50/0.50. The PZT was alloyed with up to 9 mole% PMS. A compromise among the “good” electromechanical properties was achieved in a ceramic which contained 7 mole% PMS and sintered at 1250 °C for 2 h. The set of values was: $d_{33} = 230$ pC/N, $Q_m = 1520$, $k_p = 0.66$, $K^T = 675$, $\tan \delta = 0.53\%$.

From the information provided above, the highlights of the existing literature on PZT-PMnN, and PZT-PMS type ceramics can be summarized as follows:

(1) In the PZT-PMnN material system high drive ceramics with Q_m values like 1000 and piezoelectric constant of d_{33} around 300 have been developed. However, it is noted that the effect of Zr/Ti ratio has not been studied fully, and no work has been reported on PSLZT-PMnN type ceramics.

(2) In the PZT-PMS system, additions of PMS are limited due to the possibility of existence of the pyrochlore phase. With 10 mole% PMS addition into a PSZT type ceramics with $Q_m = 1250-1500$ and $d_{33} = 230-374$ pC/N could be manufactured. Again, the effect of Zr/Ti ratio covering the T and R phases has not been studied. Also, no information is available on PSLZT-PMS type systems.

(3) The effects of combined additions of PMnN and PMS on PZT type ceramics have not been studied at all. In this context, PSLZT-PMnN-PMS ceramics have never been the subject of earlier investigations on PZT based material systems.

5.2 Compositions Studied

The starting ceramic in quest for high Q_m was the PSLZT with the composition $\text{Pb}_{0.94}\text{Sr}_{0.05}\text{La}_{0.01}(\text{Zr}_{0.54}\text{Ti}_{0.46})_{0.9975}\text{O}_3$. This ceramic had a d_{33} value of 640 pC/N but exhibited a rather too low Q_m of 70. The aim in this part of the thesis was to modify this base PSLZT in chemical composition to enhance its Q_m . For this purpose, three distinct set of experiments were planned:

- (a) Incorporate Mn and Nb in the form of the niobate $\text{Pb}(\text{Mn}_{1/3}\text{Nb}_{2/3})\text{O}_3$ (as PMnN) to the B-site of the ceramic by substituting increasing amounts of MnN for (Zr,Ti) positions,
- (b) Optimize the Zr/Ti ratio of the PSLZT ceramic for the PMnN substitution which yields higher Q_m ,
- (c) Modify the PSLZT of optimized PMnN content with Sb^{5+} additions to increase the Q_m to still higher values. This modification was based on the

addition of Mn, Nb, and Sb in the form of the mixed niobate-antimonate $\text{Mn}_{1/3}[\text{Nb}_{2-x/3}\text{Sb}_{x/3}]\text{O}_3$.

The chemical formulations of the PSLZT ceramics for high Q_m research are summarized in Table 5.2. The samples of the ceramics in Table 5.2 were synthesized from powders of PbO, ZrO₂, TiO₂, SrCO₃, La₂O₃, MnCO₃, Nb₂O₅ and Sb₂O₃ in accordance with the mixed oxide technique. The XRD patterns of the calcined powders of the PSLZT-PMnN group revealed the formation of pure perovskite phase during that stage of the thermal treatment. A typical XRD pattern belonging to this group is presented in Figure 5.4.

The green ceramic discs produced from these powders were sintered by a thermal schedule in which the heating and cooling rates were 4 °C/min, and the soaking was done at 1240 °C for 2 h.

Table 5.2 Chemical formulations of PZT samples.

Sample Designation	Sample Composition
1.0[PSLZT] - 0.0[PMnN]	$\text{Pb}_{0.94}\text{Sr}_{0.05}\text{La}_{0.01}[(\text{Zr}_{0.54}\text{Ti}_{0.46})_{0.9975}\text{O}_3]$
0.99[PSLZT] - 0.01[PMnN]	$0.99[\text{Pb}_{0.94}\text{Sr}_{0.05}\text{La}_{0.01}(\text{Zr}_{0.54}\text{Ti}_{0.46})_{0.9975}\text{O}_3] - 0.01[\text{Pb}(\text{Mn}_{1/3}\text{Nb}_{2/3})\text{O}_3]$
0.97[PSLZT] - 0.03[PMnN]	$0.97[\text{Pb}_{0.94}\text{Sr}_{0.05}\text{La}_{0.01}(\text{Zr}_{0.54}\text{Ti}_{0.46})_{0.9975}\text{O}_3] - 0.03[\text{Pb}(\text{Mn}_{1/3}\text{Nb}_{2/3})\text{O}_3]$
0.95[PSLZT] - 0.05[PMnN]	$0.95[\text{Pb}_{0.94}\text{Sr}_{0.05}\text{La}_{0.01}(\text{Zr}_{0.54}\text{Ti}_{0.46})_{0.9975}\text{O}_3] - 0.05[\text{Pb}(\text{Mn}_{1/3}\text{Nb}_{2/3})\text{O}_3]$
0.93[PSLZT] - 0.07[PMnN]	$0.93[\text{Pb}_{0.94}\text{Sr}_{0.05}\text{La}_{0.01}(\text{Zr}_{0.54}\text{Ti}_{0.46})_{0.9975}\text{O}_3] - 0.07[\text{Pb}(\text{Mn}_{1/3}\text{Nb}_{2/3})\text{O}_3]$
0.91[PSLZT] - 0.09[PMnN]	$0.91[\text{Pb}_{0.94}\text{Sr}_{0.05}\text{La}_{0.01}(\text{Zr}_{0.54}\text{Ti}_{0.46})_{0.9975}\text{O}_3] - 0.09[\text{Pb}(\text{Mn}_{1/3}\text{Nb}_{2/3})\text{O}_3]$
0.90[PSLZT] - 0.10[PMnN]	$0.90[\text{Pb}_{0.94}\text{Sr}_{0.05}\text{La}_{0.01}(\text{Zr}_{0.54}\text{Ti}_{0.46})_{0.9975}\text{O}_3] - 0.10[\text{Pb}(\text{Mn}_{1/3}\text{Nb}_{2/3})\text{O}_3]$
0.97[PSLZT] – 0.03[PMnN] 52/48	$0.97[\text{Pb}_{0.94}\text{Sr}_{0.05}\text{La}_{0.01}(\mathbf{Zr}_{0.52}\mathbf{Ti}_{0.48})_{0.9975}\text{O}_3] - 0.03[\text{Pb}(\text{Mn}_{1/3}\text{Nb}_{2/3})\text{O}_3]$
0.97[PSLZT] – 0.03[PMnN] 53/47	$0.97[\text{Pb}_{0.94}\text{Sr}_{0.05}\text{La}_{0.01}(\mathbf{Zr}_{0.53}\mathbf{Ti}_{0.47})_{0.9975}\text{O}_3] - 0.03[\text{Pb}(\text{Mn}_{1/3}\text{Nb}_{2/3})\text{O}_3]$
0.97[PSLZT] – 0.03[PMnN] 54/46	$0.97[\text{Pb}_{0.94}\text{Sr}_{0.05}\text{La}_{0.01}(\mathbf{Zr}_{0.54}\mathbf{Ti}_{0.46})_{0.9975}\text{O}_3] - 0.03[\text{Pb}(\text{Mn}_{1/3}\text{Nb}_{2/3})\text{O}_3]$
0.97[PSLZT] – 0.03[PMnN] 55/45	$0.97[\text{Pb}_{0.94}\text{Sr}_{0.05}\text{La}_{0.01}(\mathbf{Zr}_{0.55}\mathbf{Ti}_{0.45})_{0.9975}\text{O}_3] - 0.03[\text{Pb}(\text{Mn}_{1/3}\text{Nb}_{2/3})\text{O}_3]$
0.97[PSLZT] – 0.03[PMnN] 56/44	$0.97[\text{Pb}_{0.94}\text{Sr}_{0.05}\text{La}_{0.01}(\mathbf{Zr}_{0.56}\mathbf{Ti}_{0.44})_{0.9975}\text{O}_3] - 0.03[\text{Pb}(\text{Mn}_{1/3}\text{Nb}_{2/3})\text{O}_3]$
0.97[PSLZT] - 0.028[PMnN] – 0.002[PMS]	$0.97[\text{Pb}_{0.94}\text{Sr}_{0.05}\text{La}_{0.01}(\text{Zr}_{0.53}\text{Ti}_{0.47})_{0.9975}\text{O}_3] - 0.028[\text{Pb}(\text{Mn}_{1/3}\text{Nb}_{2/3})\text{O}_3] - 0.002[\text{Pb}(\text{Mn}_{1/3}\text{Sb}_{2/3})\text{O}_3]$
0.97[PSLZT] - 0.026[PMnN] - 0.004[PMS]	$0.97[\text{Pb}_{0.94}\text{Sr}_{0.05}\text{La}_{0.01}(\text{Zr}_{0.53}\text{Ti}_{0.47})_{0.9975}\text{O}_3] - 0.026[\text{Pb}(\text{Mn}_{1/3}\text{Nb}_{2/3})\text{O}_3] - 0.004[\text{Pb}(\text{Mn}_{1/3}\text{Sb}_{2/3})\text{O}_3]$
0.97[PSLZT] - 0.024[PMnN] - 0.006[PMS]	$0.97[\text{Pb}_{0.94}\text{Sr}_{0.05}\text{La}_{0.01}(\text{Zr}_{0.53}\text{Ti}_{0.47})_{0.9975}\text{O}_3] - 0.024[\text{Pb}(\text{Mn}_{1/3}\text{Nb}_{2/3})\text{O}_3] - 0.006[\text{Pb}(\text{Mn}_{1/3}\text{Sb}_{2/3})\text{O}_3]$

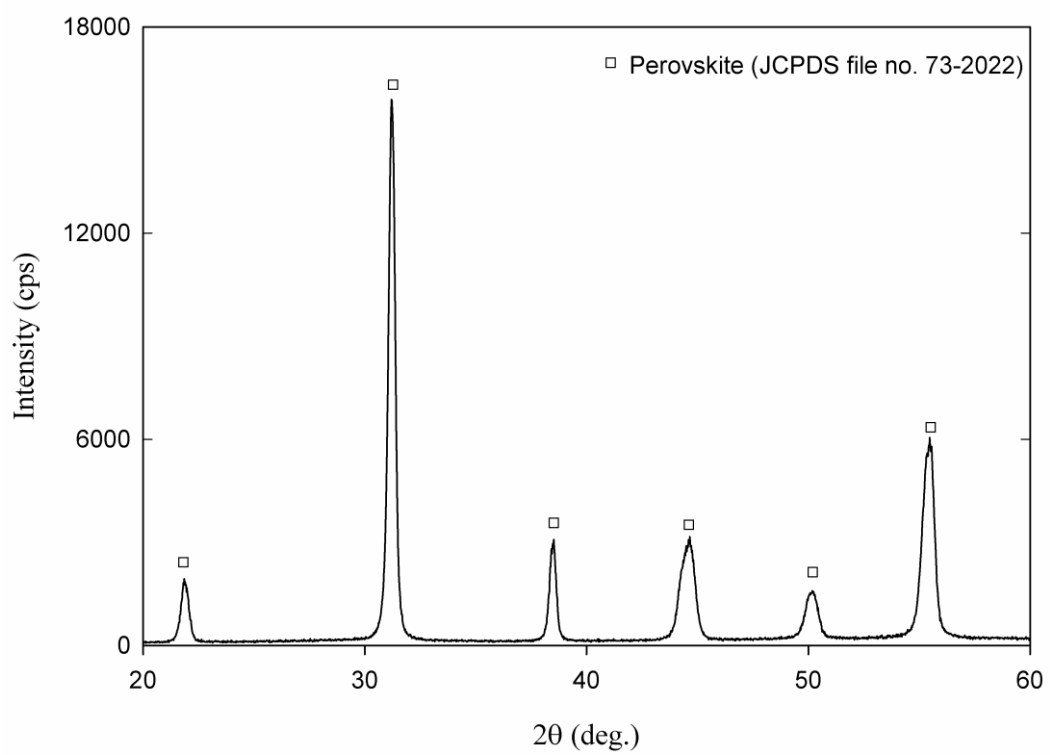


Figure 5.4 The XRD pattern of 0.97[PSLZT] - 0.03[PMnN] powder.

5.3 Results and Discussion

5.3.1 PMnN Addition

The data on physical and electrical properties of PSLZT-PMnN content are given in Table 5.3. PMnN addition was very effective on both the densification of the ceramics and their electromechanical properties. SEM images of thermally etched surfaces of PSLZT samples doped with $\text{Pb}(\text{Mn}_{1/3}\text{Nb}_{2/3})\text{O}_3$ are shown in Figure 5.5. The simultaneous doping of Mn^{2+} and Nb^{5+} refined the microstructure. As the amount of PMnN increased the microstructure became finer. The average grain size was decreased from approximately 4 μm to 1 μm when the PMnN addition was increased from 0.01 mole to 0.10 mole. The inhibition of grain growth is attributed to the greater difficulty of diffusion accompanying the lattice shrinkage caused by Mn. As a result of finer microstructure, the density of doped samples, which are tabulated in Table 5.3, reached to values of about 99 % TD.

Table 5.3 Physical and electrical properties of $(1-x)[\text{PSLZT}]-x[\text{PMnN}]$ ceramics.

x	0	0.01	0.03	0.05	0.07	0.09	0.10
d_{33} (pC/N)	640	645	660	550	490	455	440
k_p	0.56	0.54	0.60	0.59	0.56	0.51	0.52
Q_m	70	90	400	660	590	308	280
K^T	1800	2293	1940	1430	1282	1435	1546
$\tan \delta$ (%)	1.55	1.47	0.90	1.06	1.26	1.25	1.22
Density (% TD)	98.29 (± 0.07)	98.35 (± 0.08)	98.68 (± 0.06)	98.44 (± 0.07)	98.19 (± 0.08)	98.20 (± 0.06)	98.42 (± 0.07)
Open/Closed Porosity (vol%)	0.63/ 1.08	0.65/ 1.00	0.49/ 0.83	0.67/ 0.89	0.71/ 1.10	0.83/ 0.97	0.68/ 0.90

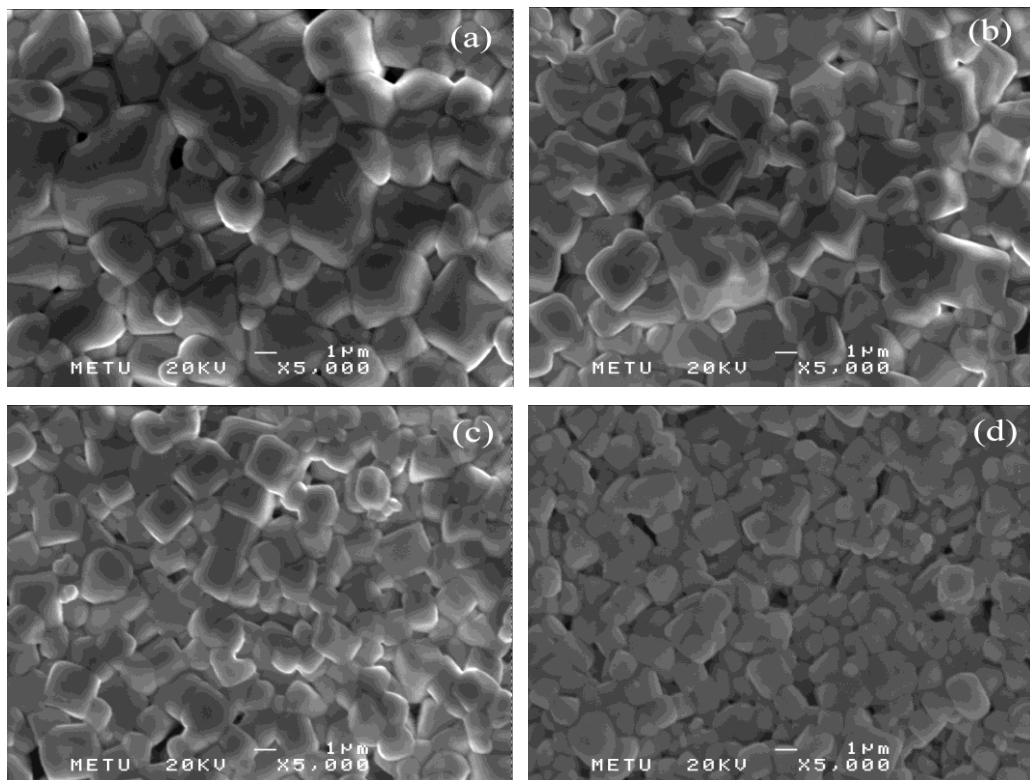


Figure 5.5 SEM micrographs of PSLZT samples doped with (a) 0.01, (b) 0.05, (c) 0.07 and (d) 0.10 mole PMnN.

The XRD patterns of PMnN doped PSLZT samples are shown in Figure 5.6. All of the samples had pure perovskite structure. The experimental diffraction lines of any MPB composition consisted of three separated peaks between 2θ values of 43° and 46° . Two of the peaks, with the intensity of the one being approximately half of the other, corresponded to the line splitting of the tetragonal phase and the third corresponded to the central peak of the rhombohedral phase. In order to resolve for the tetragonal and rhombohedral fractions, Peakfit v4.0 software was used to deconvolute the peaks assuming Lorentzian line shape [75].

The results obtained by processing the peak intensities in Equation (4-1) are shown in Figure 5.7. The composition without the PMnN dopant was mainly tetragonal. PMnN doping into PSLZT caused an increase in rhombohedral fraction. On further increasing the PMnN dopant content beyond 0.06 mole the perovskite structure changed from tetragonal to rhombohedral symmetry. It was concluded from these results that the $(\text{Mn}_{1/3}\text{Nb}_{2/3})$ doping in the B-site of the formulation of these ceramics shifted the MPB to the Ti-rich region. The incorporation of Mn into B-site of perovskite structure stabilized the rhombohedral phase against the tetragonal one [12].

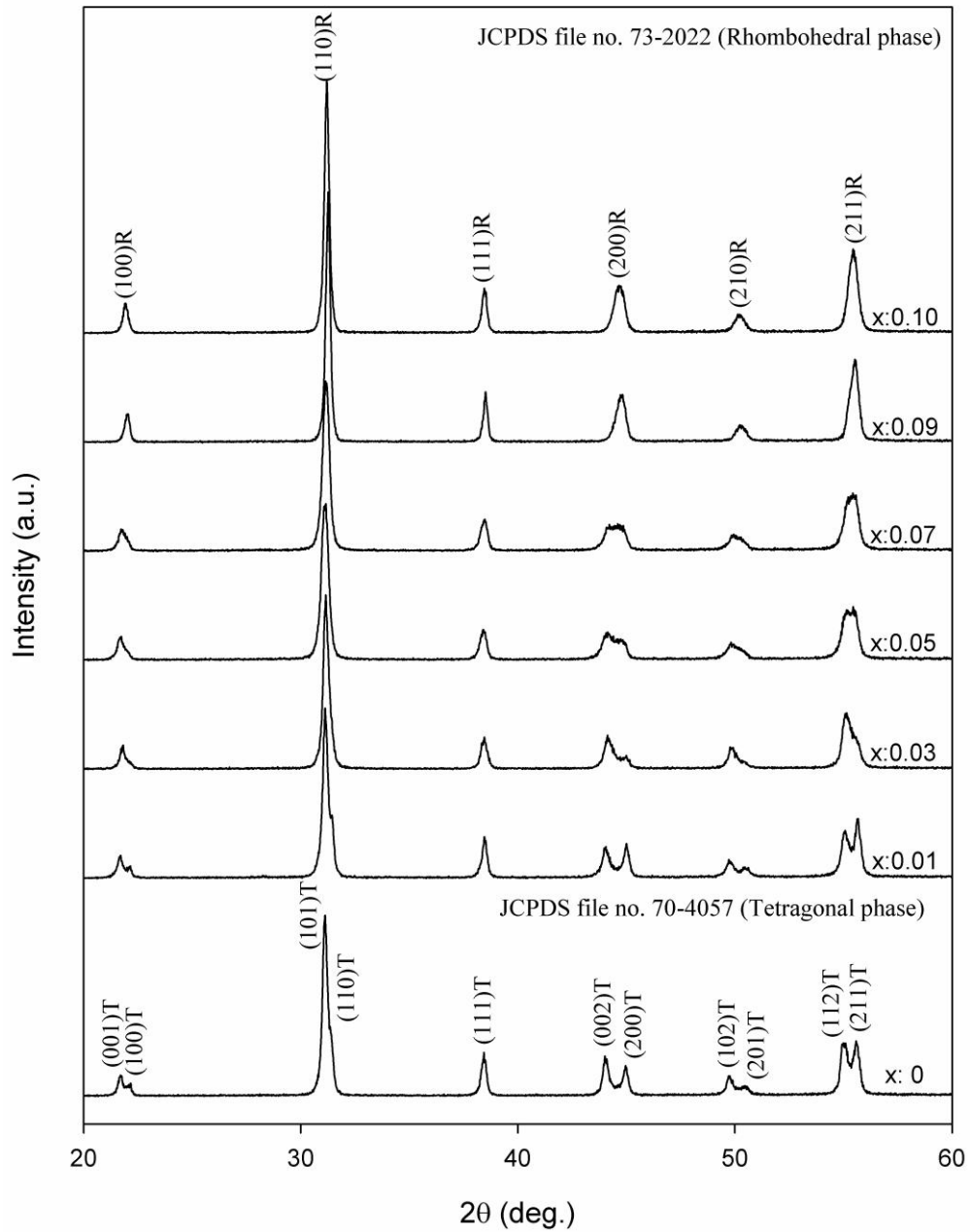


Figure 5.6 The XRD patterns of $(1-x)[\text{PSLZT}]-x[\text{PMnN}]$ samples. The values of x in the figure indicate the PMnN content in the PSLZT-PMnN.

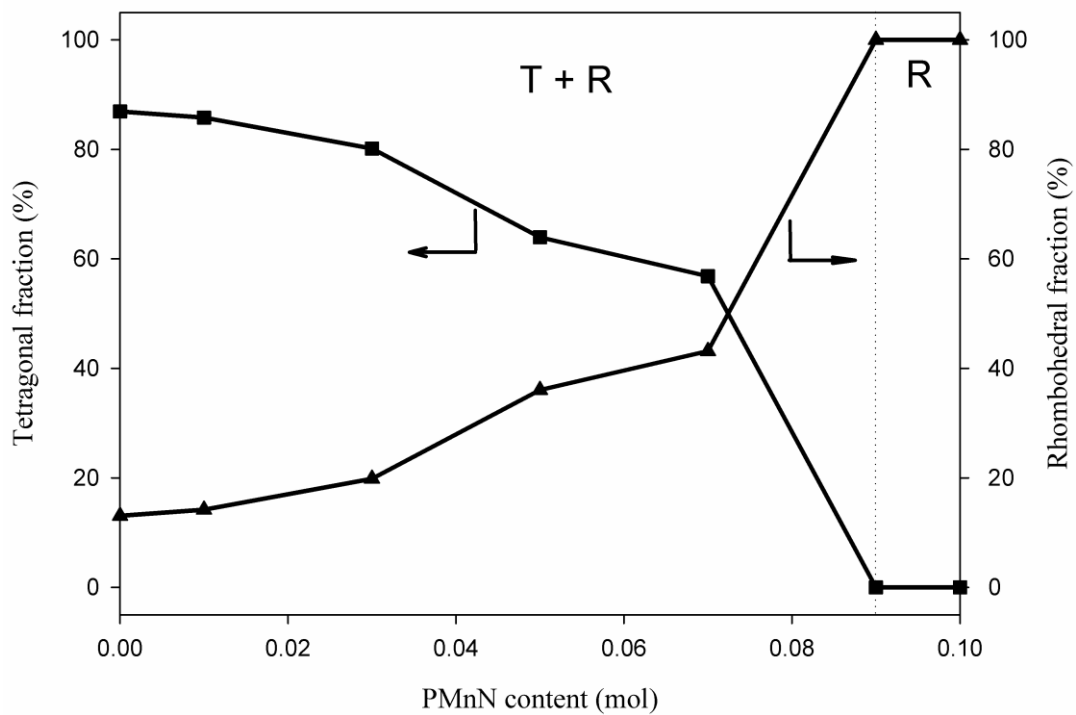


Figure 5.7 Relative proportions of tetragonal and rhombohedral modifications in [PSLZT] – [PMnN] ceramics with varying PMnN content.

The effect of Mn^{2+} and Nb^{5+} doping on the dielectric and piezoelectric properties of PSLZT-based ceramics were examined. The variation in these properties as a function of $\text{Pb}(\text{Mn}_{1/3}\text{Nb}_{2/3})\text{O}_3$ content were given in Table 5.3. Obviously, additions of PMnN caused rather interesting changes in electromechanical properties which could be attributed to the conflicting individual effects exerted by Mn^{2+} and Nb^{5+} .

The variations in the electromechanical properties of PSLZT ceramics doped with PMnN are also shown graphically in Figure 5.8 and Figure 5.9. Piezoelectric strain constant, d_{33} , electromechanical coupling factor, k_p and dielectric constant, K^T , reached to their maximum values when PMnN addition is increased from 0.01 to 0.03 mole. PMnN addition into PSLZT caused a transition from tetragonal phase dominant region to a tetragonal- rhombohedral coexistence region and finally to single rhombohedral phase as previously given in Figure 5.7. Since the activation energy for domain motion is low near the two coexisting phases, the compositions near that region between 0.01 and 0.03 mole PMnN exhibited higher piezoelectric and dielectric values as shown in Figure 5.8.

In Figure 5.9, mechanical quality factor, Q_m , and tangent loss, $\tan \delta$, changed in almost the opposite sense with increasing amount of PMnN. Dielectric loss shows higher values for undoped and 0.01 mole PMnN doped compositions in which the tetragonal and rhombohedral phases coexisted. On the other hand, as expected, mechanical quality factor exhibited lower values at this level of doping. Further doping caused Q_m to increase and reach the maximum value at 0.05 mole PMnN. This effect can be correlated to the decreasing grain size of ceramics with PMnN addition. In addition to the phase coexistence, the domain wall motion is also affected by the grain size. Since grain boundaries act as additional pinning points, the domain wall motion is inhibited as the grain size decreased [29]. After reaching the highest value of 660, the Q_m value decreased upon doping with PMnN beyond 0.05 mole. At this level of doping, the phase constitution of the ceramic is dominant over the grain size and Q_m value decreased to 280 towards the single rhombohedral phase region.

The ceramics designated as 0.97[PSLZT] - 0.03[PMnN] displayed the highest d_{33} values coupled with a large k_p and low $\tan \delta$. Therefore, despite the higher Q_m values attained with 0.05[PMnN] and 0.07[PMnN], the one having 0.03[PMnN] was chosen as the optimized composition. The examination of changes in dielectric and piezoelectric properties of doped PSLZT samples leads to the determination of optimum composition as 0.97[PSLZT] - 0.03[PMnN] with maximum d_{33} and k_p values of 660 pC/N and 0.60, respectively. This composition also exhibits high Q_m (400) and dielectric constant (1940) values and a low loss tangent value of 0.90%.

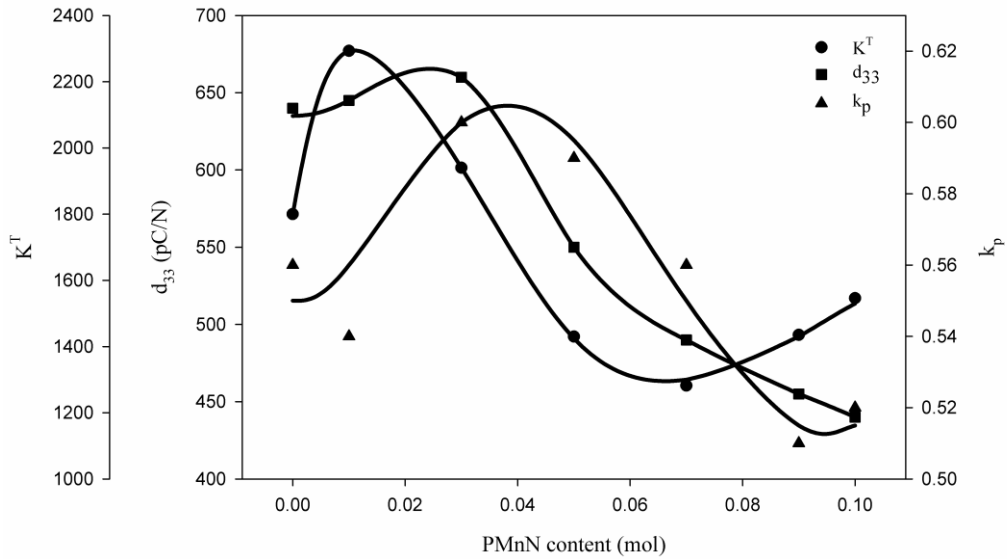


Figure 5.8 Variation of piezoelectric and dielectric properties as a function of PMnN doping.

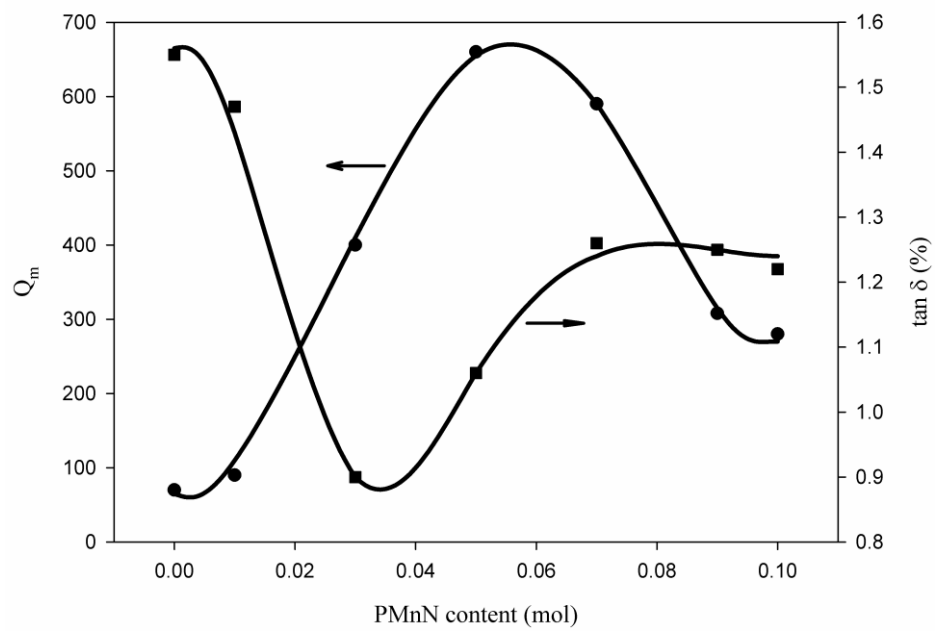


Figure 5.9 Variation of mechanical quality factor and loss tangent value as a function of PMnN doping.

Figure 5.10 shows the polarization versus field hysteresis loops for undoped and PMnN-doped PSLZT samples. The square-like hysteresis loop of PSLZT sample became round or “propeller-shaped” with an increase in PMnN doping. This change in the shape of loop is related to the defect dipoles which inhibit the orientation of the ferroelectric domains leading to “pinched” hysteresis loops. These pinched loops are typical of the hard piezoelectrics [82]. The defect dipoles are formed by acceptor ions and oxygen vacancies. However, it is unlikely to have oxygen vacancies in PSLZT-PMnN ceramics since the $(\text{Mn}_{1/3}\text{Nb}_{2/3})^{4+}$ ion substitution for Ti^{4+} or Zr^{4+} in B-site of the chemical formulation leads to no valent compensation. But the oxygen vacancies may be produced due to loss of oxygen from the crystal lattice during sintering at high temperature. Li et al. [82] proposed that there may be some preferable substitutions of B-site ions by the Mn^{2+} ions which also leads to the formation of oxygen vacancies.

The oxygen vacancies trapped on the domain walls pin the domain orientation causing round hysteresis loop and increases the mechanical quality factor, Q_m [67]. In Figure 5.10 the coercive field and remanance polarization values decreased upto 0.05 mole PMnN doping and increased again beyond this point. This is in good agreement with the change in Q_m values with PMnN addition. It increased to a maximum value of 660 for 0.05 mole PMnN and decreased again with further doping. The decrease in grain size is also believed to be effective on the domain orientation since grain boundaries act as pinning sites for domain wall movement. As far as the ceramic system studied is concerned, the grain size decreased with increasing PMnN-doping as shown in Figure 5.5; this caused the pinning of domain wall movement and decreased the remanent polarization values.

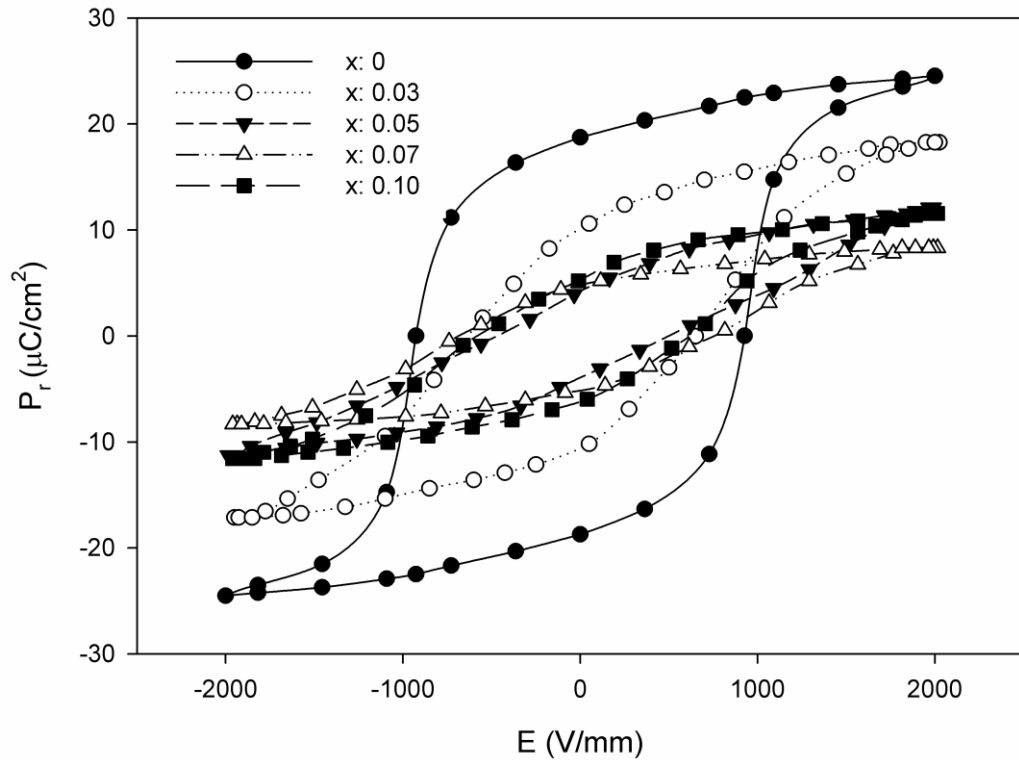


Figure 5.10 Ferroelectric hysteresis loops of $(1-x)[\text{PSLZT}]-x[\text{PMnN}]$ ceramics.

Figure 5.11 shows T_C as a function of $(\text{Mn}_{1/3}\text{Nb}_{2/3})$ doping in PSLZT ceramics. The peak values in dielectric constant correspond to the position of Curie temperature. With increasing $(\text{Mn}_{1/3}\text{Nb}_{2/3})$ addition, a reduction in both the Curie temperature and the dielectric constant of PSLZT-PMnN was observed and as a result the maximum dielectric constant value corresponding to the Curie temperature was shifted toward room temperature. The lowering of Curie temperature and dielectric constant can be attributed to the lattice shrinkage due to the formation of oxygen vacancies with Mn doping. The Curie temperature of PSLZT ceramic was 272°C and decreased to a value of 205°C at the maximum doping level of 0.10 PMnN.

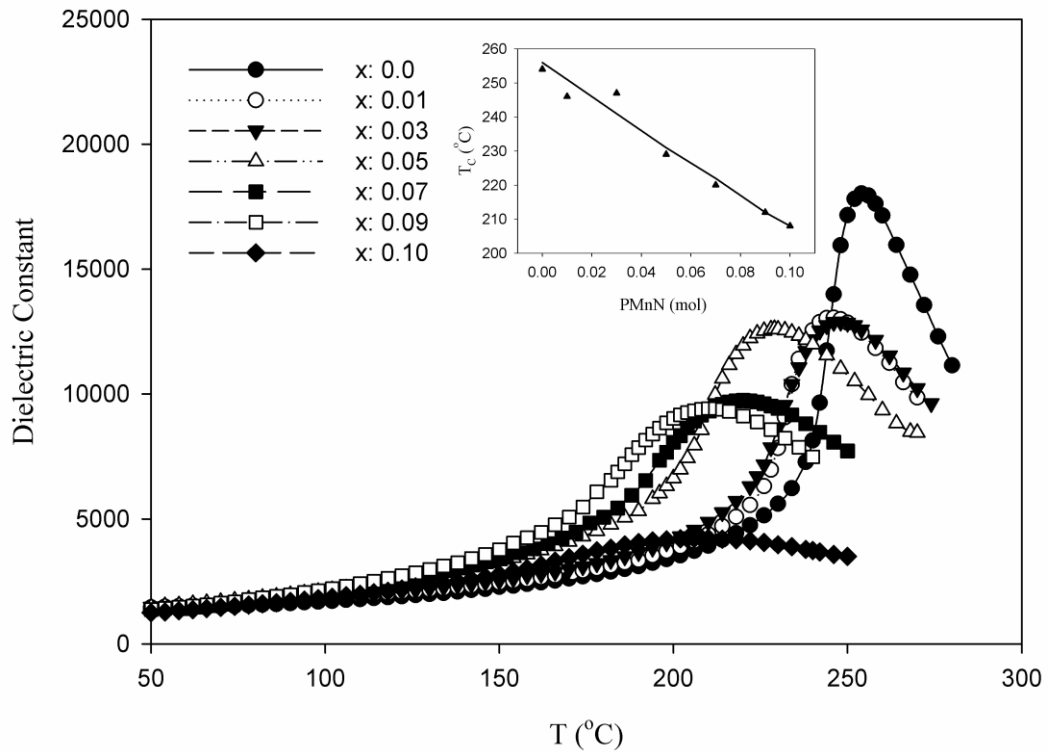


Figure 5.11 The change in the dielectric constant $(1-x)[\text{PSLZT}]-x[\text{PMnN}]$ ceramics with temperature.

5.3.2 Zr/Ti Ratio

This part of the study was performed in order to determine the new composition of the MPB which had shifted away from the Zr/Ti ratio of 54/46 because of the simultaneous Mn^{2+} and Nb^{5+} doping as mentioned in Section 5.3.1. For this purpose, the Zr/Ti ratio of the $0.97[\text{PSLZT}] - 0.03[\text{PMnN}]$ composition was altered between the values of 52/48 and 56/44. Various physical and electrical properties measured for these compositions are listed in Table 5.4. The values of %TD for the 0.03 mole PMnN doped PSLZT ceramics were all in excess of 98%. Hence good densification was obtained during sintering. The XRD patterns of the $0.97[\text{PSLZT}] - 0.03[\text{PMnN}]$ ceramics with varying Zr/Ti ratio are given in Figure

5.12. As the Zr/Ti ratio increased, a transition occurred from tetragonal to rhombohedral phase as shown in Figure 5.13. For the composition with the maximum Zr/Ti ratio of 56/44, the perovskite structure formed in completely rhombohedral symmetry.

Table 5.4 Physical and electrical properties of 0.97[PSLZT]-0.03[PMnN] ceramics with different Zr/Ti ratio.

Zr/Ti	52/48	53/47	54/46	55/45	56/44
d_{33} (pC/N)	560	690	660	585	510
k_p	0.57	0.63	0.60	0.57	0.57
Q_m	315	638	400	371	320
K^T	2006	2110	1940	1098	1164
$\tan \delta$ (%)	0.74	0.99	0.90	0.73	0.74
Density (%TD)	98.54 (± 0.05)	98.95 (± 0.07)	98.68 (± 0.06)	98.92 (± 0.06)	98.54 (± 0.04)
Open/Closed Porosity (vol%)	0.38/ 1.08	0.40/ 0.65	0.49/ 0.83	0.48/ 0.60	0.54/ 0.92

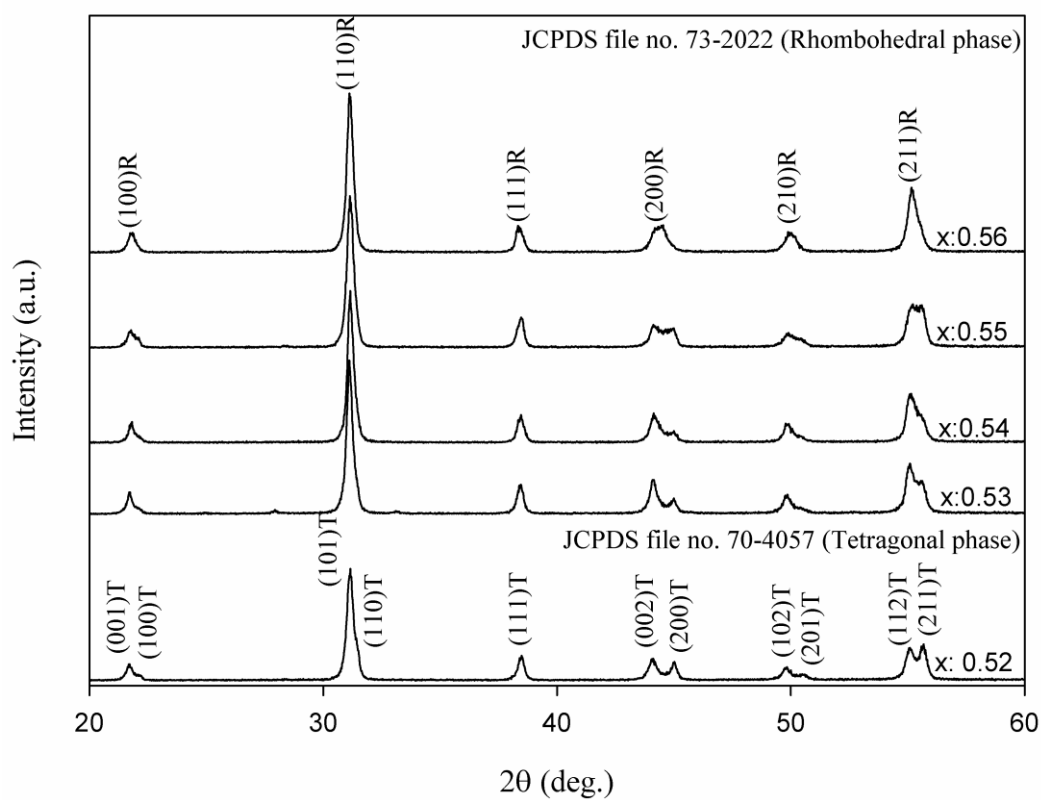


Figure 5.12 The XRD patterns of $0.97[\text{Pb}_{0.94}\text{Sr}_{0.05}\text{La}_{0.01}(\text{Zr}_x\text{Ti}_{1-x})_{0.9975}\text{O}_3]-0.03[\text{Pb}(\text{Mn}_{1/3}\text{Nb}_{2/3})\text{O}_3]$ samples. The values of x in the figure indicate the Zr content in the $0.97[\text{PSLZT}]-0.03[\text{PMnN}]$.

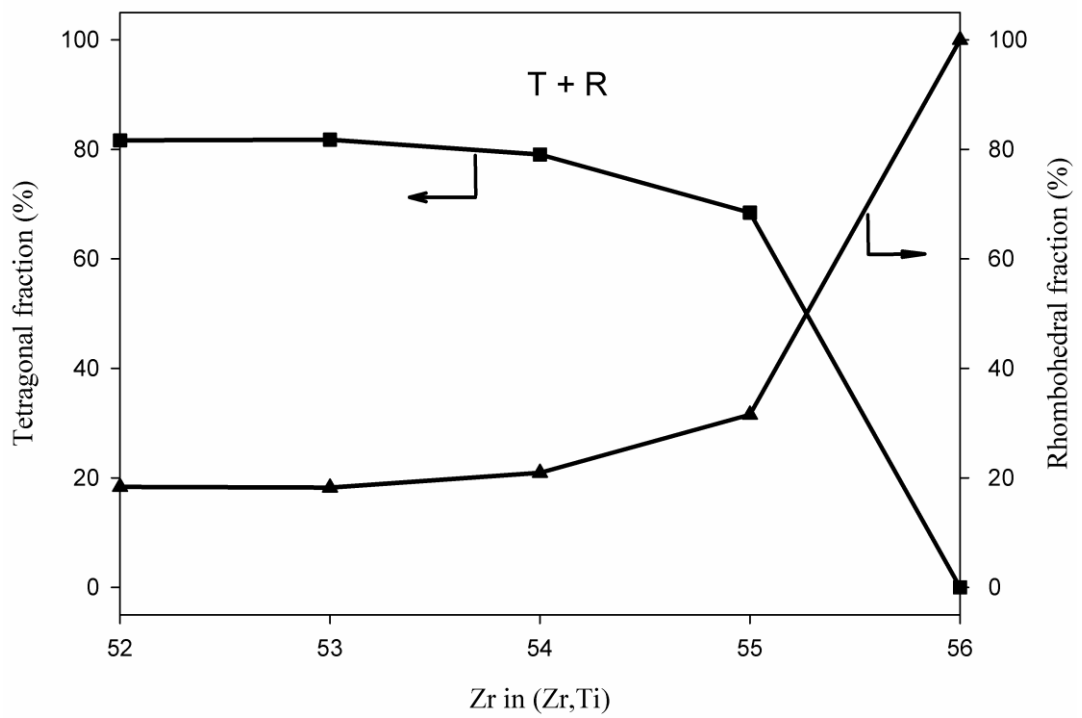


Figure 5.13 Relative proportions of tetragonal and rhombohedral modifications in 0.97[PSLZT]-0.03[PMnN] ceramics with varying Zr/Ti ratio.

The data for the electrical properties in Table 5.4 are presented also graphically in Figure 5.14 and Figure 5.15. The maximum values of $d_{33} = 690$ pC/N and $k_p = 0.63$ were obtained at $x = 0.53$. It is the result of coexistence of tetragonal and rhombohedral phases at this composition. The coexistence region provides highest number of possible polarization directions arising from 6 in tetragonal and 8 in rhombohedral phases. The dielectric constant and mechanical quality factor were also maximized at this particular composition. Combining these results with the x-ray studies, it can be concluded that the morphotropic phase boundary of 0.97[PSLZT] – 0.03[PMnN] ceramics was at the Zr/Ti ratio of 53/47.

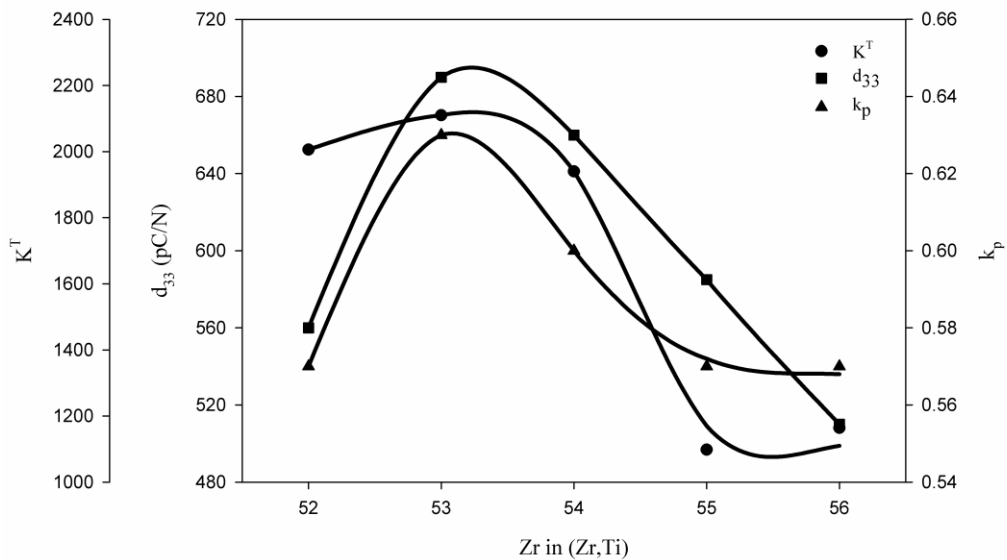


Figure 5.14 Variation of piezoelectric strain coefficient, dielectric constant and coupling factor as a function of Zr/Ti ratio in 0.97[PSLZT]-0.03[PMnN] ceramics.

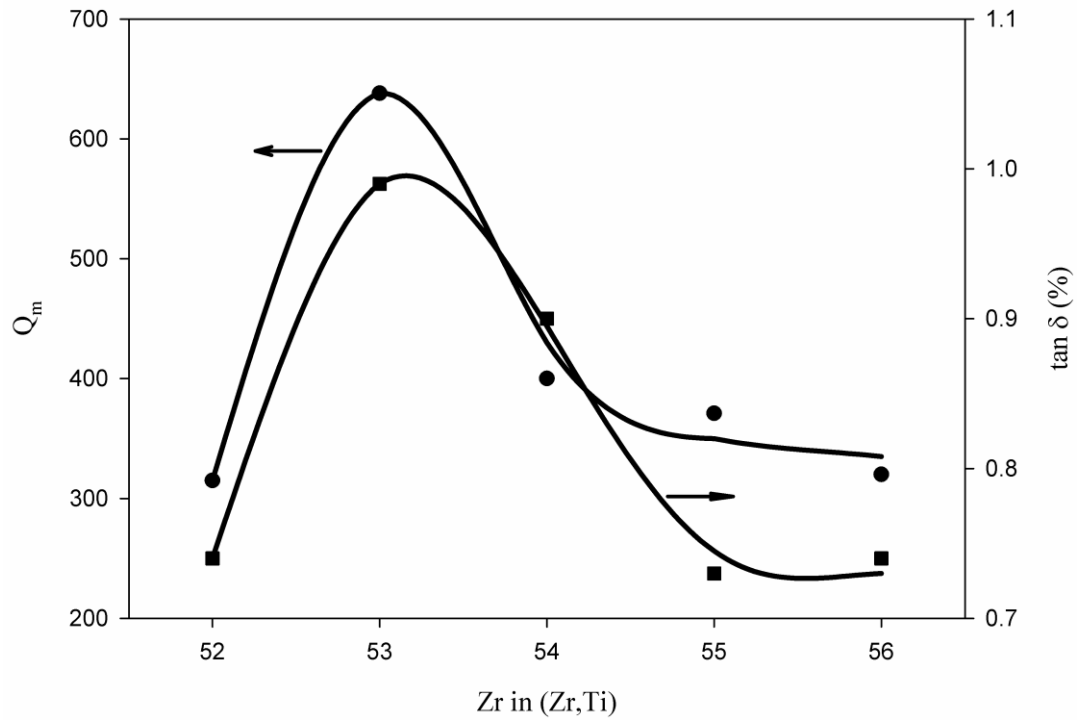


Figure 5.15 Variation of mechanical quality factor and loss tangent as a function of Zr/Ti ratio in 0.97[PSLZT]-0.03[PMnN] ceramics.

Figure 5.16 shows the change in Curie temperature of 0.97[PSLZT] – 0.03[PMnN] ceramics with varying Zr/Ti ratio. The maximum peak temperature (T_C) decreased only slightly as the Zr/Ti ratio was increased. Curie temperature of the composition 52/48 was 252 °C and decreased to 245 °C as the Zr/Ti ratio reached to 55/45.

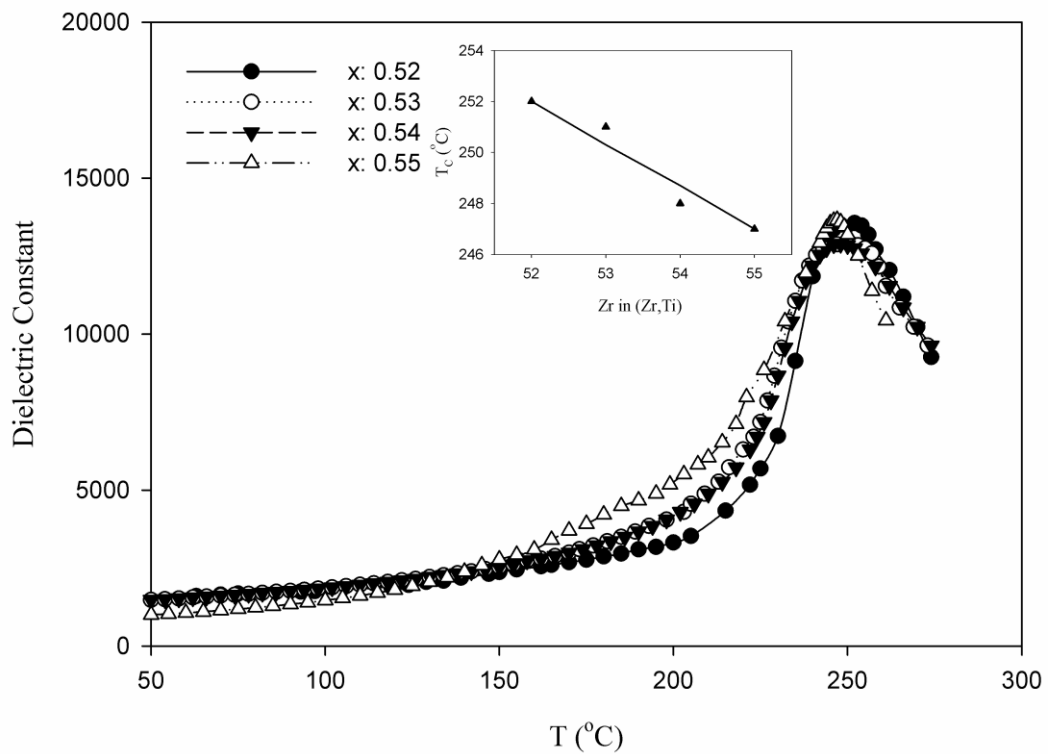


Figure 5.16 The change in the dielectric constant of $0.97[\text{Pb}_{0.94}\text{Sr}_{0.05}\text{La}_{0.01}(\text{Zr}_x\text{Ti}_{1-x})_{0.9975}\text{O}_3]-0.03[\text{Pb}(\text{Mn}_{1/3}\text{Nb}_{2/3})\text{O}_3]$ ceramics with temperature.

5.3.3 PMS Addition

The $0.97[\text{PSLZT}] - 0.03[\text{PMnN}]$ ceramic with Zr/Ti ratio of 53/47, being the MPB composition, was further doped with $\text{Pb}((\text{Mn}_{1/3}\text{Sb}_{2/3})\text{O}_3)$ (PMS) in order to obtain higher Q_m values. The dielectric, piezoelectric and physical properties of $0.97[\text{PSLZT}] - 0.03[\text{PMnN}]$ based samples doped with different amounts of PMS are given in Table 5.5. The %TD values in excess of ~99% indicate the good densification during sintering process. The dielectric constant, K^T , electromechanical coupling factor, k_p and piezoelectric constant, d_{33} decreased,

whereas the mechanical quality factor, Q_m , increased with increasing amount of PMS in the system.

Table 5.5 Physical and electrical properties of 0.97[PSLZT]-(0.03-y)[PMnN]-(y)[PMS] ceramics with different Zr/Ti ratio.

y	0	0.002	0.004	0.006
d_{33} (pC/N)	690	650	590	540
k_p	0.63	0.58	0.56	0.57
Q_m	638	892	1005	1240
K^T	2110	1986	1934	1913
$\tan \delta$ (%)	0.99	0.79	0.82	0.89
Density (%TD)	98.95 (± 0.07)	98.88 (± 0.06)	99.00 (± 0.05)	99.12 (± 0.06)
Open/Closed Porosity	0.40/0.65	0.36/0.76	0.40/0.60	0.36/0.52

SEM images of PSLZT-PMnN-PMS ceramics with different PMS content are given in Figure 5.17. The increase in PMS content from 0.002 mole to 0.006 mole resulted in a decrease in grain size from approximately 3.2 to approximately 1.6 μm , respectively.

XRD patterns of 0.97[PSLZT] - 0.03[PMnN] ceramics modified by PMS are depicted in Figure 5.18. The results show that all ceramic specimens had pure perovskite structure. The dominant phase was tetragonal for all the samples. As seen in Figure 5.19, addition of 0.006 mole PMS into this ceramic composition caused a ~5 vol% decrease in the fraction of tetragonal phase.

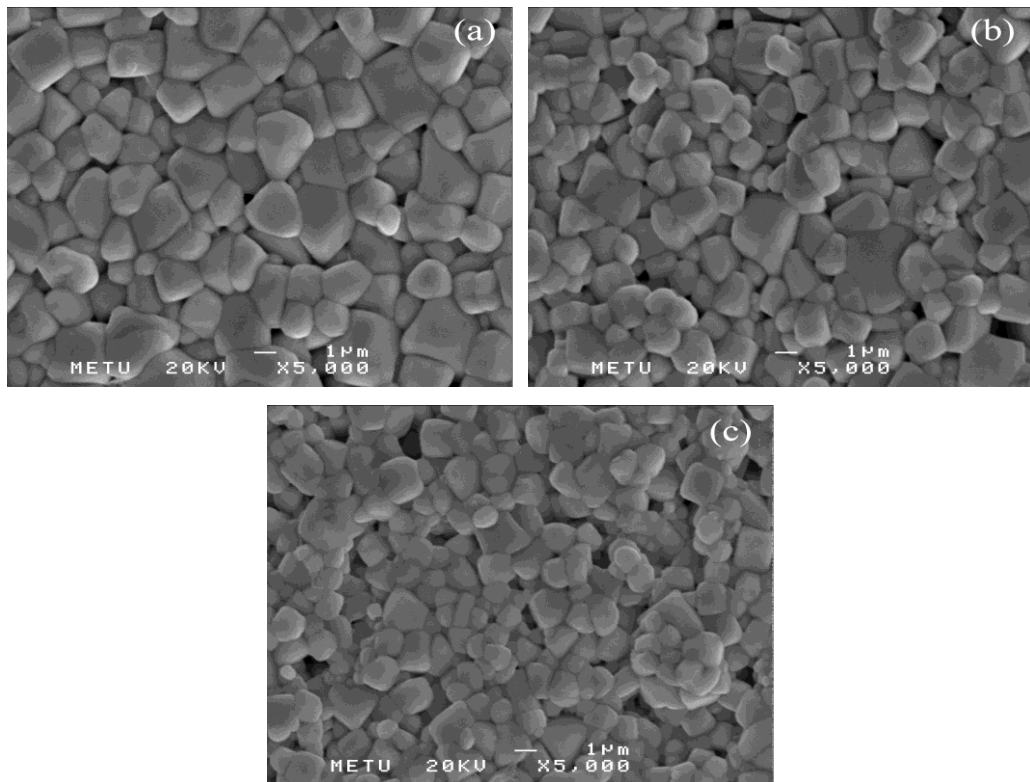


Figure 5.17 SEM micrographs of PSLZT-PMnN-PMS samples:

(a) 0.97[PSLZT]-0.028[PMnN]-0.002[PMS],

(b) 0.97[PSLZT]-0.026[PMnN]-0.004[PMS],

(c) 0.97[PSLZT]-0.024[PMnN]-0.006[PMS].

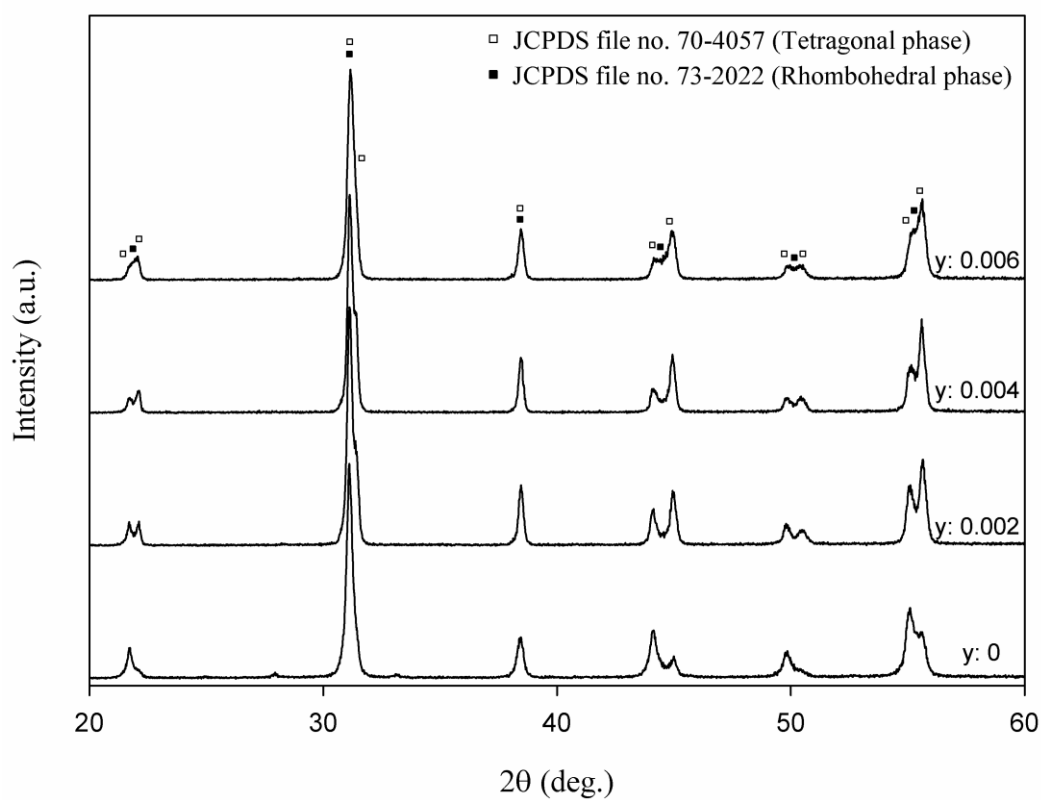


Figure 5.18 XRD patterns of $0.97[\text{PSLZT}]-(0.03-y)[\text{PMnN}]-y[\text{PMS}]$ samples sintered at $1240\text{ }^{\circ}\text{C}$ for 2h. The values of y in the figure indicate the PMS content in the PSLZT-PMnN-PMS.

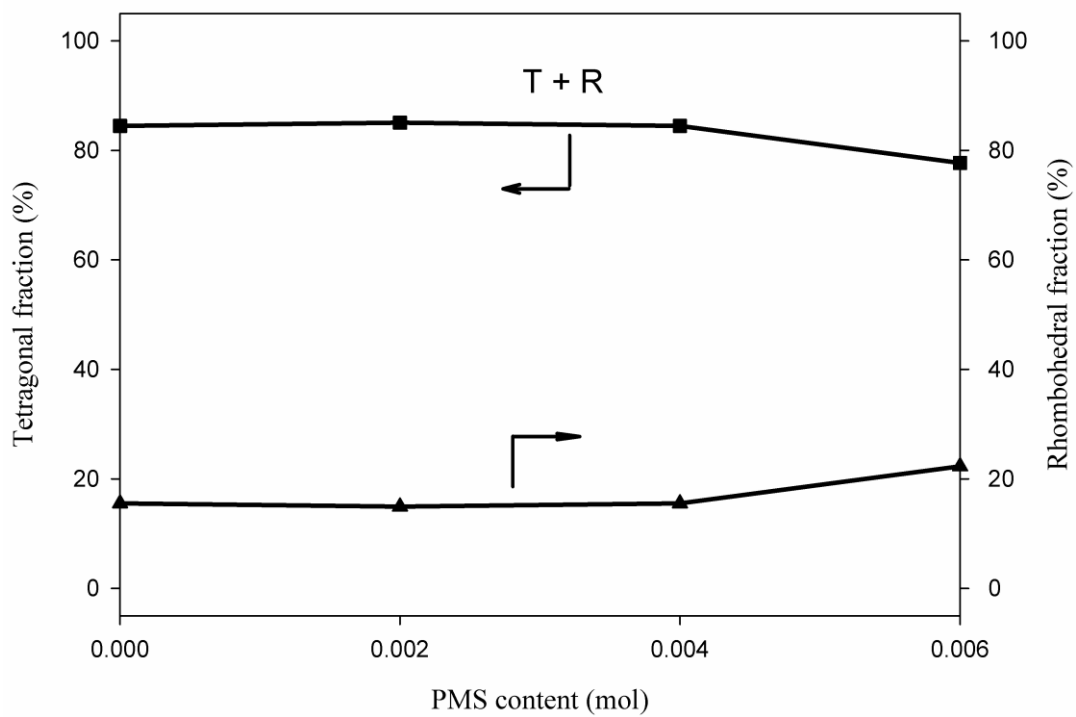


Figure 5.19 Variations of relative contents of tetragonal and rhombohedral phases with the amount of PMS doping.

The variation in electrical properties of the samples with the amount of PMS dopant is shown in Figure 5.20 and Figure 5.21. As the amount of PMS increased the dielectric constant and d_{33} values decreased. On the other hand, mechanical quality factor reached to a maximum value of 1240 at 0.006 mole PMS. This opposite variation of Q_m and d_{33} is due to the decreasing grain size with increasing PMS as shown in Figure 5.17. Smaller grain size leads to more grain boundaries which in turn provide more domain walls. The higher the amount of domain walls, the higher the internal friction in the ceramic during domain movement. This causes higher mechanical quality factor whereas piezoelectric strain constant, dielectric constant and coupling factor values decreased due to the difficult domain motion. However, electromechanical coupling factor, k_p , value of 0.57 at 0.006 mole PMS doping is still quite a good value for hard-drive applications of piezoelectric ceramics.

Figure 5.22 shows P-E hysteresis curves of specimens according to the amount of PMS addition. PMS substitution caused a rapid decrease in remanent polarization whereas it led an increase in the coercive field values. Since the piezoelectric strain coefficient, d_{33} , of a piezoelectric ceramic is proportional to its remanent polarization value, d_{33} values given in Table 5.5 decreased monotonously with increasing PMS content. On the other hand, high coercive electric field value is a characteristic of hard type piezoelectric ceramics. This is also reflected in the increasing Q_m values of the ceramics with increasing PMS addition.

The variation of dielectric constant with temperature was illustrated for 0.97[PSLZT] – (0.03-y)[PMnN] – (y)[PMS] compositions in Figure 5.23. PMS addition had a negative effect on the Curie temperature. The T_C of the $y = 0.006$ composition, having the optimum electrical properties, was 235 °C.

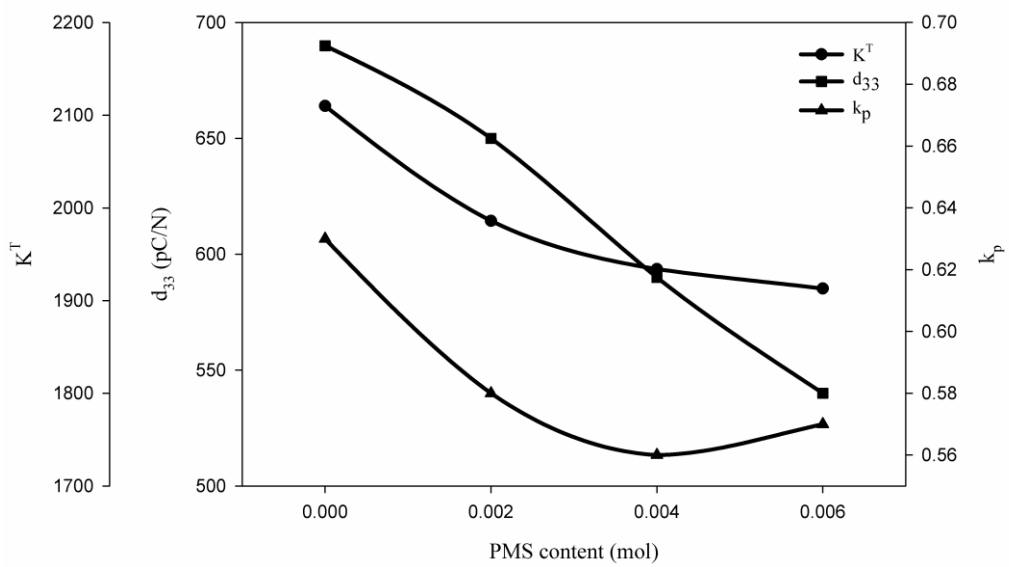


Figure 5.20 Variation of piezoelectric strain coefficient, dielectric constant and coupling factor as a function of PMS additions.

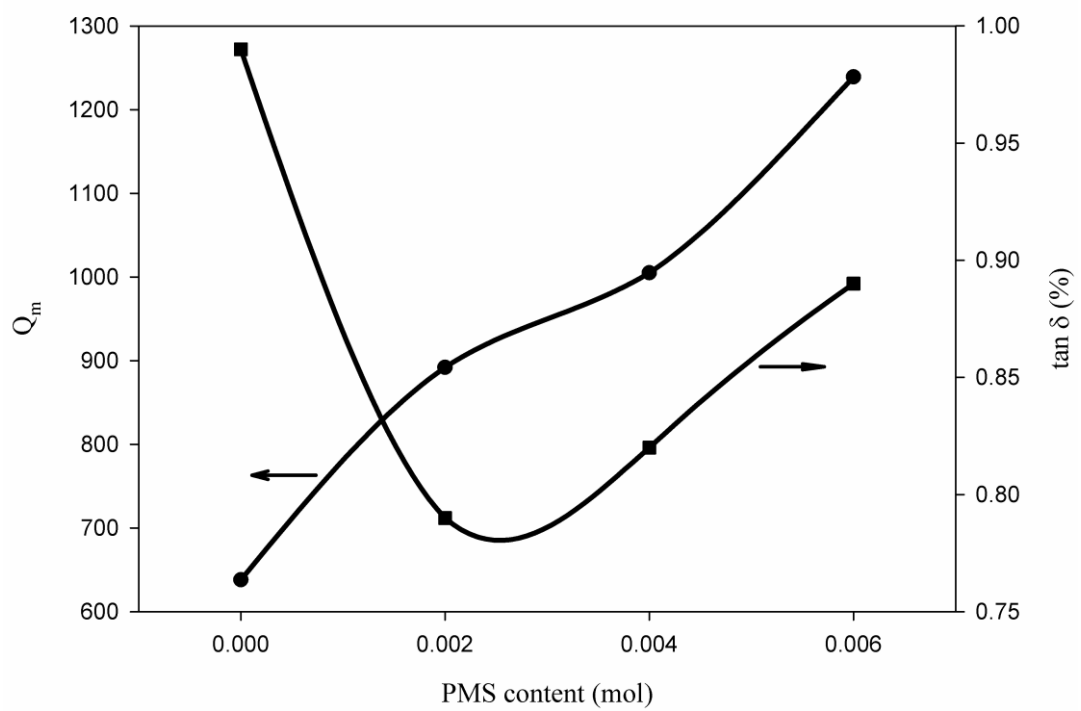


Figure 5.21 Variation of mechanical quality factor and loss tangent as a function of PMS additions.

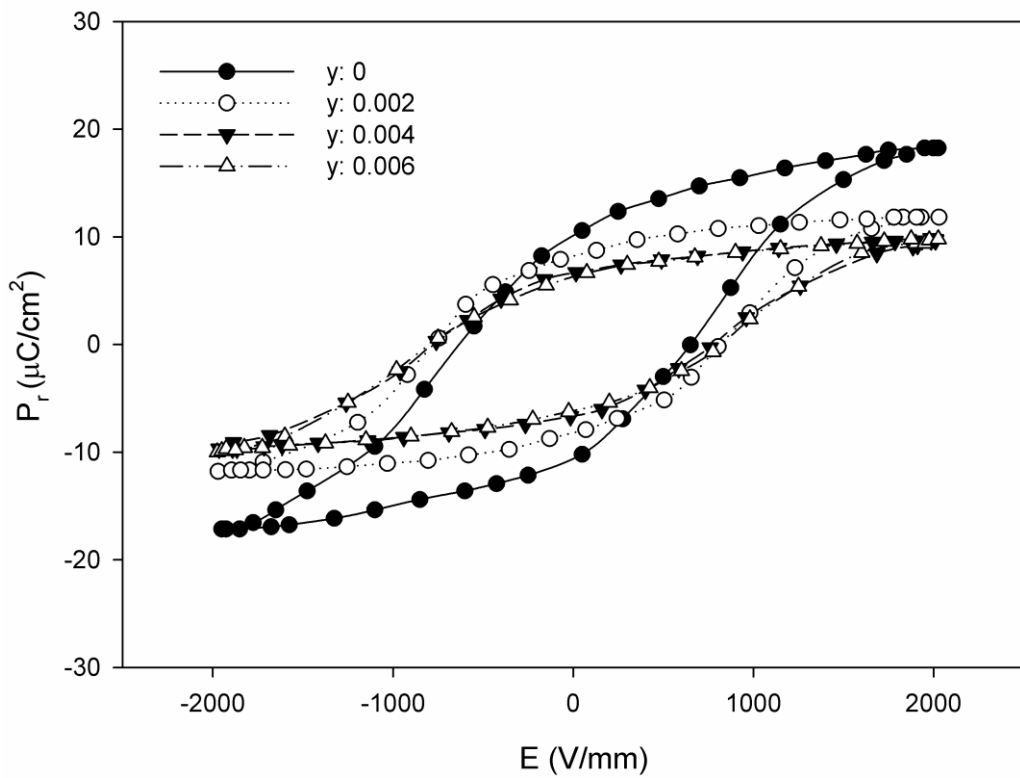


Figure 5.22 Ferroelectric hysteresis loops of 0.97[PSLZT]-(0.03- y)[PMnN]-(y)[PMS] ceramics.

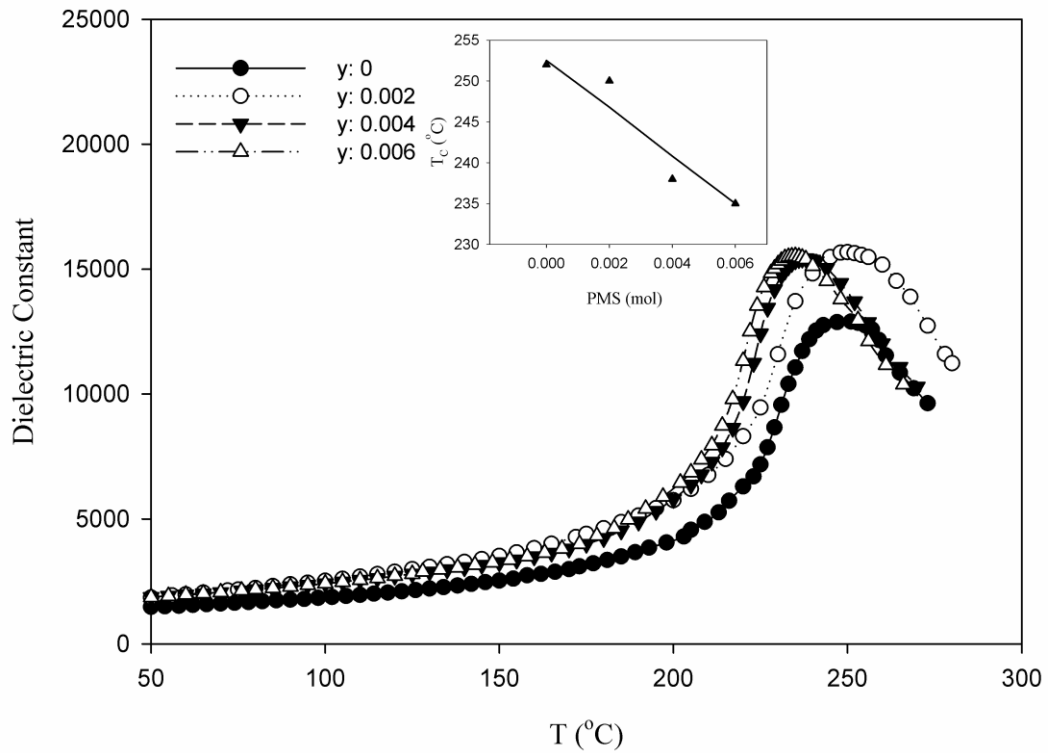


Figure 5.23 Variation of dielectric constant of 0.97[PSLZT]-(0.03-y)[PMnN]-(y)[PMS] ceramics with temperature.

The results obtained on [PSLZT] – [PMnN] – [PMS] ceramics in the present thesis study compare quite favorably with the electromechanical data obtained in earlier studies [77, 78]. For example, in the $\text{Pb}_{0.98}\text{Sr}_{0.02}(\text{Mn}_{1/3}\text{Sb}_{2/3})_y\text{Zr}_z\text{Ti}_{1-y-z}\text{O}_3$ ceramics, Zhu et al. [77] reported $d_{33}=374$ pC/N, $Q_m=1250$, and $k_p=0.6$. The compositional parameters y and z were not disclosed. Hong-liang and coworkers [78] reported $d_{33}=230$ pC/N, $Q_m=1520$, $K^T=675$ and $k_p=0.66$ for a $\text{Pb}(\text{Mn}_{1/3}\text{Sb}_{2/3})\text{O}_3$ -PZT ceramic with PMS content of 0.06 mole. With increasing PMS content their d_{33} values declined sharply.

As previously mentioned, it is desirable for PZT-based ceramics to combine high values of Q_m (>1000), d_{33} (>300 pC/N) and k_p (>0.5) for use in hard-drive

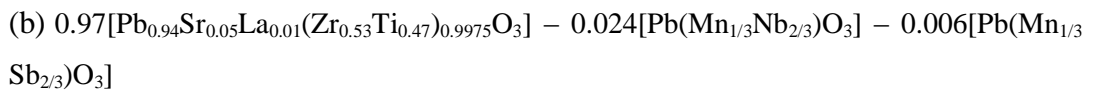
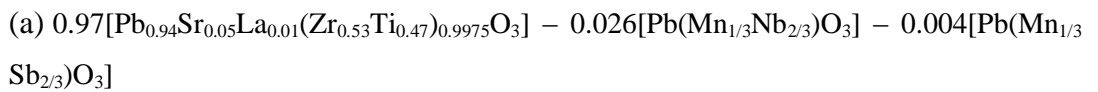
application areas. The samples doped with 0.004 and 0.006 moles of [PMS] in the present study possess the desired values of piezoelectric and dielectric properties. Hence, they are good candidates for high power electromechanical applications like ultrasonic motors.

5.4 Conclusions of the PSLZT Ceramics Modified by Mn, Nb and Sb

1. The PSLZT ceramic of composition $\text{Pb}_{0.94}\text{Sr}_{0.05}\text{La}_{0.01}(\text{Zr}_{0.54}\text{Ti}_{0.46})_{0.9975}\text{O}_3$ was modified with multiple dopants of Mn, Nb, and Sb in order to develop PZT ceramics suitable for use in piezoelectric motors.

2. Mn and Nb were introduced to the B-site of the PSLZT in accordance with the stoichiometry ($\text{Mn}_{1/3}\text{Nb}_{2/3}$) so that the total site charge remained as 4^+ . The PSLZT with 0.03 mole of $\text{Pb}(\text{Mn}_{1/3}\text{Nb}_{2/3})\text{O}_3$ per mole of the ceramic had a Q_m of 400 and d_{33} of 660 pC/N. With proper adjustment of the Zr/Ti ratio of 53/47 these parameters could be improved further to Q_m of 638 and d_{33} of 690 pC/N. The latter composition was on the MPB.

3. The Q_m values of PSLZT-PMnN ceramics could be enhanced drastically by introducing Mn and Sb to the MnN site of the PZT composition. Q_m values in excess of 1000 were attained by using PMS addition of 0.006 mole per mole of PZT. The specific compositions that could be used for piezoelectric motors were:



The attendant Q_m and d_{33} values were:

Ceramic (a): $Q_m = 1005$, $d_{33} = 590$ pC/N,

Ceramic (b): $Q_m = 1239$, $d_{33} = 540$ pC/N.

CHAPTER 6

ULTRASONIC MOTOR (USM) APPLICATION

6.1 Hard-Drive Applications and Requirements

Structural and electrical properties of piezoelectric ceramics have been broadly studied for many years. However, their usage in high-power/hard-drive devices, such as **ultrasonic motors**, was actively studied only in the last decade. The piezoelectric elements in these devices are electrically driven to high mechanical vibrations in the vicinity of their resonance frequencies. A piezoelectric ceramic which is intended to be used in hard-drive applications is desired to combine a high mechanical quality factor ($Q_m, > 1000$) with high piezoelectric constant ($d_{33}, > 200$ pC/N) and high electromechanical coupling coefficient ($k, > 0.5$) [5, 6].

For high-power applications, high Q_m is the most important requirement since it is the parameter of dissipation of energy during the transformation between the mechanical and electrical energies. If Q_m value is low, then the loss of energy in the materials will cause heat and then deteriorate the piezoelectric properties. So it is necessary to have a piezoelectric that exhibits a high Q_m value with high k_p and d_{33} . In order to satisfy these requirements of ultrasonic motor applications, many ternary and quaternary solid-solutions have been manufactured by chemical modifications [6].

6.2 Ultrasonic Motors

Ultrasonic motor is a type of motor in which ultrasonic vibration of piezoelectric element is utilized to gain a driving force, which then drives the motor using friction. The audible frequency range is between 50 Hz to 20 kHz. Sound waves with frequencies above 20 kHz are called ultrasonic waves. The use of piezoelectric ceramics as the source of ultrasonic vibration in ultrasonic motors was proposed in the early 1970s. Siemens and Matsushita Electrical Industries put this idea into practice between 1970 and 1972. In this applications, the amplitude of vibration was small and high torque and power values could not be obtained [1, 5].

In the ultrasonic motor, a voltage is applied to the piezoelectric ceramic element to generate alternating vibrations, either in the ceramic body or in an attached metal part. The magnitude of the oscillations is very small; of the order of 1 μm . The resonance effect of the ceramics in the ultrasonic range is utilized in order to obtain higher values.

The oscillations are mechanically adjusted in the USM to obtain rotational or linear movement. It is possible to obtain high speeds since the applied frequencies are very high, in the order of tens of kilohertz, although the magnitude of an individual cycle of the movement is of the order of micrometers.

The traveling wave ultrasonic motors appear as the new generation of ultrasonic motors, appropriate for many applications and their technology has received increasing interest in the last decades. Ultrasonic motors have been used in automated camera focusing systems, X-Y positioning systems, and in the drivers of watches while production of devices in transport and office automation systems is vigorously being researched [1, 97-99].

Piezoelectric motors provide very high torques at low speeds. The rotor part of the motor instantaneously clamps when the electrical power source is switched off. This is due to the high friction between the piezoelectric element and the attached

piece. This property makes the motor ideal for a variety of gearless positioning systems. As additional advantages of ultrasonic motors, there is no magnetic interference and the noise emission is low [99].

6.3 Operating Principle and Features

In order to drive the USM, initially an AC voltage is applied to one or more piezoelectric elements which in turn causes the elements begin to vibrate mechanically with a typical oscillation amplitude of $\sim 1 \mu\text{m}$ due to the converse piezoelectric effect. The key point of operation in the piezoelectric motors is the conversion of these vibrations into a smooth linear or rotary movement.

Several techniques have been developed for operation of ultrasonic motors, resulting in a variety of different motor types [100]. All these different types are based on a frictional driving principle. The piezoelectric ceramic element of the motor is generally called as vibrator. During operation, it is in physical contact with the moving part of the motor (rotor) and drives the latter via friction forces. In contrast, an air gap separates the stator and the rotor in conventional electrical motors.

Because of the ultrasonic driving frequencies, piezoelectric motors are often also named ultrasonic motors. In order to obtain high speeds and high mechanical output power, the piezo-motor has to be driven at an AC voltage of very high frequency. In practice, piezo-motors are operated at a certain resonant frequency of the stator vibrator. As a result, the driving frequency is directly related to the dimensions of the motor. This results in some upper limitation for the driving frequency. Practical operation frequencies are generally between 20 and 100 kHz, i.e., in the ultrasonic range. Since the sound waves of these frequencies are not audible for humans, ultrasonic motors exhibit low noise emission.

Operation of the motor at the resonant frequency of the piezoelectric element is mandatory in order to achieve high output power, high efficiency and low driving voltages. Large mechanical vibrations can be obtained with even small electric fields if the stator is driven in resonance. In non-resonant operation, the same amplitudes require much higher electric fields. PZT ceramics exhibit a hysteretic behavior due to their ferroelectric characteristic which leads to high dielectric power losses at very high field strengths. The corresponding rise in temperature leads to the degradation of the electrical properties and hence decreases the output power. At Curie temperature, the ceramic completely loses its piezoelectric properties. The Curie temperatures of PZT ceramics suitable for the use in motors are about 300 °C. The temperature limit for continuous motor operation is about the half of the Curie temperature [101].

Piezoelectric motors have several unique properties such as low leakage of magnetic flux, high output torque and large breaking torque due to the friction force between the stator and the rotor. The torque values are at least one order larger than conventional electromagnetic motors of the same size and weight which makes the production of self-breaking piezo-motors possible. The reduction gears can be eliminated from the transmission system due to the high output torque. This means a reduction in noise emission and the possibility to construct a high rigidity positioning system. Furthermore, unique shapes, such as disks or rings can be manufactured with ultrasonic motors that are very difficult to produce with conventional electromagnetic motors.

The motor construction on which the ceramic compositions tested was chosen as the metal tube motor developed by Uchino et al. [98]. The motor consists of a metal hollow cylinder, bonded with two PZT rectangular plates poled in the thickness direction. The assembly is shown in Figure 6.1(b). Stator of the motor is the brass metal tube and the rotor is the cylindrical rod with a pair of stainless ferrule pressed with a spring.

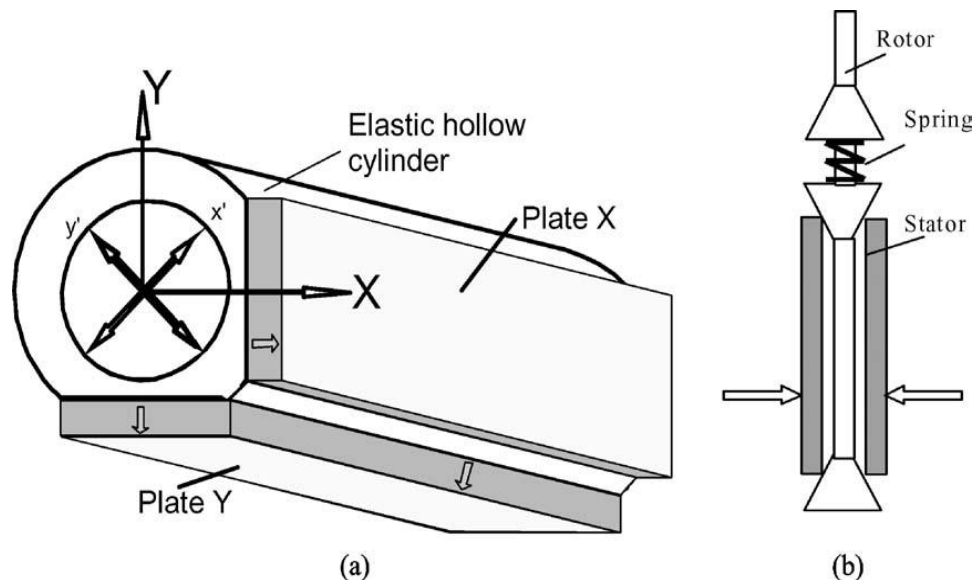


Figure 6.1 (a) Structure of the stator of metal tube motor and (b) assembly of the motor [98].

The operating principle of this motor is as follows: a bending vibration is induced along x axis when plate X in Figure 6.1a is electrically driven. Another bending mode is excited in perpendicular axis with some phase lag because of the asymmetrical plate Y which leads to an elliptical locus in a clock-wise direction as shown in Figure 6.2. On the contrary, a counter clock-wise movement is obtained when plate Y is driven. In order to drive the motor, only a single phase power supply is sufficient.

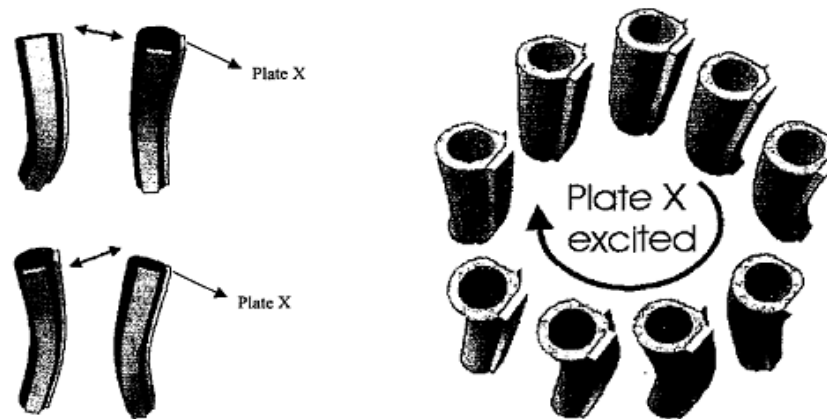


Figure 6.2 The wobbling and clock-wise motions obtained by driving plate X [100].

6.4 Experimental Procedure

A motor of same design in Figure 6.1 was constructed with different dimensions as shown in Figure 6.3. To drive the piezoelectric plates on the motor, a signal generator (Agilent 33120A) with a maximum output voltage of 10 V_{pp} and a piezo linear amplifier (Piezosystems EPA104-230) were used.

Motor parts were constructed with dimensions consistent with the values given in Figure 6.3. Stator part was made of brass whereas the rotor part was stainless steel. The photographs of the motor and its parts are shown in Figure 6.4.

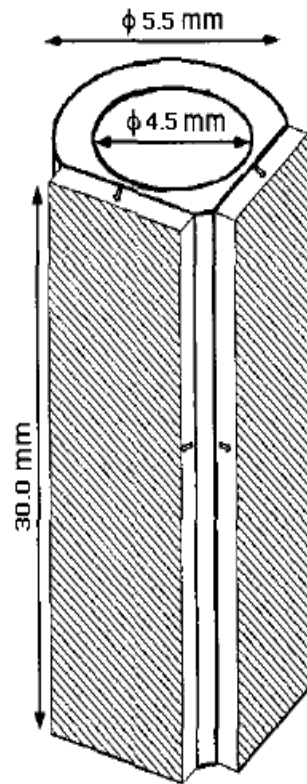


Figure 6.3 The dimensions of the stator of the metal tube motor [100].

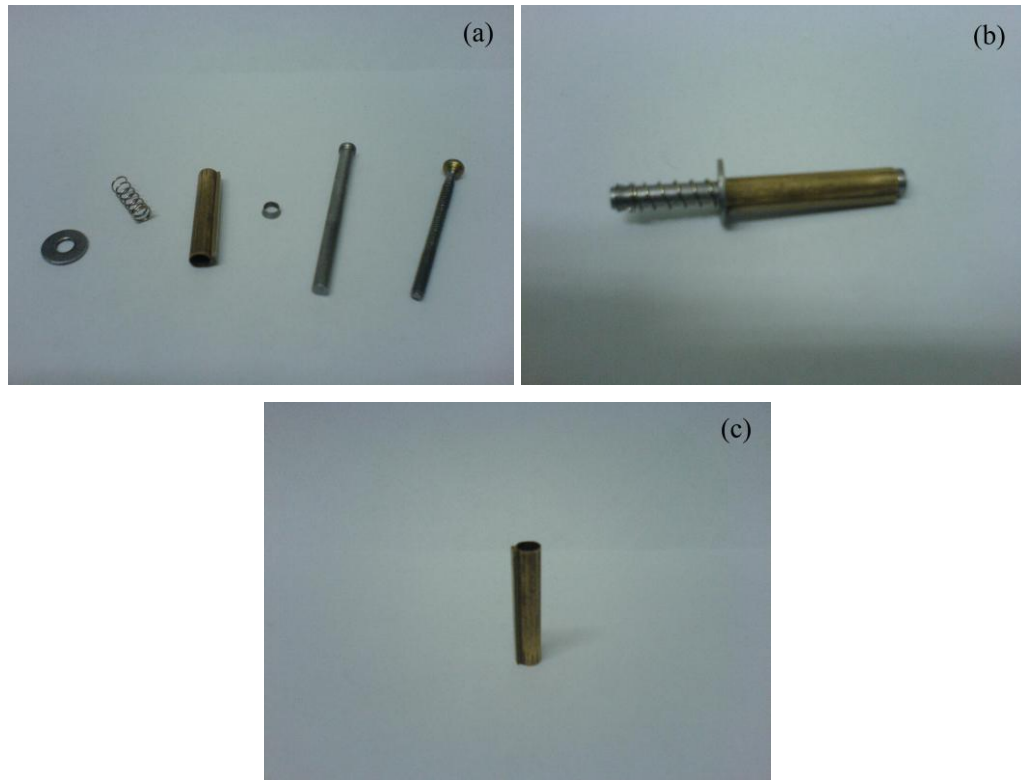


Figure 6.4 (a) Ultrasonic motor parts, (b) Assembled motor and (c) Stator bonded with a ceramic plate.

A ceramic plate with dimensions 28x2.3x1.0 mm (LxWxT) was produced by using the ceramic composition developed during this study with properties ($Q_m = 1240$, $d_{33} = 410$ pC/N and $k_p = 0.556$). The impedance spectrum of the piezoelectric resonator (plate) is shown in Figure 6.5. The lowest impedance value (470 ohm) at the first harmonic (50000 Hz) indicates the resonance frequency at which the resonator exhibits its maximum deflection movement.

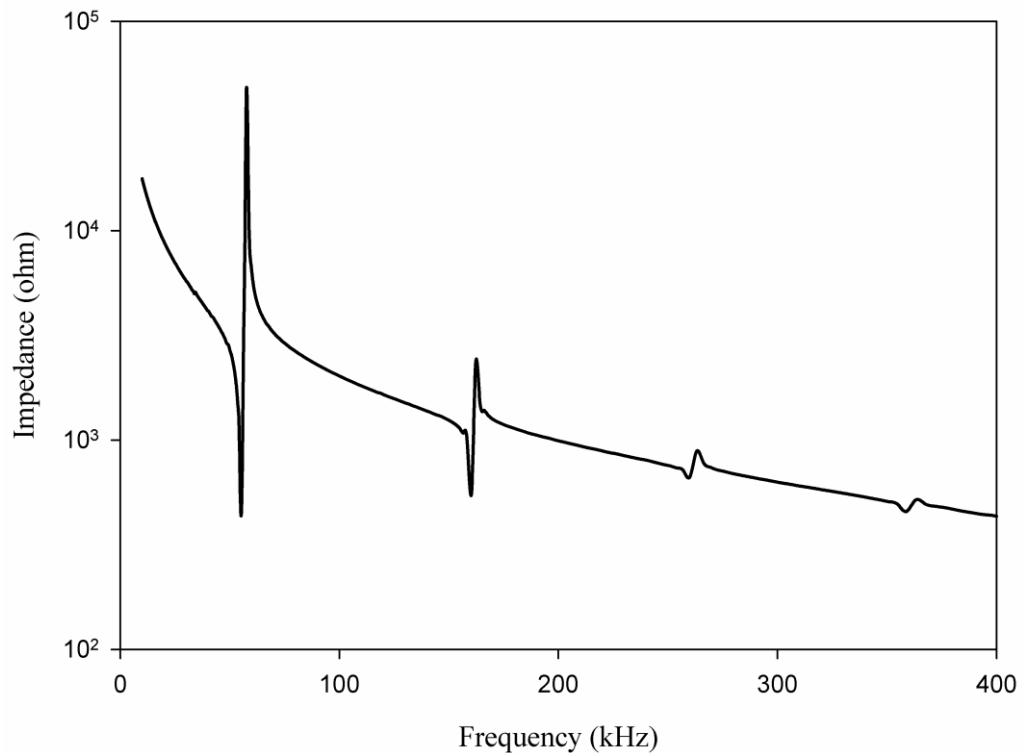


Figure 6.5 Impedance spectrum of the piezoelectric ceramic plate.

This plate was bonded to the flattened surface of the stator using epoxy glue. Impedance spectrum of the plate-stator given in Figure 6.6 shows the frequency range of 40-70 kHz since the resonance frequency of the plate lies on approximately 50 kHz. The first peak in Figure 6.6 at about 49 kHz indicates the first bending mode of the stator (Figure 6.2 – upper left) and the second peak belongs to the second bending mode (Figure 6.2 - lower left). The frequency between these two values causes the stator to provide the wobbling movement. This wobbling movement moves the rotor in clock-wise or counter-clockwise direction.

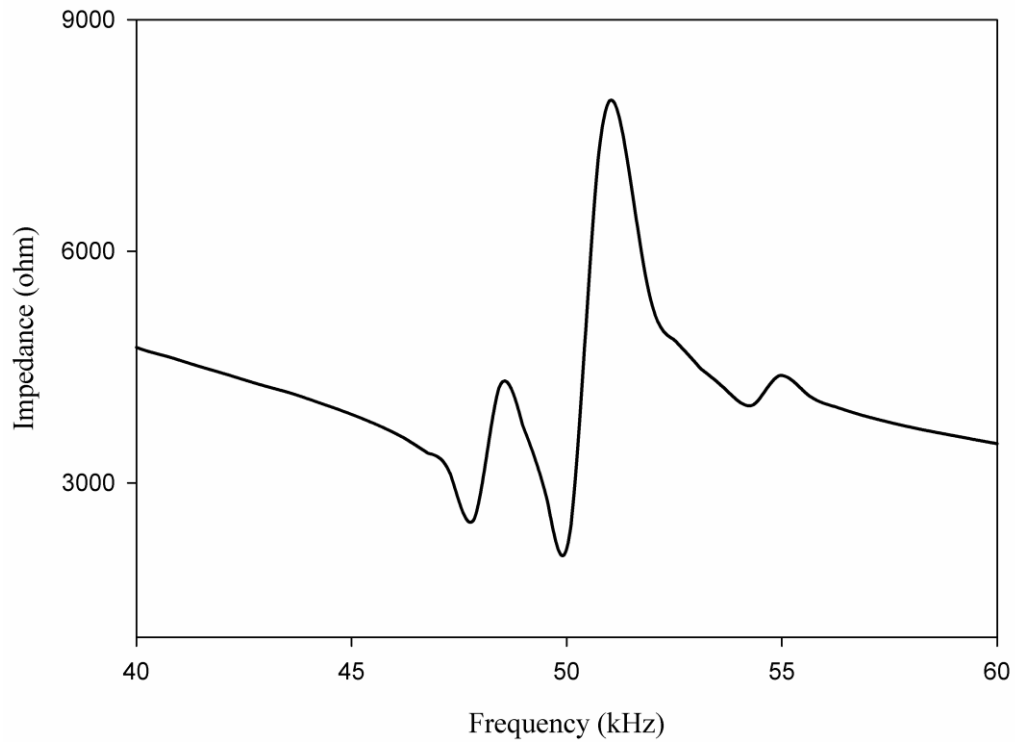


Figure 6.6 Impedance spectrum of the plate-bonded-stator.

An optical laser tachometer was used for characterization of performance of the ultrasonic motor. The speed measurements as a function of driving frequency and time were performed. The motor was driven using a signal generator (Agilent) with a maximum peak-to-peak voltage of 10V and an amplifier (Piezosystems) with the capability of magnifying the input voltage as high as 20 times as shown in Figure 6.7. Speed of motor as a function of driving frequency, driving voltage and operating time was measured.

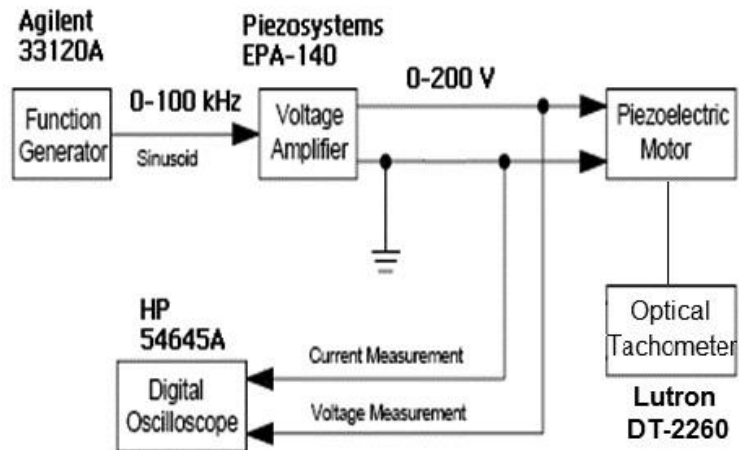


Figure 6.7 The schematic of the driving and characterization systems for ultrasonic motor.

6.5 Results and Discussion

The speed-driving frequency relation for two different driving voltages was given in Figure 6.8. The optimum driving frequency of operation for both driving voltages was approximately 50.6 kHz which is also close to resonance frequency of the motor. A maximum speed value of 200 rpm was achieved.

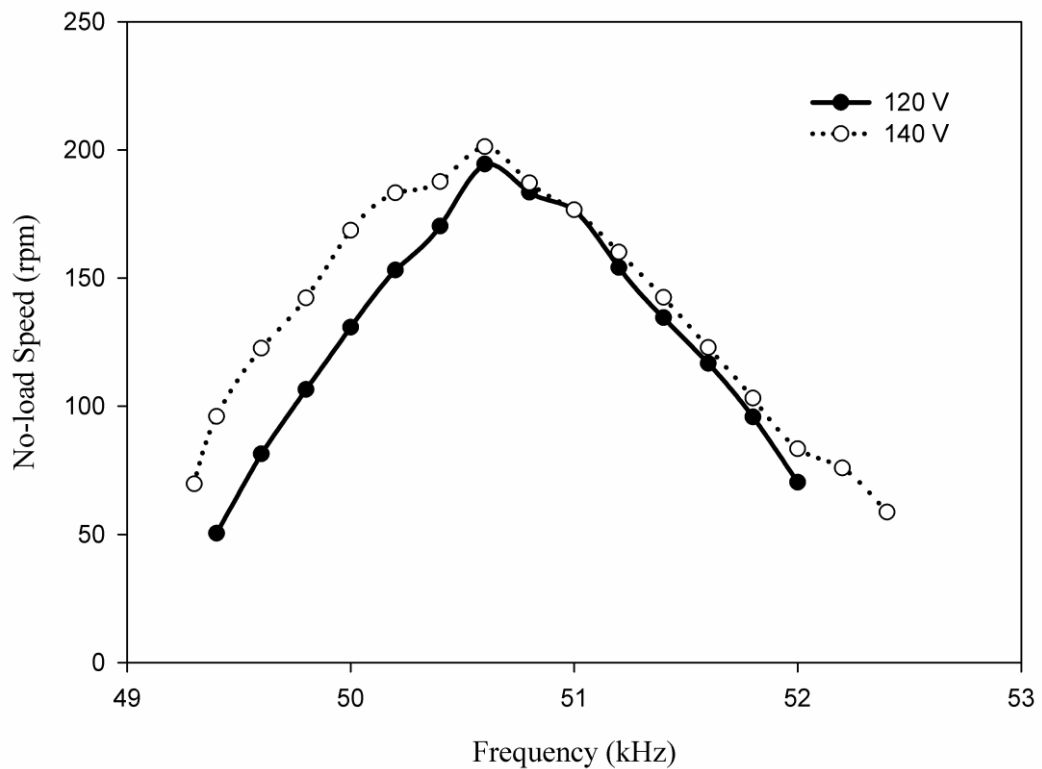


Figure 6.8 Speed-frequency characteristic of USM for different operating voltages.

Figure 6.9 shows the speed-time graph of the motor driven at 120 V_{pp}. As time passes the speed of motor decreased. After 10 min of operation, the speed was decreased approximately 10 rpm because of the heating of the piezo-ceramic element of the motor vibrating during operation at its resonance frequency [1, 102]. The speed decreases since the temperature of ceramic plate becomes closer to its Curie temperature and the magnitude of the spontaneous polarization becomes zero as the Curie temperature is approached.

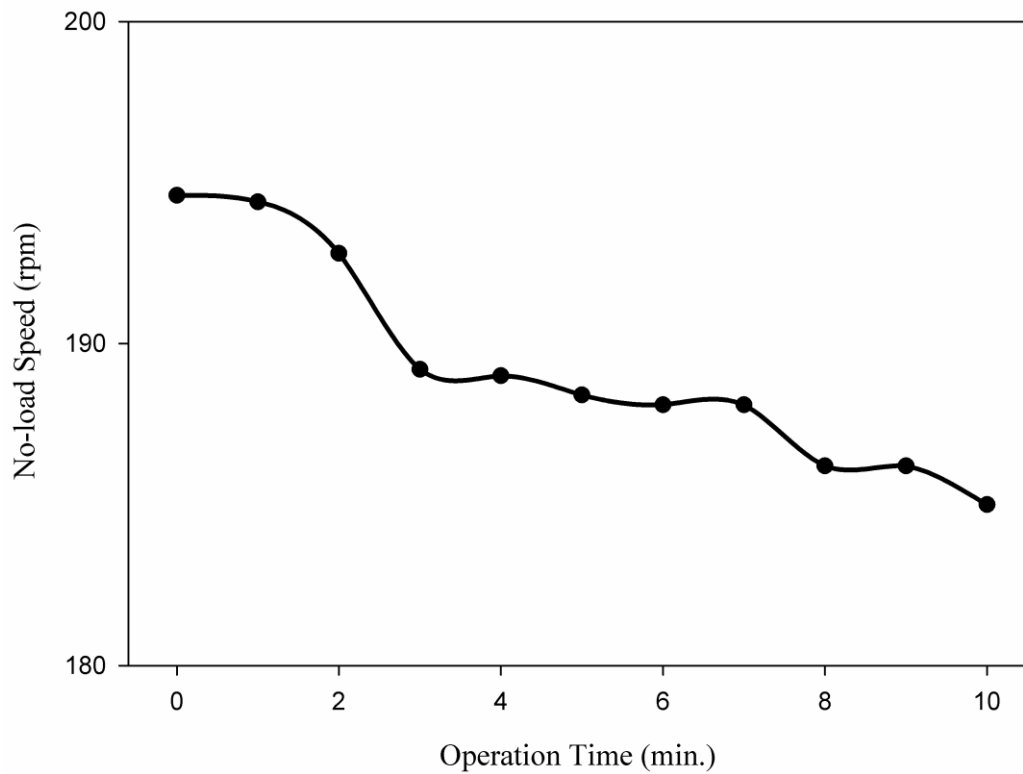


Figure 6.9 Speed-time characteristic of USM driven at 120 V_{pp}.

The measurement of torque-speed relation is difficult using the conventional torque-meters because of the small size of the motor [103]. For the torque measurements of USM, the transient characterization method which was proposed by Nakamura [104] was used. In the transient method, a load (a disc whose moment of inertia is known) is installed onto the motor and the transient speed is measured as a function of time. The transient torque of the motor can be calculated using the moment of inertia of the disc. Output mechanical power is the product of torque and angular speed whereas input electrical power is calculated by multiplying the input voltage and current. The ratio of the output power to input power is defined as the efficiency of the motor.

A metal disc was mounted onto the stator and the motor was driven using a signal generator with a maximum peak-to-peak voltage of 10 V and an amplifier. Ceramic plates of selected compositions given in Table 6.1 were also produced and bonded to the flatted surfaces of the stator. Speed of motor as a function of driving frequency, driving voltage and operating time was measured. The change in speed and efficiency with increasing torque was also determined.

Table 6.1 Compositions of the ceramics investigated for ultrasonic motor study.

No.	Composition	Q_m	d_{33} (pC/N)
1	$Pb_{0.94}Sr_{0.05}La_{0.01}[(Zr_{0.54}Ti_{0.46})_{0.9975}]O_3$	70	640
2	0.93[PSLZT]-0.07[PMnN] (Zr/Ti:54/46)	590	490
3	0.91[PSLZT]-0.09[PMnN] (Zr/Ti:54/46)	308	455
4	0.90[PSLZT]-0.10[PMnN] (Zr/Ti:54/46)	280	440
5	0.97[PSLZT]-0.03[PMnN] (Zr/Ti:54/46)	638	690
6	0.97[PSLZT]-0.024[PMnN]-0.006[PMS]	1240	540

The speed-driving frequency relations for a driving voltage of 120 V were presented in Figure 6.10. The optimum driving frequencies of operation were taken as the maximum speed values for each ceramic composition. These frequency values are close to the resonant frequencies of the ceramics in plate shape. The plot of the speed values as a function of torque was shown in Figure 6.11. The efficiency curves that were obtained by dividing the output mechanical power to input electrical power were also illustrated.

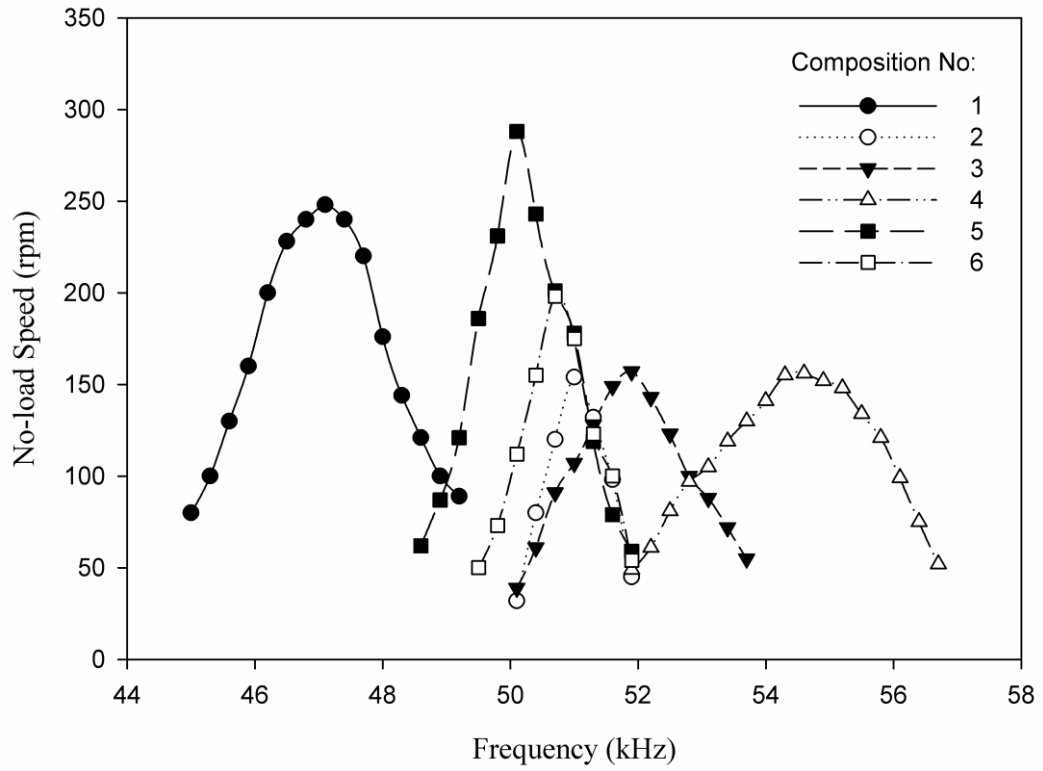


Figure 6.10 Speed of the motor as a function of driving frequency for ceramic plates of different compositions.

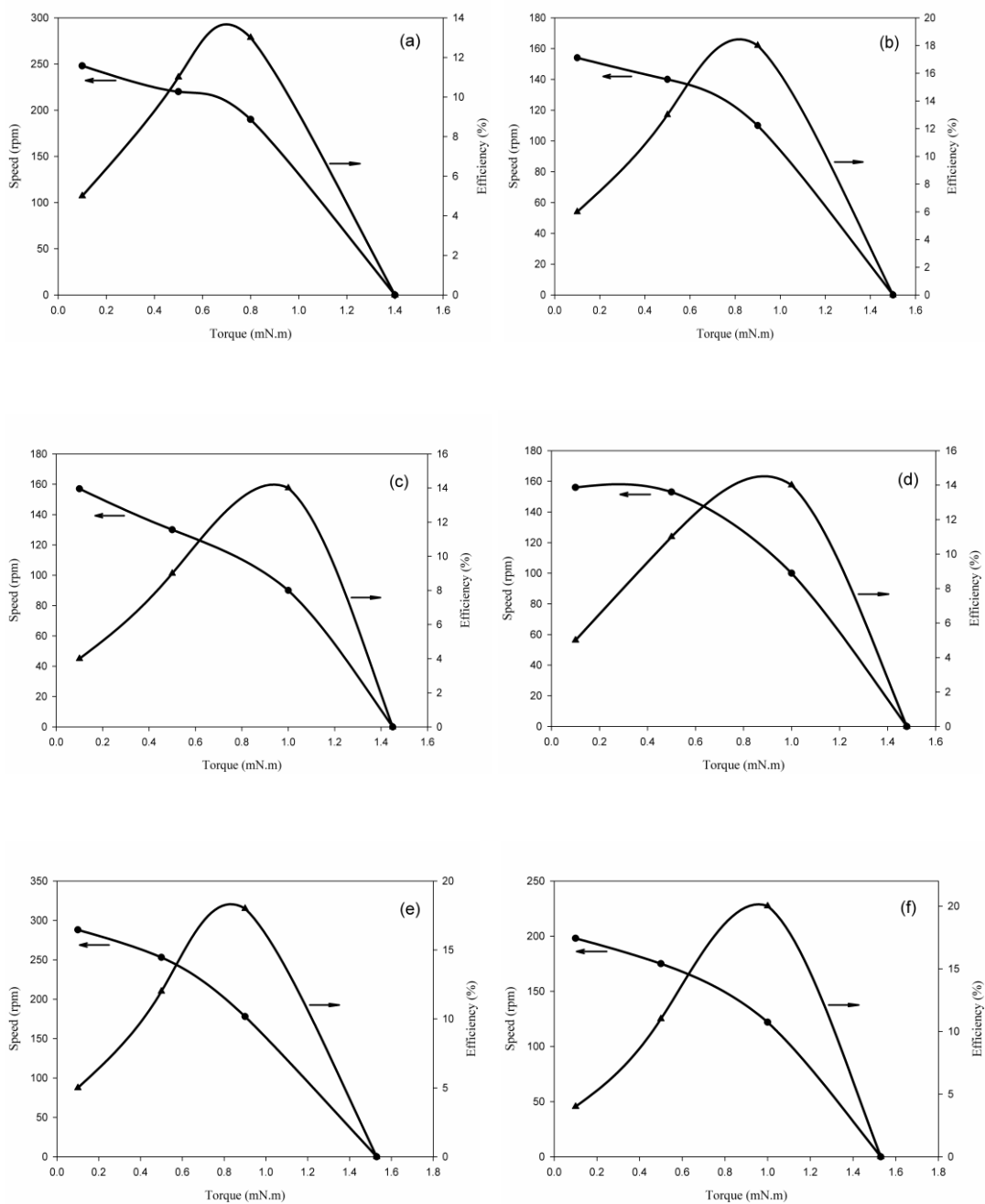


Figure 6.11 Load characteristics of the ultrasonic motor for composition number (a) 1, (b) 2, (c) 3, (d) 4, (e) 5 and (f) 6 given in Table 6.1.

Speed of the motor decreased as the torque increased. The maximum efficiency of 20% at 120 V and the maximum torque 1.53 mNm were obtained for the composition with the highest Q_m value and this efficiency value is similar to other cylindrical type motors. Efficiency value is directly proportional to the product of torque and angular velocity and inversely proportional to the input power which is the product of voltage and current.

The dependency of the performance of the ultrasonic motor to the piezoelectric properties of the ceramic plate was determined. The variation of no-load speed of the motor with dielectric strain constant is given in Figure 6.12. High d_{33} value ceramics provide higher speed since the deflection of the piezoceramic during vibration is higher. The change in speed with mechanical quality factor is also plotted in Figure 6.13. The decrease in speed of the motor was higher for ceramics with low Q_m values. Maximum torque and efficiency values are obtained for the ceramic with the highest mechanical quality factor. Since the temperature rise and degradation of piezoelectric properties are lower in high Q_m ceramics.

6.6 Conclusions of the Ultrasonic Motor Application

1. An ultrasonic motor (USM) called as *metal tube motor* which produces rotational movement by utilizing two rectangular piezoelectric ceramic plates was constructed using the ceramics developed in this study. A set of samples with different compositions and hence different electrical properties were prepared for this purpose.

2. A system including a voltage generator, a linear amplifier and an optical tachometer was used to determine the driving voltage and the optimum driving frequencies of operation for each ceramic composition. The driving value was determined as 120 V_{pp} from speed measurements and the frequency value was selected as the one which leads to the maximum no-load speed.

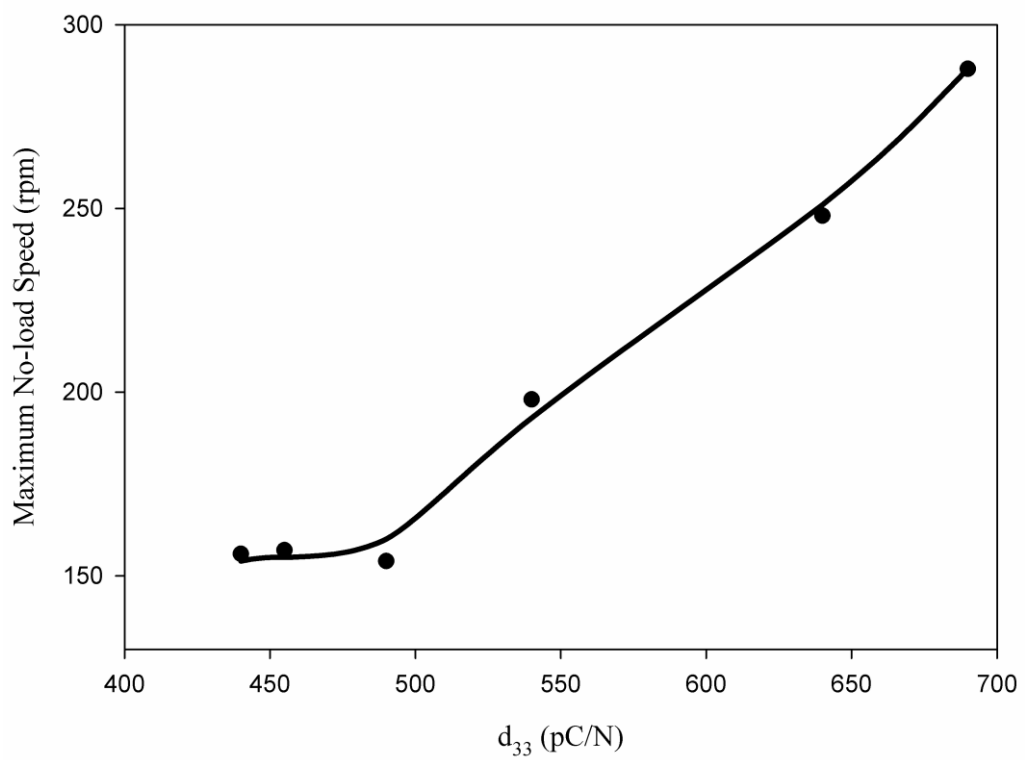


Figure 6.12 The dependency of no-load speed of the ultrasonic motor to the piezoelectric strain coefficient of ceramic plate.

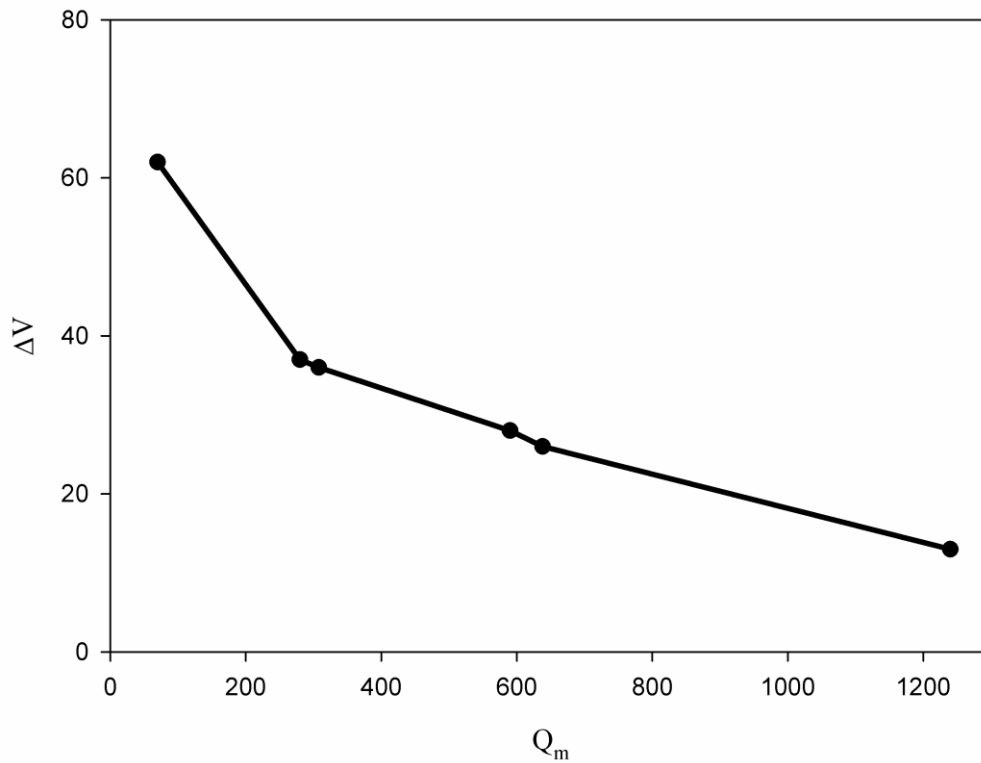


Figure 6.13 The variation of decrease in the speed of ultrasonic motor with mechanical quality factor of ceramic plate.

3. For each ceramic composition, the speed of USM decreased with time because of the heating of the piezo-ceramic element of the motor vibrating during operation at its resonance frequency. But, as expected, this decrease was lower in ceramics with high Q_m . For the composition with Q_m value of 1240 the decrease in speed was 13 rpm after 10 min of operation whereas it was 62 rpm for the composition with Q_m value of 70.

4. The dependency of the performance of an ultrasonic motor to the piezoelectric properties of the ceramic plate was determined. The maximum efficiency of 20% at 120 V_{pp} and the maximum torque 1.53 mNm were obtained for the composition with the highest Q_m value and this efficiency value is similar to other cylindrical

type motors. On the other hand, maximum no-load speed of 250 rpm was obtained for the ceramic composition with highest d_{33} value.

CHAPTER 7

SUMMARY AND CONCLUSIONS

Piezoelectric ultrasonic motors are used in a variety of application areas such as camera autofocus lenses, robotics, surgery devices, precise positioning devices and etc. Ultrasonic motors (USM) can produce high torque at low speeds and with a high efficiency. Also, since no magnetic field is used for operation there is no interference possibility.

Since the operation principle of USM is the transformation of the vibration movement of piezoelectric element under high electric fields to rotation or linear movement, this vibration movement result in temperature rise in ceramic. Temperature rise in a piezoelectric body leads to degradation of piezoelectric parameters of the material which in turn lowers the operation duration of USM.

There are various types of USMs that are produced with different design criteria. But the demand for electrical properties of piezoelectric body used in USM is independent of the design of the motor assembly. In order to have a piezoelectric element with high vibration amplitude which can be used for long operation periods without heating, both mechanical quality factor, Q_m and piezoelectric constant, d_{33} values must be high. When the Q_m value is low, the piezoelectric element in USM faces more with vibration which causes temperature rise in the ceramic. In addition to that, a low d_{33} value will result in small vibration amplitudes during operation; this lowers the performance of the motor.

In order to achieve the objectives of the thesis, the initial study was devoted to the experimental work which included the production of PZT-based piezoelectric ceramic materials which would have high mechanical quality factor with high piezoelectric properties.

These electrical properties of piezoelectric ceramics could be enhanced by doping. Because Q_m and d_{33} are competing properties, multi-doping is necessary in order to have high Q_m and high d_{33} values together. For this purpose, both acceptor and donor dopants were used. PZT ceramic was first doped with Sr and La in order to provide high piezoelectric properties, but they as expected resulted in low Q_m values. This ceramic doped further with additives selected from a group of donor and acceptor oxides such as MnO, Nb₂O₅ and Sb₂O₃.

PZT ceramics modified with simultaneous additions of Sr and La were produced with pure perovskite structure through conventional ceramic processing techniques. The incorporation of Sr²⁺ into the PZT lattice stabilized the tetragonal symmetry over the rhombohedral one and enhanced the grain growth during sintering. Although La³⁺ had similar effect on the stability of the tetragonal phase it had the tendency of decreasing the grain size. In the co-doped ceramics, satisfactory densification could be attained due to effective development of the microstructure consisting of a mixture of large and small grains.

PSLZT ceramics prepared in this study were essentially soft in nature. Sr had a dominant role in the improvement of the piezoelectric moduli and the dielectric constant. Combination of Sr and La as co-dopants had great implications on the dielectric and piezoelectric properties of the PZT ceramics. A remarkably high strain coefficient d_{33} of 640 pC/N was attained in the PSLZT ceramic containing 1 at% La and 5 at% Sr, the Zr/Ti ratio being the one on the MPB. The Curie temperature of this particular ceramic was 272 °C.

Mn, Nb and Sb occupied the B-site of the perovskite lattice. Since Mn is an acceptor dopant substituting Ti⁴⁺ and Zr⁴⁺, it acted as a hardening agent and

increased the Q_m value. The concentration of oxygen vacancies increased in the presence of this hardener which led to shranked crystal structure that blocked the domain wall motion, these stabilized domains caused higher Q_m values. On the other hand, Nb^{5+} and Sb^{5+} doping, which are donor dopants, provided a small decrease in d_{33} and other piezoelectric and dielectric properties. As a result, a new piezoelectric ceramic named as 0.97[PSLZT] – 0.024[PMnN] – 0.006[PMS] was produced with appropriate properties of $K^T = 1913$, $Q_m = 1240$, $d_{33} = 540$ pC/N, $\tan \delta = 0.89\%$, $k_p = 0.57$ and $T_c = 235$ °C. The obtained piezoelectric and dielectric properties make this composition a good candidate for high power applications.

The ceramics, with optimum piezoelectric and dielectric properties, given in each section of the experimental results chapters are listed in Table 7.1. The uncertainties in these values throughout the thesis are ± 5 in K^T , ± 3 in Q_m , ± 2 pC/N in d_{33} , $\pm 0.01\%$ in $\tan \delta$, and ± 2 °C in T_c .

The piezoelectric ceramics produced during this study were also used to construct a USM assembly. For each ceramic element, motor characterization in terms of speed, torque and efficiency was performed. A system including a voltage generator, a linear amplifier and an optical tachometer was used to determine the driving voltage and the optimum driving frequencies of operation for each ceramic composition. The driving value was chosen as $120 V_{pp}$ from speed measurements and the frequency value was selected as the one which leads to the maximum no-load speed.

The dependency of performance parameters of selected motor design to the electrical properties was determined. Increasing d_{33} values resulted in higher speed whereas high Q_m values provided higher torque values and longer operation times with small loss in speed. The maximum efficiency of 20% at $120 V_{pp}$ and the maximum torque 1.53 mNm were obtained for the composition with the highest Q_m value and this efficiency value is similar to other cylindrical type motors. On the other hand, maximum no-load speed of 250 rpm was achieved for the ceramic composition with highest d_{33} value.

Table 7.1 The ceramics, with optimum dielectric and piezoelectric properties, developed in this study.

Section No.	Composition	Q_m	d_{33} (pC/N)	k_p	K^T	$\tan \delta$ (%)
4.3.1	$Pb_{0.95}Sr_{0.05}(Zr_{0.54}Ti_{0.46})O_3$	345	305	0.44	1138	0.44
4.3.2	$Pb_{0.94}Sr_{0.05}La_{0.01}(Zr_{0.54}Ti_{0.46})O_3$	70	640	0.56	1800	1.55
5.3.1	0.97[PSLZT]-0.03[PMnN] (Zr/Ti:54/46)	400	660	0.60	2293	1.47
5.3.2	0.97[PSLZT]-0.03[PMnN] (Zr/Ti:53/47)	638	690	0.63	2110	0.99
5.3.3	0.97[PSLZT]-0.024[PMnN]- 0.006[PMS]	1240	540	0.57	1913	0.89

The following studies are recommended as extensions to this study for future work:

1. The structural and electrical characteristics of piezoelectric ceramics depend on process factors such as sintering temperature and time. The variation of the piezoelectric and dielectric properties with sintering parameters should be determined in order to find the optimum sintering regime for developed compositions.
2. The electrical characterization of the developed ceramics was performed under low field values (0.5 V/mm). Since these piezoelectric ceramics can also be used in high field application areas due to their good

electromechanical properties, a study of high field characterization would be essential for other applications of the materials.

3. The developed ceramics may be applied to other ultrasonic motor designs and other high-power electromechanical applications like piezoelectric transformers. Also, investigating the variations of piezoelectric and dielectric parameters with respect to temperature and frequency will substantially improve our understanding on these compositions.

REFERENCES

1. T. Sashida and T. Kenjo, *An Introduction to Ultrasonic Motors*. 1993: Clarendon Press.
2. B. Jaffe, W. R. Cook, and H. Jaffe, *Piezoelectric Ceramics*. 1971: Academic Press.
3. ed. R. C. Buchanan, *Ceramic Materials for Electronics*. 2004: Marcel Dekker Inc.
4. K. Nagata, J. Thongrueng and K. Kato, *Evaluation of the Reliability of Piezoelectric Ceramic Transformers*. Japanese Journal of Applied Physics, 1997. **36**: pp. 6103-6105.
5. S. Ueha, Y. Tomikawa, M. Kurosawa, and N. Nakamura, *Ultrasonic Motors*. 1993: Oxford Science Publications.
6. H. Chen, X. Guo and Z. Meng, *Processing and Properties of PMMN-PZT Quaternary Piezoelectric Ceramics for Ultrasonic Motors*. Materials Chemistry and Physics, 2002. **75**: pp. 202-206.
7. D. Hong-liang, P. Zhi-bin, L. Zhi-min, L. Fa, Z. Dong-mei, Z. Wan-cheng and Q. Shao-bo, *Effect of Sintering Temperature and Composition on Microstructure and Properties of PMS-PZT Ceramics*. Transactions of Nonferrous Metals Society of China, 2006. **16**: pp. s165-s169.

8. G. H. Haertling, *Ferroelectric Ceramics: History and Technology*. Journal of the American Ceramic Society, 1999. **82**: pp. 797-818.
9. A. J. Moulson and J. M. Herbert, *Electroceramics*. 1990: Chapman&Hall.
10. S. L. Swartz, *Topics in Electronic Ceramics*. IEEE Transaction on Electrical Insulation, 1990. **25**: pp. 935-987.
11. R. Rai, S. Sharma, and R. N. P. Choudhary, *Dielectric and Piezoelectric Studies of Fe Doped PLZT Ceramics*. Materials Letters, 2005. **59**: pp. 3921-3925.
12. J. Long, H. Chen, and Z. Meng, *Effects of Compositions and Nb-doping on Microstructure and Piezoelectric Properties of PMS–PZ–PT System*. Materials Science and Engineering B, 2003. **99**: pp. 445-448.
13. J. H. Yoo, H. S. Yoon, K. H. Yoon, Y. H. Jeong, and C. Y. Park, *Piezoelectric Characteristics of PMN-PZT Ceramics for Piezoelectric Transformer*. IEEE Ultrasonics Symposium Proceedings, 1998. **1**: pp. 981-984.
14. G. Deng, Q. Yin, A. Ding, X. Zheng, W. Cheng, and P. Qiu, *High Piezoelectric and Dielectric Properties of La-doped $0.3\text{Pb}(\text{Zn}_{1/3}\text{Nb}_{2/3})\text{O}_3$ - $0.7\text{Pb}(\text{Zr}_x\text{Ti}_{1-x})\text{O}_3$ Ceramics Near Morphotropic Phase Boundary*. Journal of the American Ceramic Society, 2005. **88**: pp. 2310-2314.
15. H.E. Çamurlu and M. Timuçin, *Production and Characterization of PMN-PT Piezoceramics Modified by Yttrium and Bismuth*. Key Engineering Materials, 2004. **264-268**: pp. 1193-1996.

16. APC Int. Ltd., *Piezoelectricity Theory, Piezo Manufacture, Applications and Reference Book*. http://www.americanpiezo.com/piezo_theory/index.html, Last accessed: December 2010.
17. T. Takenaka and H. Nagata, *Current Status and Prospects of Lead-Free Piezoelectric Ceramics*. *Journal of the European Ceramic Society*, 2005. **25**: pp. 2693-2700.
18. M. Ichiki, L. Zhang, M. Tanaka, and R. Maeda, *Electrical Properties of Piezoelectric Sodium-Potassium Niobate*. *Journal of the European Ceramic Society*, 2004. **24**: pp. 1693-1697.
19. M. A. Mohiddon and K. L. Yadav, *Effect of Heating Rate on Dielectric and Pyroelectric Properties of Double Doped PZT*. *Advances in Applied Ceramics*, 2008. **107**: pp. 310-317.
20. A. Safari, *Applications of Ferroelectric Ceramics Materials*. <http://www.rci.rutgers.edu/~ecerg/projects/ferroelectric.html>, Last accessed: December 2010.
21. T. Senda and R.C. Bradt, *Grain Growth in Sintered ZnO and ZnO-Bi₂O₃ Ceramics*. *Journal of the American Ceramic Society*, 1990. **73**: pp. 106-114.
22. *IRE Standards on Piezoelectric Crystals : Measurement of Piezoelectric Ceramics*, Proceedings of the IRE, 1961. **49**: pp. 1161-1169.
23. S. Zhao, H. Wu, and Q. Sun, *Study on PSN-PZN-PZT Quaternary Piezoelectric Ceramics Near the Morphotropic Phase Boundary*. *Materials Science and Engineering B*, 2005. **123**: p. 203-210.

24. M. Cerqueira, R. S. Nasar, E. R. Leite, E. Longo and J. A. Varela, *Sintering and Characterization of PLZT (9/65/35)*. *Ceramics International*, 2000. **26**: pp. 231-236.
25. M. T. Larrea, *Microwave-assisted Acid Dissolution of Sintered Advanced Ceramics for Inductively Coupled Plasma Atomic Emission Spectrometry*. *Journal of Analytical Atomic Spectrometry*, 1997. **12**: pp. 1323-1332.
26. C. B. Sawyer, and C. H. Tower, *Rochelle Salt as a Dielectric*. *Physical Review*, 1930. **35**: pp. 269-273.
27. J. H. Belding and M. G. McLaren, *Behavior of Modified Lead Zirconate-Lead Titanate Piezoelectric Ceramics under High Electric Fields*. *American Ceramic Society Bulletin*, 1970. **49**: pp. 1025-1029.
28. S. S. Chiang, M. Nishioka, R. M. Fulrath, and J. A. Pask, *Effect of Processing on Microstructure and Properties of PZT Ceramics*. *American Ceramic Society Bulletin*, 1981. **60**: pp. 484-489.
29. L. Wu, C. C. Wei, T. S. Wu, and H. C. Liu, *Piezoelectric Properties of Modified PZT Ceramics*. *Journal of Physics C: Solid State Physics*, 1983. **16**: pp. 2813-2821.
30. Z. Weilie, Z. Peilin, and L. Sidong, *Piezoelectric Ceramics with High Coupling and High Temperature Stability*. *Ferroelectrics*, 1990. **101**: pp. 173-177.
31. S. K. Nag and D. C. Agrawal, *Piezoelectric and Mechanical Properties of Ceria-Doped Lead Zirconate Titanate Ceramics*. *Journal of Materials Science*, 1992. **27**: pp. 4125-4130.

32. C. Moure, M. Villegas, J. F. Fernandez, and P. Duran, *Microstructural and Piezoelectric Properties of Fine Grained PZT Ceramics Doped with Donor and/or Acceptor Cations*. *Ferroelectrics*, 1992. **127**: pp. 113-118.
33. T. Yamamoto, *Optimum Preparation Methods for Piezoelectric Ceramics and Their Evaluation*. *American Ceramic Society Bulletin*, 1992. **71**: pp. 978-985.
34. J. F. Fernandez, C. Moure, M. Villegas, P. Duran, M. Kosec, and G. Drazic, *Compositional Fluctuations and Properties of Fine-Grained Acceptor-Doped PZT Ceramics*. *Journal of the European Ceramic Society*, 1998. **18**: pp. 1695-1705.
35. C. Galassi, E. Roncari, C. Capiani, and F. Craciun, *Processing and Characterization of High Q_m Ferroelectric Ceramics*. *Journal of the European Ceramic Society*, 1999. **19**: pp. 1237-1241.
36. F. Kulcsar, *Electromechanical Properties of Lead Titanate Zirconate Ceramics with Lead Partially Replaced by Calcium or Strontium*. *Journal of the American Ceramic Society*, 1959. **42**: pp. 49-51.
37. P. R. Chowdhury and S. B. Deshpande, *Effect of Dopants on the Microstructure and Lattice Parameters of Lead Zirconate-Titanate Ceramics*. *Journal of Materials Science*, 1987. **22**: pp. 2209-2215.
38. C. K. Liang and L. Wu, *Microstructure and Properties of Cr_2O_3 -Doped Ternary Lead Zirconate Titanate Ceramics*. *Journal of the American Ceramic Society*, 1993. **76**: pp. 2023-2026.
39. S. W. Lin, C. P. Chin, T. K. Fan, and K. C. Kao, *Effects of Electric and Magnetic Fields on the Resonance Frequency of Piezoelectric Ceramics*. *Ferroelectrics*, 1988. **88**: pp. 67-71.

40. C. A. Randall, N. Kim, J. P. Kucera, W. Cao, and T. R. ShROUT, *Intrinsic and Extrinsic Size Effects in Fine-Grained Morphotropic-Phase Boundary Lead Zirconate Titanate Ceramics*. Journal of the American Ceramic Society, 1998. **81**: pp. 677-688.
41. R. Lal, R. Krishnan, and P. Ramakrishnan, *Transition between Tetragonal and Rhombohedral Phases of PZT Ceramics Prepared from Spray-Dried Powders*. British Ceramic Transactions Journal, 1988. **87**: pp. 99-102.
42. C. Bedoya, Ch. Muller, J.-L. Baudour, V. Madigou, M. Anne, and M. Roubin, *Sr-doped $PbZr_{1-x}Ti_xO_3$ Ceramic: Structural Study and Field-Induced Reorientation of Ferroelectric Domains*. Materials Science and Engineering B, 2000. **75**: pp. 43-52.
43. K. P. Rema and V. Kumar, *Structure-Property Relationship in Mn-Doped $(Pb_{0.94}Sr_{0.06})(Zr_{0.53}Ti_{0.47})O_3$* . Journal of the American Ceramic Society, 2008. **91**: pp. 164-168.
44. O. Muller and R. Roy, *Crystal Chemistry of Non-Metallic Materials, The Major Ternary Structural Families*. 1974: Springer-Verlag, Berlin Heidelberg New York.
45. K. H. Hardtl and D. Hennings, *Distribution of A-Site and B-Site Vacancies in $(Pb,La)(Ti,Zr)O_3$ Ceramics*. Journal of the American Ceramic Society, 1972. **55**: pp. 230-231.
46. A. Garg and D. C. Agrawal, *Effect of Rare Earth (Er, Gd, Eu, Nd and La) and Bismuth Additives on the Mechanical and Piezoelectric Properties of Lead Zirconate Titanate Ceramics*. Materials Science and Engineering B, 2001. **86**: pp. 134-143.

47. D. Kuscer, J. Korzekwa, M. Kosec, and R. Skulski, *A- and B-compensated PLZT x/90/10: Sintering and Microstructural Analysis*. Journal of the European Ceramic Society, 2007. **27**: pp. 4499-4507.
48. G. H. Haertling and C. E. Land, *Hot-pressed (Pb,La)(Zr,Ti)O₃ Ferroelectric Ceramics for Electrooptic Applications*. Journal of the American Ceramic Society, 1971. **54**: pp. 1-11.
49. C. Galassi, D. Piazza, F. Craciun, and P. Verardi, *Electrical Investigation of Sintering Factors Influence on PLZT Ceramics*. Journal of the European Ceramic Society, 2004. **24**: pp. 1525-1528.
50. F. Kulcsar, *Electromechanical Properties of Lead Titanate Zirconate Ceramics Modified with Certain Three- or Five-Valent Additions*. Journal of the American Ceramic Society, 1959. **42**: pp. 343-349.
51. A. Tawfik, *Elastic Properties of Sound Wave Velocity of PZT Transducers Doped with Ta and La*. Journal of the American Ceramic Society, 1985. **68**: pp. C317-C319.
52. M. Hammer and M. J. Hoffman, *Detailed X-ray Diffraction Analyses and Correlation of Microstructural and Electromechanical Properties of La-doped PZT Ceramics*. Journal of Electroceramics, 1998. **2:2**: pp. 75-84.
53. B. Praveenkumar, H. H. Kumar, D. K. Kharat, and B. S. Murty, *Investigation and Characterization of La-doped PZT Nanocrystalline Ceramic Prepared by Mechanical Activation Route*. Materials Chemistry and Physics, 2008. **112**: pp. 31-34.
54. P. K. Mehta, B. D. Padalia, M. V. R. Murty, A. M. Varaprasad, and K. Uchino, *X-ray Structural Determinations on Sr and La Doped PZT*. Ferroelectrics Letters, 1987. **7**: pp. 121-129.

55. K. Ramam and M. Lopez, *Effect of Strontium Doping on Dielectric, Ferroelectric and Piezoelectric Properties of PLZTN Ceramics*. Materials Science and Engineering B, 2007. **145**: pp. 41-47.
56. K. Ramam and K. Chandramouli, *Dielectric and Piezoelectric Properties of Combinatory Effect of A-Site Isovalent and B-Site Acceptor Doped PLZT Ceramics*. Ceramics-Silikaty, 2009. **53**: pp. 189-194.
57. E. Boucher, B. Guiffard, L. Lebrun, and D. Guyomar, *Effects of Zr/Ti Ratio on Structural, Dielectric and Piezoelectric Properties of Mn- and (Mn,F)-doped Lead Zirconate Titanate Ceramics*. Ceramics International, 2006. **32**: pp. 479-485.
58. R. A. Pferner, G. Thurn, and F. Aldinger, *Mechanical Properties of PZT Ceramics with Tailored Microstructures*. Materials Chemistry and Physics, 1999. **61**: pp. 24-30.
59. S. K. Saha and D. C. Agrawal, *Composition Fluctuations and Their Influence on the Properties of Lead Zirconate Titanate Ceramics*. American Ceramic Society Bulletin, 1992. **71**: pp. 1424-1428.
60. P. Gerber, U. Böttger, and R. Waser, *Composition Influences on the Electrical and Electromechanical Properties of Lead Zirconate Titanate Thin Films*. Journal of Applied Physics, 2006. **100**: pp. 124105-1 to 8.
61. M. J. Hoffmann, M. Hammer, A. Endriss, and D. C. Lupascu, *Correlation between Microstructure, Strain Behavior, and Acoustic Emission of Soft PZT Ceramics*. Acta Materialia, 2001. **49**: pp. 1301-1310.

62. R. A. Langman, R. B. Runk, and S. R. Butler, *Isothermal Grain Growth of Pressure-Sintered PLZT Ceramics*. Journal of the American Ceramic Society, 1973. **56**: pp. 486-488.
63. X. Dai, A. DiGiovanni, and D. Viehland, *Dielectric Properties of Tetragonal Lanthanum Modified Lead Zirconate Titanate Ceramics*. Journal of Applied Physics, 1993. **74**: pp. 3399-3405.
64. K. Okazaki and K. Nagata, *Effects of Grain Size and Porosity on Electrical and Optical Properties of PLZT Ceramics*. Journal of the American Ceramic Society, 1973. **56**: pp. 82-86.
65. L. Pdungsap, N. Udomkan, S. Boonyuen, and P. Winotai, *Optimized Conditions for Fabrication of La-dopant PZT Ceramics*. Sensors and Actuators A, 2005. **122**: pp. 250-256.
66. C. H. Wang, *The Piezoelectric and Dielectric Properties of PZT-PMN-PZN*. Ceramics International, 2004. **30**: pp. 605-611.
67. S. J. Yoon, A. Joshi, and K. Uchino, *Effect of Additives on the Electromechanical Properties of $Pb(Zr,Ti)O_3$ - $Pb(Y_{2/3}W_{1/3})O_3$ Ceramics*. Journal of the American Ceramic Society, 1997. **80**: pp. 1035-1039.
68. R. S. Nasar, M. Cerqueira, E. Longo, J. A. Varela, and A. Beltran, *Experimental and Theoretical Study of the Ferroelectric and Piezoelectric Behavior of Strontium-doped PZT*. Journal of the European Ceramic Society, 2002. **22**: pp. 209-218.
69. H. Zheng, I. M. Reaney, W. E. Lee, N. Jones, and H. Thomas, *Effects of Sr Substitution in Nb-doped PZT Ceramics*. Journal of the European Ceramic Society, 2001. **21**: pp. 1371-1375.

70. L. Sun, C. Feng, Q. Sun, and H. Zhou, *Study on $Pb(Zr,Ti)O_3$ - $Pb(Zn_{1/3}Nb_{2/3})O_3$ - $Pb(Sn_{1/3}Nb_{2/3})O_3$ - $Pb(Mn_{1/3}Sb_{2/3})O_3$ Quinary System Piezoelectric Ceramics*. *Materials Science and Engineering B*, 2005. **122**: pp. 61-66.
71. S. Hallaert and E. Sarraute, *Piezoelectric Transformers; Principles, Structures and Modeling*. *Actuators*, 1998. **98**: pp. 337-340.
72. T. B. Weston, A. H. Webster, and V. M. McNamara, *Lead Zirconate-Lead Titanate Piezoelectric Ceramics with Iron Oxide Additions*. *Journal of the American Ceramic Society*, 1969. **52**: pp. 253-257.
73. L. X. He, and C. E. Li, *Effects of Addition of MnO on Piezoelectric Properties of Lead Zirconate Titanate*. *Journal of Materials Science*, 2000. **35**: pp. 2477-2480.
74. R. D. Shannon and C. T. Prewitt, *Effective Ionic Radii in Oxides and Fluorides*. *Acta Crystallographica*, 1969. **B25**: pp. 925-946.
75. R. Rai and S. Sharma. *Structural and Dielectric Properties of Sb-doped PLZT Ceramics*. *Ceramics International*, 2004. **30**: pp. 1295-1299.
76. N. Kim, W. Huebner, S. J. Jang, and T. R. Shrout, *Dielectric and Piezoelectric Properties of Lanthanum-Modified Lead Magnesium Niobium-Lead Titanate Ceramics*. *Ferroelectrics*, 1989. **93**: pp. 341-349.
77. M. T. Lanagan, N. Yang, D. C. Dube, and S. J. Jang, *Dielectric Behavior of the Relaxor $Pb(Mg_{1/3}Nb_{2/3})O_3$ - $PbTiO_3$ Solid Solution System in the Microwave Region*. *Journal of the American Ceramic Society*, 1989. **72**: pp. 481-483.

78. A. Safari and E. K. Akdoğan, *Piezoelectric and Acoustic Materials for Transducer Applications*. 2008: Springer.
79. T. Wu, M. Shyu, C. Chung, and H. Lee, *Phase Transition and Ferroelectric Characteristics of $Pb[(Mg_{1/3}Nb_{2/3})_{1-x}Ti_x]O_3$ Ceramics Modified with $La(Mg_{1/3}Nb_{2/3})O_3$* . Journal of the American Ceramic Society, 1995. **78**: pp. 2168-2174.
80. O. Ise, K. Satoh, and Y. Mamiya, *High Power Characteristics of Piezoelectric Ceramics in $Pb(Mn_{1/3}Nb_{2/3})O_3$ - $PbTiO_3$ - $PbZrO_3$ System*. Japanese Journal of Applied Physics, 1999. **38**: pp. 5531-5534.
81. S. Priya, H. W. Kim, and K. Uchino, *Low Temperature Coefficient of Resonance Frequency Composition in the System $Pb(Zr,Ti)O_3$ - $Pb(Mn_{1/3}Nb_{2/3})O_3$* . Journal of the American Ceramic Society, 2004. **87**: pp. 1907-1911.
82. B. Li, Z. Zhu, G. Li, and A. Ding, *Microstructure and Electromechanical Properties in $PMnN$ -PZT Ceramics Sintered at Different Temperatures*. Journal of Materials Science and Technology, 2005. **21**: pp. 386-390.
83. C. Y. Chen, Y. Hu, H. R. Lin, and W. Y. Wei, *Influence of the Sintering Temperature on Phase Development in PMN -PZT Ceramics*. Ceramics International, 2007. **33**: pp. 263-268.
84. S. Takahashi, Y. Sasaki, S. Hirose, and K. Uchino, *Stability of $PbZrO_3$ - $PbTiO_3$ - $Pb(Mn_{1/3}Sb_{2/3})O_3$ Piezoelectric Ceramics under Vibration-Level Change*. Japanese Journal of Applied Physics, 1995. **34**: pp. 5328-5331.
85. D. J. Lee, D. W. Shin, S. H. Jeong, H. I. Chae, H. H. Kim, and K. J. Lim, *Piezoelectric Characteristics of PZ-PT-PMS Ceramics with Addition of*

CeO_2 . Proceedings of the 5th International Conference on Properties and Applications of Dielectric Materials, 1997. **2**: pp. 875-878.

- 86.** S. J. Yoon, H. W. Kang, S. L. Kucheiko, H. J. Kim, H. J. Jung, D. K. Lee, and H. K. Ahn, *Piezoelectric Properties of $Pb[Zr_{0.45}Ti_{0.5-x}Lu_x(Mn_{1/3}Sb_{2/3})_{0.05}]O_3$ Ceramics*. Journal of the American Ceramic Society, 1998. **81**: pp. 2473-2476.
- 87.** Y. Gao, K. Uchino, and D. Viehland, *Effects of Rare Earth Metal Substitutions on the Piezoelectric and Polarization Properties of $Pb(Zr,Ti)O_3$ - $Pb(Sb,Mn)O_3$ Ceramics*. Journal of Applied Physics, 2002. **92**: pp. 2094-2099.
- 88.** Z. G. Zhu, B. S. Li, G. R. Li, W. Z. Zhang, and Q. R. Yin, *Microstructure and Piezoelectric Properties of PMS-PZT Ceramics*. Materials Science and Engineering B, 2005. **117**: pp. 216-220.
- 89.** J. H. Yoo, Y. W. Lee, S. M. Hwang, H. S. Yoon, H. S. Jeong, J. S. Kim, and C. S. Yoo, *Piezoelectric Properties of PNW-PMN-PZT Ceramics for High Power Piezoelectric Transformer*. Proceedings of the 12th IEEE International Symposium on Applications of Ferroelectrics, 2000. **1**: pp. 495-498.
- 90.** G. Feng, W. Chun-juan, L. Xiang-chun, and T. Chang-sheng, *Effect of Tungsten on the Structure and Piezoelectric Properties of PZN-PZT Ceramics*. Ceramics International, 2007. **33**: pp. 1019-1023.
- 91.** H. W. Chung, S. H. Lim, G. H. Kim, D. H. Li, E. S. Lee, B. D. Ahn, and S. Y. Lee, *Fabrication and Characterization of Piezoelectric $Pb(Zr,Ti)O_3$ - $Pb(Mn,W,Sb,Nb)O_3$ Step-Down Piezoelectric Transformer*. Science and Actuators A, 2006. **128**: pp. 350-354.

92. H. Du, S. Qu, J. Che, Z. Liu, X. Wei, and Z. Pei, *The Effect of Composition on Microstructure and Properties of PNW-PMS-PZT Ceramics for High-Power Piezoelectric Transformer*. *Materials Science and Engineering A*, 2005. **393**: pp. 36-41.
93. Y. D. Hou, M. K. Zhu, H. Wang, B. Wang, H. Yan, and C. S. Tian, *Piezoelectric Properties of New MnO₂-Added 0.2 PZN-0.8 PZT Ceramic*. *Materials Letters*, 2004. **58**: pp. 1508-1512.
94. C. Y. Chen and H. L. Lin, *Piezoelectric Properties of Pb(Mn_{1/3}Nb_{2/3})O₃-PbZrO₃-PbTiO₃ Ceramics with Sintering Aid of 2CaO-Fe₂O₃ Compound*. *Ceramics International*, 2004. **30**: pp. 2075-2079.
95. C. S. Kim, S. K. Kim, and S. Y. Lee, *Fabrication and Characterization of PZT-PMWSN Thin Film Using Pulsed Laser Deposition*. *Materials Science in Semiconductor Processing*, 2003. **5**: pp. 93-96.
96. R. Zhang, Z. Yang, X. Chao, and C. Kang, *Effects of CeO₂ Addition on the Piezoelectric Properties of PNW-PMN-PZT Ceramics*. *Ceramics International*, 2009. **35**: pp. 199-204.
97. S. Manuspiya, P. Larotanakul, and K. Uchino, *Integration of Piezoelectric Transformer and an Ultrasonic Motor*. *Ultrasonic*, 2003. **41**: pp. 83-87.
98. K. Uchino, S. Cagatay, B. Koc, S. Dong, P. Bouchilloux, and M. Strauss, *Micro Piezoelectric Ultrasonic Motors*. *Journal of Electroceramics*, 2004. **13**: pp. 393-401.
99. K. Spanner, *Survey of the Various Operating Principles of Ultrasonic Piezomotors*. http://www.pi-usa.us/technotes/Actuator2006_SurveyoftheVariousOperatingPrinciplesofUltrasonicPiezomotors_c.pdf, Last accessed: December 2010.

100. B. Koç, S. Çağatay, and K. Uchino, *A Piezoelectric Motor Using Two Orthogonal Bending Modes of a Hollow Cylinder*. IEEE Transactions on Ultrasonic, Ferroelectrics and Frequency Control, 2002. **49**: pp. 495-500.
101. A. Frangi, A. Corigliano, M. Binci, and P. Faure, *Finite Element Modeling of a Rotating Piezoelectric Ultrasonic Motor*. Ultrasonics, 2005. **43**: pp. 747-755.
102. G. Bal and E. Bekiroglu, *Servo Speed Control of Travelling-Wave Ultrasonic Motor Using Digital Signal Processor*. Sensors and Actuators A, 2004. **109**: pp. 212–219.
103. S. Yener, *Design and Characterization of Piezoelectric Ultrasonic Motors*. Ph.D. Thesis, Pennsylvania State University, 2004.
104. K. Nakamura, M. Kurosawa, H. Kurebayashi, and S. Ueha, *An Estimation of Load Characteristics of an Ultrasonic Motor by Measuring Transient Responses*. IEEE Transactions on Ultrasonics Ferroelectric and Frequency, 1991. **38**: pp. 481-485.

APPENDIX A

PIEZOELECTRIC CHARACTERIZATION DATA OF PZT CERAMICS

Table A.1 Sample diameter (\varnothing), resonance frequency (f_r), antiresonance frequency (f_a), impedance at resonance ($|Z_m|$), and capacitance at 1 kHz (C) values for PSZT ceramics measured in HP 4194A Impedance/Gain-Phase Analyzer.

Sample*	\varnothing (mm.)	f_a (kHz)	f_r (kHz)	$ Z_m $ (Ω)	C (pF)
PSZ _z T (z:0.50)	13.18	199.45	189.95	9.00	1350
PSZ _z T (z:0.52)	13.10	199.00	180.90	7.90	1500
PSZ _z T (z:0.54)	13.17	185.90	175.02	13.50	1137
PSZ _z T (z:0.56)	13.23	189.34	176.23	27.57	752
PSZ _z T (z:0.58)	13.30	188.12	180.46	49.00	707
PSZ _z T (z:0.60)	13.02	193.63	183.12	37.45	705

* t (thickness of all samples) = 1.0±0.03 mm. (prior to electroding)

Table A.2 Sample diameter (\varnothing), resonance frequency (f_r), antiresonance frequency (f_a), impedance at resonance ($|Z_m|$), and capacitance at 1 kHz (C) values for PSLZT ceramics measured in HP 4194A Impedance/Gain-Phase Analyzer.

Sample*	\varnothing (mm.)	f_a (kHz)	f_r (kHz)	Z_m (Ω)	C (pF)
PSL _y ZT (y:0.005)	13.08	201.01	179.10	30.45	1550
PSL _y ZT (y:0.01)	13.23	156.40	136.15	34.08	2076
PSL _y ZT (y:0.02)	13.07	190.80	169.30	25.47	2234
PSL _y ZT (y:0.03)	13.12	193.50	174.40	27.98	2255
PSL _y ZT (y:0.04)	13.23	191.62	175.25	33.73	2154
PSL _y ZT (y:0.05)	13.26	188.70	175.26	52.38	1733
PSLZ _z T (z:0.50)	13.19	183.91	172.70	71.38	1132
PSLZ _z T (z:0.52)	13.33	176.12	162.75	44.00	1770
PSLZ _z T (z:0.54)	13.23	156.40	136.15	34.08	2076
PSLZ _z T (z:0.56)	13.22	157.19	139.08	47.00	1340
PSLZ _z T (z:0.58)	13.28	158.62	147.34	110.00	720
PSLZ _z T (z:0.60)	13.30	158.69	148.14	122.56	580
PS _x LZT (x:0.00)	12.64	185.75	173.25	143.00	878
PS _x LZT (x:0.01)	12.80	185.95	167.88	91.00	988
PS _x LZT (x:0.02)	13.07	168.72	152.12	75.00	1172
PS _x LZT (x:0.03)	13.03	156.88	138.65	61.00	1430
PS _x LZT (x:0.04)	13.30	159.75	141.00	42.42	1810
PS _x LZT (x:0.05)	13.23	156.40	136.15	34.08	2076

* t (thickness of all samples) = 1.0±0.03 mm. (prior to electroding)

Table A.3 Sample diameter (\varnothing), resonance frequency (f_r), antiresonance frequency (f_a), impedance at resonance ($|Z_m|$), and capacitance at 1 kHz (C) values for (1-x-y)[PSLZT]-(x)[PMnN]-(y)[PMS] ceramics measured in HP 4194A Impedance/Gain-Phase Analyzer.

Sample*	\varnothing (mm.)	f_a (kHz)	f_r (kHz)	$ Z_m $ (Ω)	C (pF)
0.99[PSLZT]-0.01[PMnN]	12.96	162.55	144.05	22.43	2589
0.97[PSLZT]-0.03[PMnN]	12.68	188.35	160.58	4.42	2098
0.95[PSLZT]-0.05[PMnN]	12.70	200.88	172.00	3.44	1557
0.93[PSLZT]-0.07[PMnN]	12.81	203.16	177.26	4.55	1413
0.91[PSLZT]-0.09[PMnN]	12.85	200.20	179.05	8.94	1580
0.90[PSLZT]-0.10[PMnN]	12.85	197.80	175.42	8.51	1730
0.97[PSLZT]-0.03[PMnN] Zr/Ti:52/48	12.66	201.73	175.22	5.52	2160
0.97[PSLZT]-0.03[PMnN] Zr/Ti:53/47	12.75	199.72	166.97	2.17	2310
0.97[PSLZT]-0.03[PMnN] Zr/Ti:54/46	12.68	188.35	160.58	4.42	2098
0.97[PSLZT]-0.03[PMnN] Zr/Ti:55/45	12.72	195.46	168.57	8.31	1195
0.97[PSLZT]-0.03[PMnN] Zr/Ti:56/44	12.70	201.80	174.41	9.2	1260
0.97[PSLZT]-0.028[PMnN]-0.002[PMS]	12.68	198.95	171.65	1.91	2142
0.97[PSLZT]-0.026[PMnN]-0.004[PMS]	12.68	195.38	169.57	1.81	2094
0.97[PSLZT]-0.024[PMnN]-0.006[PMS]	12.70	197.74	171.57	1.46	2082

* t (thickness of all samples) = 1.0±0.03 mm. (prior to electroding)

APPENDIX B

X-RAY AND DENSITY DATA OF PZT CERAMICS

Table B.1 Lattice parameters, tetragonality, theoretical and experimental density values of $\text{Pb}_{0.95}\text{Sr}_{0.05}(\text{Zr}_z\text{Ti}_{1-z})\text{O}_3$ ceramics.

z	Structure	c_T (Å)	a_T (Å)	$(c/a)_T$	a_R (Å)	$\rho_{\text{exp.}}$ (g/cm³)	$\rho_{\text{theo.}}$ (g/cm³)
0.50	T	4.1405	4.0418	1.0244	-	7.65	7.90
0.52	T	4.1339	4.0387	1.0235	-	7.66	7.94
0.54	T+R	4.1335	4.0474	1.0212	4.0879	7.67	7.92
0.56	T+R	4.1303	4.0543	1.0187	4.0845	7.69	7.92
0.58	R	-	-	-	4.0909	7.64	7.89
0.60	R	-	-	-	4.0947	7.62	7.89

Table B.2 Lattice parameters, tetragonality, theoretical and experimental density values of $\text{Pb}_{0.95-y}\text{Sr}_{0.05}\text{La}_y(\text{Zr}_{0.54}\text{Ti}_{0.46})\text{O}_3$ ceramics.

y	Structure	c_T (Å)	a_T (Å)	$(c/a)_T$	a_R (Å)	$\rho_{\text{exp.}}$ (g/cm ³)	$\rho_{\text{theo.}}$ (g/cm ³)
0	T+R	4.1335	4.0474	1.0212	4.0879	7.67	7.917
0.005	T+R	4.1314	4.0440	1.0216	4.1054	7.64	7.813
0.01	T+R	4.1258	4.0392	1.0214	4.0716	7.77	7.90
0.02	T+R	4.1231	4.0462	1.0190	4.0811	7.81	7.904
0.03	T+R	4.1141	4.0460	1.0168	4.0855	7.77	7.871
0.04	T+R	4.1088	4.0441	1.0159	4.0741	7.71	7.913
0.05	T+R	4.1078	4.0491	1.0144	4.0779	7.61	7.875

Table B.3 Lattice parameters, tetragonality, theoretical and experimental density values of $\text{Pb}_{0.94}\text{Sr}_{0.05}\text{La}_{0.01}(\text{Zr}_z\text{Ti}_{1-z})\text{O}_3$ ceramics.

z	Structure	c_T (Å)	a_T (Å)	$(c/a)_T$	a_R (Å)	$\rho_{\text{exp.}}$ (g/cm ³)	$\rho_{\text{theo.}}$ (g/cm ³)
0.50	T	4.1253	4.0265	1.0245	-	7.72	7.87
0.52	T	4.1215	4.0397	1.0202	-	7.71	7.87
0.54	T+R	4.1258	4.0392	1.0214	4.0716	7.77	7.90
0.56	T+R	4.0994	4.0446	1.0136	4.0711	7.75	7.88
0.58	R	-	-	-	4.0726	7.71	7.93
0.60	R	-	-	-	4.0761	7.73	7.93

Table B.4 Lattice parameters, tetragonality, theoretical and experimental density values of $\text{Pb}_{0.99-x}\text{Sr}_x\text{La}_{0.01}(\text{Zr}_{0.54}\text{Ti}_{0.46})\text{O}_3$ ceramics.

x	Structure	c_T (Å)	a_T (Å)	$(c/a)_T$	a_R (Å)	$\rho_{\text{exp.}}$ (g/cm ³)	$\rho_{\text{theo.}}$ (g/cm ³)
0	T+R	4.1256	4.0412	1.0208	4.0711	7.40	7.87
0.01	T+R	4.1255	4.0409	1.0209	4.0709	7.53	7.88
0.02	T+R	4.1257	4.0408	1.0210	4.0714	7.60	7.90
0.03	T+R	4.1258	4.0401	1.0212	4.0715	7.65	7.90
0.04	T+R	4.1257	4.0393	1.0214	4.0716	7.72	7.89
0.05	T+R	4.1258	4.0392	1.0214	4.0716	7.77	7.90

Table B.5 Lattice parameters, tetragonality, theoretical and experimental density values of $(1-x)[\text{PSLZT}] - (x)[\text{PMnN}]$ ceramics.

x	Structure	c_T (Å)	a_T (Å)	$(c/a)_T$	a_R (Å)	$\rho_{\text{exp.}}$ (g/cm ³)	$\rho_{\text{theo.}}$ (g/cm ³)
0	T+R	4.1258	4.0392	1.0214	4.0716	7.77	7.90
0.01	T+R	4.1109	4.0256	1.0211	4.0647	7.88	8.01
0.03	T+R	4.1000	4.0257	1.0184	4.0552	7.94	8.05
0.05	T+R	4.1063	4.0277	1.0195	4.0620	7.90	8.03
0.07	T+R	4.0928	4.0290	1.0158	4.0603	7.90	8.05
0.09	R	-	-	-	4.0411	7.92	8.08
0.10	R	-	-	-	4.0544	7.94	8.07

Table B.6 Lattice parameters, tetragonality, theoretical and experimental density values of 0.97[PSLZT] – 0.03[PMnN] ceramics with different Zr/Ti ratio.

Zr/Ti ratio	Structure	c_T (Å)	a_T (Å)	$(c/a)_T$	a_R (Å)	$\rho_{exp.}$ (g/cm ³)	$\rho_{theo.}$ (g/cm ³)
52/48	T+R	4.1027	4.0238	1.0196	4.0507	7.92	8.04
53/47	T+R	4.1005	4.0257	1.0185	4.0556	7.95	8.04
54/46	T+R	4.1000	4.0257	1.0184	4.0552	7.94	8.05
55/45	T+R	4.1023	4.0295	1.0180	4.0562	7.95	8.04
56/44	R	-	-	-	4.0712	7.84	7.96

Table B.7 Lattice parameters, tetragonality, theoretical and experimental density values of 0.97[PSLZT] – (0.03-y)[PMnN] – (y)[PMS] ceramics.

y	Structure	c_T (Å)	a_T (Å)	Tetragonality (c/a)	a_R (Å)	$\rho_{exp.}$ (g/cm ³)	$\rho_{theo.}$ (g/cm ³)
0.0	T+R	4.1005	4.0257	1.0185	4.0556	7.95	8.04
0.002	T+R	4.1053	4.0311	1.0184	4.0706	7.95	8.04
0.004	T+R	4.1012	4.0306	1.0175	4.0663	7.93	8.01
0.006	T+R	4.0963	4.0334	1.0156	4.0807	7.95	8.02

CURRICULUM VITAE

PERSONAL INFORMATION

Surname, Name: Kalem, Volkan
Nationality: Turkish (TC)
Date and Place of Birth: 30 March 1979 , Sivas
Marital Status: Single
Phone: +90 312 210 59 13
Fax: +90 312 210 25 18
email: vkalem@metu.edu.tr

EDUCATION

Degree	Institution	Year of Graduation
M.Sc.	ITU, Materials Science and Eng.	2003
B.Sc.	Anadolu University, Ceramic Eng.	2001
High School	Kütahya High School	1997

WORK EXPERIENCE

Year	Place	Enrollment
2005- Present	METU Department of Metallurgical and Materials Eng.	Res. Asst.
2001-2004	ITU Department of Materials Science and Eng.	Res. Asst.

FOREIGN LANGUAGES

Advanced English

PUBLICATIONS

1. Kalem V., Çam İ., Timuçin M., "Dielectric and Piezoelectric Properties of PZT Based Ceramics Doped with Strontium and Lanthanum", accepted by Ceramics International (2010).
2. Kalem V., Özalp R., Özen G., Altın F., Öveçoğlu M.L., "Kinetic Study and Optical Investigations of some TeO₂-GeO₂ Glasses", Key Engineering Materials, Vols. 264-268 (2004) pp. 1919-1922.
3. Kalem V., Altın F., Öveçoğlu M.L., Özen G., Özkal B., "Crystallization Behaviour of some TeO₂-GeO₂ Glasses", Key Engineering Materials, Vols. 264-268 (2004) pp. 1915-1918.